Reconstitution and Characterization of Kinetochore Units Assembled on Centromeric Nucleosome Templates

Inaugural-Dissertation

zur

Erlangung des Doktorgrades

Dr. rer. nat.

der Fakultät für Biologie

an der

Universität Duisburg-Essen

vorgelegt von

Kai Walstein

aus Marl

durchgeführt am

Max-Planck-Institut für molekulare Physiologie

Abteilung für mechanistische Zellbiologie

Oktober 2020

Die der vorliegenden Arbeit zugrunde liegenden Experimente wurden am Max-Planck-Institut für molekulare Physiologie in der Abteilung für mechanistische Zellbiologie durchgeführt.

1. Gutachter: Prof. Dr. Andrea Musacchio

2. Gutachter: Prof. Dr. Stefan Westermann

Vorsitzender des Prüfungsausschusses: Prof. Dr. Michael Ehrmann

Tag der mündlichen Prüfung: 18.12.2020

DOI: 10.17185/duepublico/73912
URN: urn:nbn:de:hbz:464-20210218-085846-2

In the context of this doctoral work, the following articles were published:

- Dongqing Pan, Kerstin Klare, Arsen Petrovic, Annika Take, Kai Walstein, Priyanka Singh, Arnaud Rondelet, Alex W Bird, and Andrea Musacchio. 2017. CDK-regulated dimerization of M18BP1 on a Mis18 hexamer is necessary for CENP-A loading. *Elife*. 6.

- Dongqing Pan, Kai Walstein, Annika Take, David Bier, Nadine Kaiser, and Andrea Musacchio. 2019. Mechanism of centromere recruitment of the CENP-A chaperone HJURP and its implications for centromere licensing. *Nat Commun*. 10:4046.

- Kai Walstein, Arsen Petrovic, Dongqing Pan, Dorothee Vogt, and Andrea Musacchio. Preliminary title: CENP-C bridges two adjacent nucleosomes and provides the scaffold for the assembly of the inner and outer kinetochore. Manuscript in preparation

List of figures

List of tables

List of abbreviations

AID ..... Auxin-Inducible Degron

APC/C ..... Anaphase Promoting Complex / Cyclosome

ATM ..... Ataxia-Telangiectasia Mutated

ATP ..... Adenosine Triphosphate

ATR ..... Ataxia-telangiectasia and Rad9 related

AUC ..... Analytical Ultracentrifugation

Bpa ..... p-benzoyl-L-phenylalanine

C. elegans ..... *Caenorhabditis elegans*

$CaCl_2$ ..... Calcium Chloride

CAK ..... Cdk activating kinase

CATD ..... CENP-A Targeting Domain

CBB ..... Coumassie Brilliant Blue

CCAN ..... Constitutive Centromere Associated Network

CCC CDK1:Cyclin B:CAK1

CDE ..... Centromere DNA element

CDK ..... Cyclin-dependent kinase

CDS ..... Coding Sequences

CENP ..... Centromere Protein

CPC ..... Chromosomal Passenger Complex

CREST ..... Calcinosis/Raynaud's phenomenon/ Esophageal dysmotility/ Sclerodactyly/ Telangiectasia

D. melanogaster ..... *Drosophila melanogaster*

DAPI ..... 4′,6-diamidino-2-phenylindole

DMEM ..... Dulbecco's Modified Eagle Medium

DMSO ..... Dimethyl Sulfoxide

DNA ..... Deoxyribonucleic Acid

DTE ..... Dithioerythritol

E. coli ..... *Escherichia coli*

EDTA ..... Ethylenediaminetetraacetic Acid

EGFP ..... Enhanced Green Fluorescent Protein

EGTA ..... Egtazic Acid

FBS ..... Fetal Bovine Serum

GTP ..... Guanidine Triphosphate

HEPES ..... 4-(2-hydroxyethyl)-1-Piperazineethanesulfonic Acid

HFD ..... Histone Fold Domain

HJURP ..... Holliday Junction Recognition Protein

IF ..... Immunofluorescence

INCENP ..... Inner Centromere Protein

IP ..... Immunoprecipitation

IPTG ..... Isopropyl-β-D-thiogalactopyranoside

KCl ..... Potassium Chloride

LB ..... Lysogeny Broth

M18BP1 ..... Mis18 Binding Protein 1

MBP ..... Maltose-binding Protein

MCC ..... Mitotic Checkpoint Complex

$MgCl_2$ ..... Magnesium Chloride

NaCl ..... Sodium Chloride

NP-40 ..... Nonidet P-40

NPC ..... Nucleosome Core Particle

PAGE ..... Polyacrylamide Gel Electrophoresis

PBD ..... Polo Box Domain

PBS ..... Phosphate-Buffered Saline

PCR ..... Polymerase Chain Reaction

PFA ..... Paraformaldehyde

PLK ..... Polo-like kinase

PMSF ..... Phenylmethylsulfonyl Fluoride

RbAp ..... Retinoblastoma protein Associated protein

RSF ..... Remodelling and Spacing Factor

S. cerevisiae ..... *Saccharomyces cerevisiae*

S. pombe ..... *Schizosaccharomyces pombe*

SAC ..... Spindle Assembly Checkpoint

SDS ..... Sodium Dodecyl Sulfate

SEC ..... Size-Exclusion Chromatography

siRNA ..... Small Interfering Ribonucleic Acid

STLC ..... S-trityl-L-cysteine

TB ..... Terrific Broth

TBS ..... Tris-Buffered Saline

TCEP ..... Tris(2-carboxyethyl)phosphine

TEV ..... Tobacco Etch Virus

UV ..... Ultraviolet

X. laevis ..... *Xenopus laevis*

YT ..... Yeast Extract Tryptone

1 Introduction

1.1 The cell cycle

The cell cycle is a regulated series of events in eukaryotic cells resulting in the production of two daughter cells, which are accurate copies of the parent cell. Cell division consists of two consecutive steps, the complete replication of the chromosomal deoxyribonucleic acid (DNA) and the faithful segregation of replicated chromosomes into two nascent cells. The first cell cycle phase was recognized in 1882 by Flemming, who discovered the process of nuclear division, termed mitosis (Paweletz, 2001). The rest of the cell cycle was called interphase, or resting stage. When DNA was recognized in the 1940s as the agent of heredity, it became obvious, that interphase must contain a DNA duplication event to preserve an euploid state. In 1953, Howard and Pelc discovered in a key experiment, that ^{32}P was incorporated into DNA only during interphase and that this happened with an interval of several hours to the mitotic phase (Howard and Pelc, 1953). Since then, the cell cycle conceptually consists of four distinct phases (Figure 1-1).

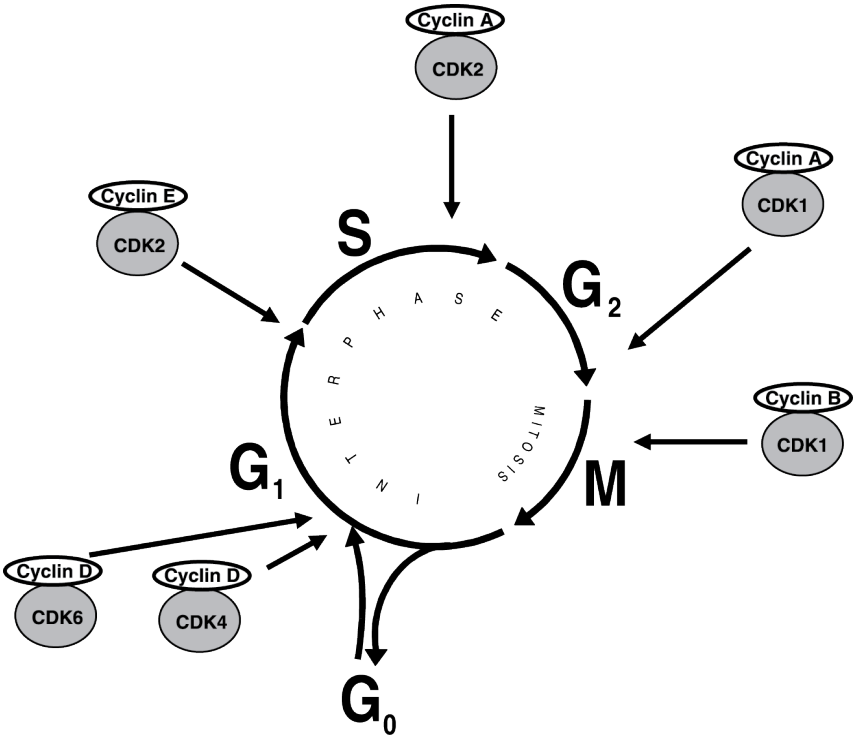

Figure 1-1 The stages of the eukaryotic cell cycle

The eukaryotic cell cycle consists of four different phases, namely G1 phase, S phase, G2 phase and M phase. In G1 phase, cells can enter a reversible quiescent state, called G0. Alternatively, cells can progress through the cell cycle. In S phase, cells replicate their DNA, which is equally distributed to the daughter cells during M phase. Cell cycle progression is controlled by Cdk activity. Figure adapted from (Vermeulen et al., 2003)

In M phase, the chromosomes are segregated during mitosis followed by cytokinesis, the division of the cytoplasm. In the first gap phase, termed G1 phase, cells grow back to an optimal size. In G1 phase, cells can reenter a new cycle of DNA replication and cell division or, if the supply of nutrients is poor, enter a non-dividing state, called G0 phase (Vermeulen et al., 2003). During S phase, the DNA replication is initiated at many sites called origins of replication. Each of these origins is licensed in G1 phase by the formation of a prereplication complex. In S phase, the prereplication complex is dismantled and cannot be reassembled before the cell has entered the next G1 phase. This prevents multiple rounds of DNA replication from the same origin of replication (Blow and Hodgson, 2002). The duplicated DNA molecules, the sister chromatids, become linked to each other by the pentameric cohesin complex (Toth et al., 1999). In G2 phase, cells prepare their chromatin and cytoskeleton for the drastic changes that will occur during mitosis. The integrity of the replicated DNA is further checked, and mitotic entry is delayed in case of non-replicated or damaged DNA.

The transition from one phase of the cell cycle to the next is strictly regulated by key regulatory proteins, the cyclin-dependent kinases (CDK) (Uhlmann et al., 2011). The activity of these serine/threonine protein kinases depends on the binding of regulatory subunits, termed cyclins. Whereas CDK levels are constant during the cell cycle, cyclins are expressed and destroyed at specific points and thereby regulate CDK activity in a timely manner (Morgan, 1995). Five CDKs have been identified in humans to be involved in cell cycle regulation. CDK2, CDK4 and CDK6 act as interphase-specific CDKs, whereas CDK1 is the mitosis-specific CDK. CDK7 acts as a CDK activating kinase (CAK) (Fisher and Morgan, 1994). D-type cyclins bind to CDK4 and 6 in G1 phase and the phosphorylation of their downstream targets leads to the expression of E-type cyclins. CDK2-Cyclin E is essential to drive the G1/S phase transition (Ohtsubo et al., 1995; Sherr, 1994). During late S phase CDK2-Cyclin A promotes the transition from S phase to G2 phase. A-type cyclins activate CDK1 to facilitate the onset of mitosis and are subsequently degraded to enable the complex formation of CDK1-Cyclin B (Arellano and Moreno, 1997). CDK1-Cyclin B will drive the cells through mitosis until Cyclin B is rapidly degraded to promote mitotic exit. In contrast to the cell cycle in humans, where specific CDK-Cyclin complexes form to drive the various events, cell cycle progression in *Saccharomyces cerevisiae* (*S. cerevisiae*) is controlled by a single CDK, known as Cdc28, that binds to different

cyclins during the cell cycle (Mendenhall and Hodge, 1998). Although the number of CDKs has expanded in higher eukaryotes, the underlying principle of phosphorylation-driven cell cycle regulation is the same in fungi, plants and animals (Gunbin et al., 2011).

The transitions between cell cycle stages are controlled by various checkpoints. These checkpoints send inhibitory signals when they detect problems (Hartwell and Weinert, 1989). The restriction point in G1 phase marks the point of no return; if the cell passes this checkpoint, it is committed to enter the cell cycle. Cells starved of serum before the restriction point enter a G0-like state, while cells starved later continue through mitosis (Pardee, 1974). DNA damage checkpoints are performed before the cell enters S-phase and also after DNA replication at the G2/M phase border. Two key protein kinases, ataxia-telangiectasia mutated (ATM) and ataxia-telangiectasia and Rad9 related (ATR), act as sensors of DNA damage and activate two transducer kinases CHK1 and CHK2. They also stabilize p53, which induces the expression of genes involved in cell cycle progression and apoptosis (Abraham, 2001). Finally, during mitosis, the spindle assembly checkpoint (SAC) prevents cells from the metaphase to anaphase transition until each chromosome is properly attached to the mitotic spindle (Hoyt et al., 1991; Li and Murray, 1991).

1.2 Mitosis and the spindle assembly checkpoint

When a cell enters mitosis, the visible condensation of chromosomes is the first event defining the beginning of prophase (Figure 1-2). As a consequence of prophase compaction, transcription shuts down and the nucleus disperses. The beginning of prometaphase is characterized by nuclear envelope breakdown. The lamin fibers, that interact with inner nuclear membrane proteins, become hyperphosphorylated by CDK1-Cyclin B causing the dispersal of the nuclear envelope. At the same time, microtubules start to invade the nuclear space and make contacts with chromosomes by attaching to specialized structures, called kinetochores (McIntosh, 2016). Kinetochores are multi protein complexes which assemble exclusively on specialized chromatin. During prometaphase kinetochores show a characteristic trilaminar disk structure, as shown by early electron-microscopy studies (Rieder, 1982). First, highly dynamic spindle microtubules, which nucleate from centrosomes, are captured by

kinetochores at their wall. These lateral attachments are facilitated by a surface expansion of the outer kinetochore (Magidson et al., 2011). The lateral, unstable kinetochore-microtubule interactions are then converted into stable end-on attachments in a multi-step end-on conversion process (Tanaka, 2010). Stably bound kinetochore microtubules are getting stabilized which results in a reduced probability of catastrophic shrinkage (Hayden et al., 1990). Another way of kinetochore capture in mitotic cells, although less well understood, is the kinetochore-driven nucleation of microtubules (Khodjakov et al., 2003; Maiato et al., 2004). Capture of one microtubule by a kinetochore results in the movement of the chromosome to the spindle pole, from which the microtubule originates. When the kinetochore from the sister chromatid captures a microtubule coming from the opposite spindle pole, this bipolar attachment leads to a balance of opposing forces, which results in the alignment of the chromosomes at the spindle equator (Figure 1-2). This process is called chromosome congression and involves cytoskeletal motor proteins, in particular centromere protein (CENP)-E (Kapoor et al., 2006).

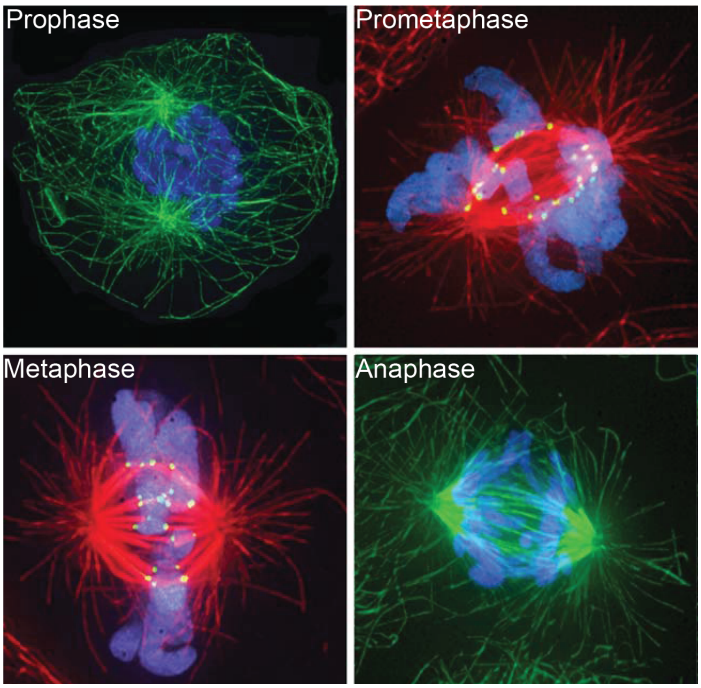

Figure 1-2 Immunofluorescence images of mitotic rat kangaroo cells

During prophase the chromosomes (blue) condense while the microtubules (green) organize in the cytoplasm. In prometaphase, the spindle microtubules (red) are captured by the kinetochores (green dots) and the chromosomes move towards the spindle equator. In metaphase, all chromosomes are properly bi-oriented and are aligned on the spindle midplane. During anaphase, the sister chromatids segregate and move towards the opposite spindle poles. Figure adapted from (McIntosh, 2016).

The desired metaphase state is defined by a complete set of chromosomes that are properly bioriented between both spindle poles forming the metaphase plate (Figure 1-2). To achieve this state, erroneous attachments need to be corrected. Besides chromosomes with one or two unattached kinetochores, the most common sorts of errors include syntelic attachments, where both kinetochores are attached to microtubules originating from the same spindle pole, and merotelic attachments, where one kinetochore is attached to both spindle poles (Cimini and Degrassi, 2005). The latter error is the most common cause for segregation errors in cultivated mammalian cells (Salmon et al., 2005). Both errors are sensed by Aurora B kinase, which is a member of the chromosomal passenger complex (CPC), along with borealin, survivin and inner centromere protein (INCENP) (Carmena et al., 2012). The CPC localizes at the inner centromere during prometaphase and metaphase (Earnshaw and Cooke, 1991). Aurora B senses erroneous end-on attachments and corrects them by phosphorylating several kinetochore subunits, in particular Hec1 and the Dam1 complex in budding yeast. These phosphorylations inhibit the microtubule binding of that particular kinetochore subunits (Tien et al., 2010). Furthermore, Aurora B has been shown to be an upstream regulator of the end-on conversion process since it stabilizes lateral attachments in human cells (Shrestha et al., 2017).

To achieve the state, in which all chromosomes are properly bioriented, anaphase onset has to be delayed even if one single chromosome has not reached biorientation (Rieder et al., 1995). The SAC is the surveillance mechanism, that monitors the status of kinetochore-microtubule attachments and prevents the premature segregation of sister chromatids (Musacchio, 2015). Unattached kinetochores catalyze the formation of diffusible mitotic checkpoint complexes (MCC), composed of BUBRI/BUB3 and CDC20/MAD2 (Hwang et al., 1998; Nilsson et al., 2008; Sudakin et al., 2001). The generation of the MCC is catalyzed by additional components including MAD1 and two mitotic kinases, MPS1 and BUB1 (Abrieu et al., 2001; Hoyt et al., 1991; Li and Murray, 1991). CDC20 itself is the mitotic co-activator of the anaphase promoting complex or cyclosome (APC/C). The MCC formation prevents the activation of the APC/C by sequestering CDC20 as long as there are unattached kinetochores. The APC/C is an E3 ligase that has two key substrates, Securin and Cyclin B, whose proteasomal degradation leads to anaphase onset (Cohen-Fix et al., 1996; Sudakin et al., 1995). Securin degradation allows the cleavage of centromeric cohesin by the enzyme

Separase enabling the physical segregation of the sister chromatid pairs (Uhlmann et al., 1999). Cyclin B degradation leads to an inactivation of CDK1 allowing mitotic exit (Murray et al., 1989). Once all kinetochores are properly bioriented, the released CDC20 eventually activates the APC/C which will initiate the metaphase to anaphase transition. Thus, the SAC is an important feedback mechanism that maintains the genomic stability by preventing premature sister chromatid segregation.

In anaphase, the sister chromatids move towards the opposite spindle poles. This movement is achieved by a shortening of microtubules and the necessary energy is provided by the hydrolysis of guanidine triphosphate (GTP) bound to assembled tubulin (Asbury, 2017). During telophase, the nuclear envelope reforms on the surface of the separated sister chromatids which are located in clusters near the spindle poles. Thus, mitosis is a series of finely regulated events, that is controlled by the SAC, a sensitive surveillance mechanism ensuring that the genetic material is faithfully segregated between the arising daughter cells.

1.3 The centromere

All mitotic events from prometaphase to anaphase depend on the fine-tuned interactions between spindle microtubules and kinetochores. Kinetochores can be divided into an inner and an outer layer. While the outer kinetochore promotes the microtubule binding and also catalyzes MCC formation, the inner kinetochore directly flanks the chromosomes throughout the cell cycle and recruits the outer kinetochore members specifically during mitosis. Kinetochore assembly is limited to unique chromatin structures, which are called centromeres (Fukagawa and Earnshaw, 2014). The centromere is a specialized region of the chromosome, that was originally defined as a region of suppressed meiotic recombination and as the "primary constriction" of the chromosome (Fukagawa and Earnshaw, 2014). Its major function is to provide the foundation for the assembly of the kinetochore and to serve as the site of sister chromatid cohesion until anaphase onset during mitosis. Although the word centromere can be translated as "central part", centromeres are not necessarily located in the center of chromosomes. From the human chromosomes, only five are considered metacentric with both chromosome arms being roughly of equal length. In the other chromosomes, the centromere is either located close to the center

(submetacentric) or it is situated in a way, that one chromosomal arm is much shorter than the other (acrocentric).

The size of a centromere varies largely between species. In *S. cerevisiae*, the centromere of each chromosome has a well-defined size of exactly 125 bps (Clarke and Carbon, 1980). This type of centromere is referred to as point centromere. However, the centromeres of most eukaryotes are more complex and organized in a configuration termed regional centromere. These centromeres are characterized by complex tandemly repeated DNA sequences flanked by pericentromeric heterochromatin. In human regional centromeres, the 171 bp α satellite DNA, which is organized in higher order repeats (Manuelidis, 1978), spans regions from several 100 kbps to 5 Mbps (Fukagawa and Earnshaw, 2014). A third type of centromere, termed holocentromere, exists in some insects, lower plants and nematodes like *Caenorhabditis elegans* (*C. elegans*) and extends along the entire length of the chromosome (Marques and Pedrosa-Harand, 2016). Thus, point centromeres and holocentromeres seem to be an evolutionary adaptation from the regional centromere configuration.

The initial understanding of regional centromeres as repetitive α-satellite sequences was soon challenged and has changed in a way that the underlying DNA sequence moved out of focus. Although repetitive DNA sequences are a common feature of regional centromeres, several findings raised doubts, that the centromere is strictly specified by its underlying DNA sequence. The most obvious evidence is the lack of repetitive DNA sequences in at least one chromosome in various species like chicken or orangutan (Locke et al., 2011; Shang et al., 2010). Another striking argument against a sequence dependence was the discovery of neocentromeres, which form at non-centromeric loci due to de novo rearrangements of chromosomes (Amor and Choo, 2002). Remarkably, human neocentromeres have been shown to behave like their satellite-DNA containing counterparts (Voullaire et al., 1993). The discovery of pseudodicentric chromosomes, in which one α-satellite array does not recruit any centromere associated proteins further questioned the role of DNA sequence as the marker of functional centromeres (Earnshaw and Migeon, 1985).

The discovery of autoantibodies against centromeres in patients suffering from calcinosis/ Raynaud's phenomenon/ esophageal dysmotility/ sclerodactyly/ telangiectasia (CREST) variant of scleroderma laid the foundation for the molecular

understanding of the centromere (Moroi et al., 1980). Three different antigens were recognized by the sera of patients suffering from CREST syndrome being designated CENP-A, CENP-B and CENP-C, from which CENP-A has been finally identified as a histone H3 variant (Earnshaw and Rothfield, 1985; Palmer et al., 1987). There is now general agreement that CENP-A is the actual molecular determinant of the centromere in eukaryotes, since it is present in virtually all organisms from *S. cerevisiae* (where CENP-A is called Cse4) to humans. As a consequence, the centromere is defined rather epigenetically than by a specific DNA sequence.

The point centromere of *S. cerevisiae* is a notable exception, because it is genetically defined by three centromere DNA elements (CDE) CDEI, CDEII and CDEIII forming together the 125 bp centromere sequence (Clarke and Carbon, 1980). The CDEIII element is specifically recognized by CBF3, a critical complex necessary for proper kinetochore function and for the recruitment of kinetochore proteins (Lechner and Carbon, 1991). Quantitative chromatin immunoprecipitation experiments could detect one single Cse4 nucleosome present at each point centromere in *S. cerevisiae (Furuyama and Biggins, 2007)*. Cse4 could furthermore be mapped to the 80 bp CDEII element in all 16 budding yeast chromosomes (Krassovsky et al., 2012). In contrast to budding yeast, higher organisms with regional centromeres do not possess specific genetic elements which define the centromere region. Thus, in these organisms CENP-A nucleosomes are the molecular determinant of the centromere.

In human regional centromeres, CENP-A nucleosomes are dispersed between canonical H3 nucleosomes. The number of CENP-A nucleosomes was estimated to be approximately 200 per centromere in human cells with a CENP-A:H3 ratio of 1:25 (Bodor et al., 2014). Although more than two thirds of the nuclear CENP-A pool were found at non-centromeric sites, taking into account the size of the human genome, the quantified number of centromeric CENP-A nucleosomes still represents nearly a 50-fold enrichment over non-centromeric CENP-A (Figure 1-3). At physiological centromeres and neocentromeres, CENP-A nucleosomes occupy two thirds of the length of the constriction and one third of constriction width and height. This level of

occupancy led to the conclusion that the centromere is probably arranged in a coiled 30 nm fiber that forms a higher order folded or looped structure (Marshall et al., 2008).

The canonical H3 nucleosome consists of DNA wrapped around a histone octamer in a left-handed manner with two copies each of histone H2A, H2B, H3 and H4 (Luger et al., 1997). Several provocative forms of the CENP-A nucleosome have been postulated including tetrameric and hexameric forms, nucleosomes with opposite

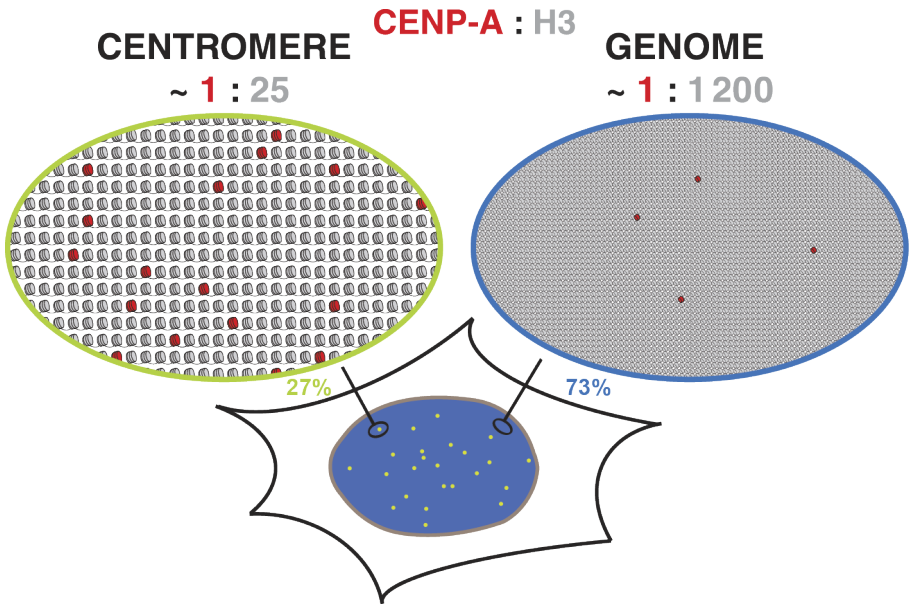

Figure 1-3 The quantitative architecture of centromeric chromatin

Less than one third of all CENP-A nucleosomes (red) is found at centromeric sites. However, the CENP-A:H3 ratio at the centromere is approximately 50-fold larger than at non-centromeric sites. Figure adapted from (Bodor et al., 2014)

handedness and heterotypic nucleosomes containing both H3 and CENP-A (Dalal et al., 2007; Dimitriadis et al., 2010; Furuyama and Henikoff, 2009; Mizuguchi et al., 2007). The crystal structure of a reconstituted human CENP-A nucleosome revealed, that CENP-A nucleosomes resemble canonical H3 nucleosomes with only minor differences (Tachiwana et al., 2011). The DNA writhe is left-handed like it is in H3 nucleosomes, but the DNA wrapping is looser in CENP-A nucleosomes allowing more flexible DNA ends (Dechassa et al., 2011; Panchenko et al., 2011; Roulland et al., 2016). While the overall organization of the CENP-A nucleosome does not seem to be very distinct from H3 nucleosomes, the actual discriminants can be found in the CENP-A histone itself.

Compared to H3, the N-terminal helix of CENP-A contains three residues less which results in a smaller protected DNA fragment in nuclease assays (Conde e Silva et al., 2007; Tachiwana et al., 2011). The N-terminal tail of CENP-A is highly divergent from H3 and several posttranslational modifications were identified. The residues Ser7, Ser16, Ser18 and Ser68 have been shown to be phosphorylated, whereas Lys124 is a ubiquitination site (Bailey et al., 2013; Kunitoku et al., 2003; Niikura et al., 2015; Yu et al., 2015). Additionally, the N-terminal methionine of CENP-A is removed and the Gly1 residue of the nascent CENP-A peptide is trimethylated (Bailey et al., 2013; Sathyan et al., 2017). Remarkably, the importance of posttranslational modifications was discussed controversially. For instance, the phosphorylation of Ser7 by the Aurora kinases A, B and C has been proposed to be important for the completion of cytokinesis, chromosome alignment, CENP-C recruitment as well as sister chromatid cohesion (Eot-Houllier et al., 2018; Goutte-Gattat et al., 2013; Kunitoku et al., 2003; Zeitlin et al., 2001). However, another study, in which endogenous CENP-A was depleted by an Auxin-inducible degron and rescued by a CENP-A Ser7 Alanine mutant, questioned the importance of CENP-A Ser7 phosphorylation in any of these processes (Barra et al., 2019).

The CENP-A targeting domain (CATD) is an important feature and consists of unique residues within loop 1 and the α2-helix. This domain contributes to the rigidity of the CENP-A nucleosomes and is necessary and sufficient for the centromere recruitment of CENP-A (Black et al., 2007; Foltz et al., 2009). Importantly, the loop 1 region contains two extra residues, Arg80 and Gly81, which form a surface-accessible bulge (Tachiwana et al., 2011). This bulge serves as a recognition motif and can be "read" by the inner kinetochore member CENP-N (Fang et al., 2015; Pentakota et al., 2017; Tian et al., 2018). The C-terminal tail of CENP-A, which contains six residues, is not evolutionary conserved, but has a considerably higher proportion of hydrophobic residues than the C-Terminus of H3. This hydrophobicity is specifically recognized by another member of the inner kinetochore, CENP-C (Kato et al., 2013). Replacing the C-Terminus of histone H3 with the C-terminal tail of CENP-A enables the recruitment of CENP-C *in vitro* and *in vivo* (Carroll et al., 2010; Guse et al., 2011). However, CENP-C can also be recruited to the centromere in HeLa cells by H3 carrying the CATD, but not the C-Terminus of CENP-A (Black et al., 2007). Furthermore, both the CATD and the CENP-A C-terminus are required to recruit CENP-C to a LacO array (Logsdon et

al., 2015). This finding is strengthened by an *in vitro* study using reconstituted H3/Cse4 chimera nucleosomes and the *S. cerevisiae* CENP-C orthologue Mif2 (Xiao et al., 2017). Thus, the histone H3 variant CENP-A is the molecular, epigenetic determinant of the centromere in all higher eukaryotes and harbors specific features recognized by members of the inner kinetochore.

1.4 The inner kinetochore

The inner kinetochore is a meshwork comprising 16 centromere proteins that is termed constitutive centromere associated network (CCAN), since most of its components permanently reside at the centromere throughout the cell cycle. Except CENP-C, which can be characterized as a large binding hub (Klare et al., 2015), all CCAN members are organized in constituent subcomplexes, namely CENP-LN, CENP-HIKM, CENP-OPQUR and CENP-TWSX (Figure 1-4). CENP-LN and CENP-HIKM bind each other and, together with CENP-C, form the stable heptameric CENP-CHIKMLN complex (Weir et al., 2016). CENP-OPQUR depends on CENP-HIKM as well as CENP-LN (Pesenti et al., 2018). The integration of CENP-TWSX within the CCAN is less well characterized and will be discussed in detail. This work focuses on the architecture and reconstitution of the human kinetochore. Though, the CCAN organization of *S. cerevisiae* is also going to be discussed and briefly compared to the human CCAN in the upcoming sections.

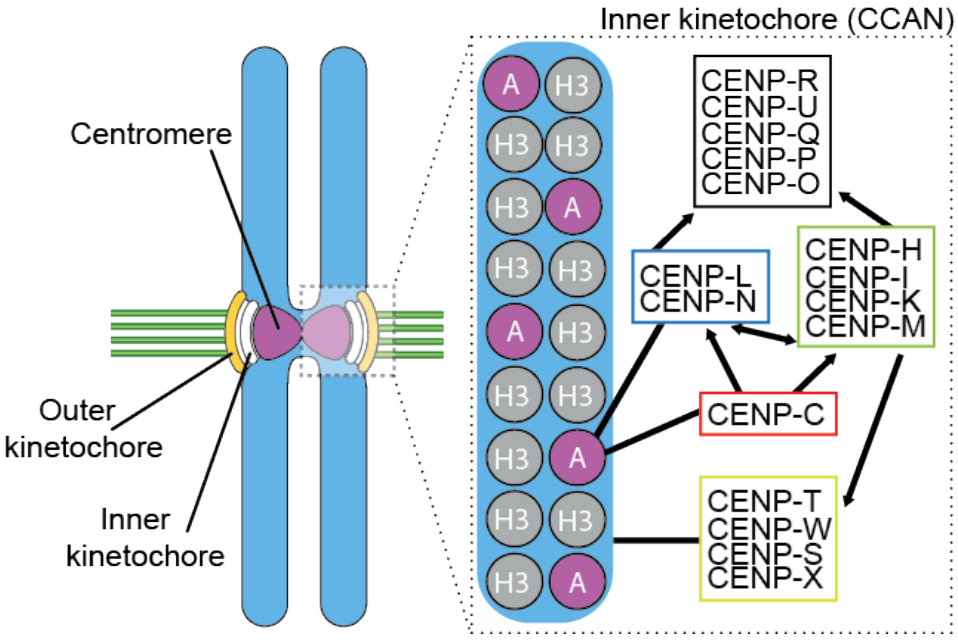

Figure 1-4 Organization of the Constitutive Centromere Associated Network (CCAN)

The CCAN flanks centromeric DNA throughout the cell cycle and consists of 16 different proteins. CENP-C and CENP-N bind directly to CENP-A nucleosomes and recruit the other CCAN components in a hierarchical manner. The CENP-TWSX complex also interacts with centromeric DNA. Figure adapted from (Weir et al., 2016)

1.4.1 The CENP-LN complex

CENP-N has been shown to specifically interact with CENP-A nucleosomes (Carroll et al., 2009; Foltz et al., 2006; Pentakota et al., 2017). This interaction is mediated by the CATD of CENP-A. Interestingly, CENP-N does not interact with pre-nucleosomal CENP-A, because it recognizes a specific histone-DNA interface that is only present in the assembled nucleosome (Pentakota et al., 2017). Like the *S. cerevisiae* orthologs Chl4 (the ortholog of CENP-N) and Iml3 (the ortholog of CENP-L), CENP-N forms a heterodimer with CENP-L (Hinshaw and Harrison, 2013; Pentakota et al., 2017; Weir et al., 2016). The binding between CENP-A and the CENP-LN complex is mediated by the N-Terminus of CENP-N, whereas the CENP-N C-Terminus is sufficient to interact with CENP-L (Pentakota et al., 2017). Mutations in CENP-N, that abolish the binding to CENP-A, strongly reduce the centromere recruitment of CENP-N (Carroll et al., 2009; Pentakota et al., 2017). CENP-LN further interacts with CENP-C, and this binding is most probably mediated by the dimer interface of CENP-LN. A CENP-N truncation mutant lacking the C-Terminus shows impaired centromere localization, indicating that CENP-A alone is not able to fully recruit CENP-N (Carroll et al., 2009). Indeed, the interaction of CENP-N with CENP-C has been shown to be crucial for the

centromere recruitment of CENP-N (Pentakota et al., 2017). Depletion of CENP-N results in strong alignment defects in mitotic cells and furthermore leads to the formation of multipolar spindles (McKinley et al., 2015). Biochemical reconstitution experiments revealed, that CENP-LN also binds the CENP-HIKM subcomplex (Weir et al., 2016).

1.4.2 The CENP-HIKM complex

The complex formation of the four CCAN members CENP-H, -I, -K and -M has been discovered and characterized by biochemical reconstitution analysis (Basilico et al., 2014). CENP-M has been originally proposed to be part of the CENP-LN complex (Cheeseman et al., 2008; Okada et al., 2006). Within the CENP-HIKM complex, CENP-M has a critical function, since it stabilizes CENP-I and thereby helps to solubilize the complex. Structural analyses revealed, that CENP-M has the fold of a small GTPase, which lost its capacity to bind and hydrolyze GTP (Basilico et al., 2014). In contrast to CENP-H, -I and -K, CENP-M does not have an ortholog in *S. cerevisiae*. The centromere recruitment of CENP-I, -K and -M has been shown to be interdependent in HeLa cells using RNAi based approaches as well as inducible knockouts (Basilico et al., 2014; McKinley et al., 2015). Depletion of CENP-M and CENP-I leads to severe chromosome alignment defects. Furthermore, depletion of CENP-HIKM subunits prevents the centromere localization of CENP-LN and vice versa (McKinley et al., 2015). CENP-HIKM further interacts with the histone-fold containing CCAN members CENP-TW, which has been demonstrated in pull-down assays with recombinant proteins (Basilico et al., 2014).

1.4.3 The CENP-OPQUR complex

The CENP-OPQUR complex is the most peripheral subcomplex of the CCAN meshwork. Its kinetochore localization depends on CENP-C, CENP-HIKM and CENP-LN. The localization of the individual CENP-OPQUR proteins is interdependent, whereas the centromere recruitment of the other CCAN members is not affected by the depletion of the CENP-OPQUR complex (McKinley et al., 2015; Pesenti et al., 2018). Two distinct functions can be assigned to different parts of the CENP-OPQUR complex. The tandem RWD domains of the CENP-OP subunits provide the binding

site for the CENP-CHIKMLN complex and thereby target the CENP-OPQUR complex to the kinetochore. The disordered, basic N-terminal tail of CENP-Q provides microtubule binding and also recruits the plus-end directed motor protein CENP-E (Amaro et al., 2010; Pesenti et al., 2018). As a consequence, cells depleted of the CENP-OPQUR complex show chromosome alignment defects (Bancroft et al., 2015; Hori et al., 2008b; Pesenti et al., 2018). Furthermore, Polo-like kinase (PLK) 1, which regulates kinetochore-microtubule attachments, is recruited by CENP-U in a phosphorylation dependent manner (Kang et al., 2006). Strikingly, chicken DT40 knockout cell lines for the CENP-OPQUR subunits are viable, but proliferate at considerably slower rates compared to WT cells (Hori et al., 2008b). In *S. cerevisiae*, the corresponding complex of CENP-OPQUR is named COMA (for Ctf19, Okp1, Mcm21 and Ame1). While the CENP-O and -P orthologs Ctf19 and Mcm21 are non-essential for viability, depletion of the CENP-Q and -U orthologs Okp1 and Ame1 is lethal. In contrast to CENP-U, its ortholog Ame1 carries an N-terminal binding motif for Mtw1, a component of the yeast Mis12 complex (Hornung et al., 2014). Thus, the Ame1-Okp1 complex is crucial to render the yeast centromere competent for the assembly of the outer kinetochore.

1.4.4 The CENP-TWSX complex

The dimeric CENP-TW and CENP-SX subcomplexes together form the tetrameric CENP-TWSX complex. Among all CCAN members, these four are the only ones harboring histone fold domains (HFDs). The sequence of CENP-T additionally contains an unstructured N-terminal region. Both subcomplexes, CENP-SX and CENP-TW, can individually bind to DNA *in vitro* and induce negative supercoiling similar to H3 and CENP-A containing histone octamers. Contrarily, the tetrameric CENP-TWSX complex induces positive supercoiling, caused by the DNA binding regions of CENP-TW. *In vitro* binding experiments and negative stain EM images revealed, that probably two copies of CENP-TWSX preferentially bind to a 100 bp linker DNA of CENP-A or H3 containing dinucleosomes (Amano et al., 2009; Hori et al., 2008a; Nishino et al., 2012; Takeuchi et al., 2014). The histone fold domains of CENP-TW have been demonstrated to be necessary for the centromere localization of the CENP-TWSX complex. Due to its DNA binding ability, CENP-TWSX has been proposed to form an axis that is independent from the rest of the CCAN, but a clear

dependence on the CENP-C-CENP-HIKM branch has been shown (Basilico et al., 2014; Hoffmann et al., 2016; Hori et al., 2008a; Klare et al., 2015; Lang et al., 2018; Pekgoz Altunkaya et al., 2016). Thus, DNA binding mediated by the HFDs and direct interactions with other CCAN members, are both required for the recruitment of CENP-TWSX to the centromere.

CENP-T is one of two CCAN members providing a link to the outer kinetochore. The intrinsically disordered N-terminal tail has two motifs that bind to the RWD domains of the NDC80 subunits SPC24 and SPC25 (Nishino et al., 2013). This interaction is CDK1 dependent in humans and the specific phosphorylation sites in CENP-T, Thr11 and Thr85, have been identified (Gascoigne et al., 2011; Huis In 't Veld et al., 2016). A third, non-canonical CDK1 site, Ser201, promotes binding to another outer kinetochore member, the MIS12 complex. Since the MIS12 complex itself interacts with NDC80, CENP-T recruits in total three NDC80 complexes upon proper CDK1 phosphorylation (Huis In 't Veld et al., 2016). Depletion of CENP-T in human cells leads to severe outer kinetochore assembly defects (Gascoigne et al., 2011). Also in chicken cells, the NDC80 binding domain of CENP-T is essential for mitotic cell progression and cell viability which demonstrates the dominance of the CENP-T pathway for the outer kinetochore assembly in that organism (Hara et al., 2018; Hori et al., 2008a; Nishino et al., 2013). In *S. cerevisiae*, the CENP-T pathway seems to be less important, since the CENP-T ortholog Cnn1 is not essential for cell viability (Malvezzi et al., 2013). However, when the interaction between MIS12 and CENP-C is disturbed by a lack of Aurora B phosphorylation, the CENP-T pathway becomes essential (Lang et al., 2018).

1.4.5 CENP-C

CENP-C is the largest CCAN protein encompassing 943 residues in humans and its sequence analysis predicts, that most of the protein, except its C-Terminus, is intrinsically disordered. Dissection of the human CENP-C sequence reveals, that the largely unstructured protein carries a linearly organized set of binding sites for members of the inner and outer kinetochore as well as two sequence-related nucleosome binding motifs (Figure 1-5). The ordered arrangement of the binding sites recapitulates the outer to inner kinetochore axis rendering CENP-C as a scaffold or "blueprint", that orders the assembly of the whole kinetochore (Klare et al., 2015). Notably, *D. melanogaster* and *C. elegans* lack all the CCAN components described so far except CENP-C.

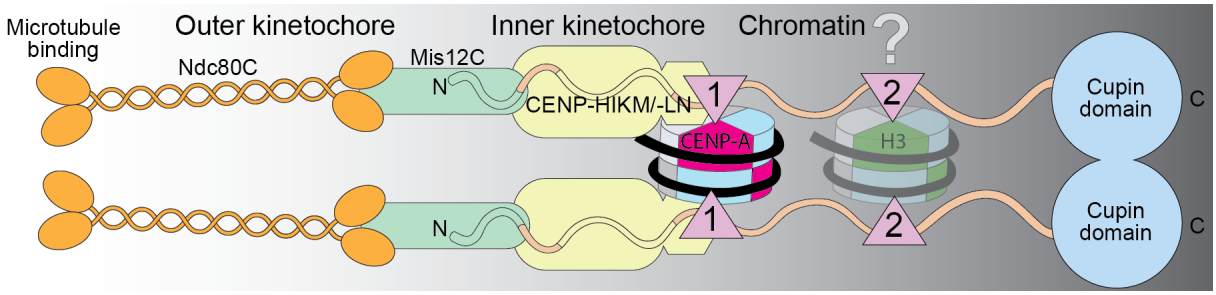

Figure 1-5 CENP-C is a binding platform for the inner and outer kinetochore

The N-Terminus of CENP-C (green region) provides a binding site for the outer kinetochore MIS12 complex, which binds the NDC80 complex. CENP-C furthermore recruits the inner kinetochore members CENP-HIKM and CENP-LN (yellow region). Two sequence-related motifs (magenta triangles) mediate the binding to nucleosomes. The central motif has a higher affinity towards CENP-A nucleosomes than the C-terminal CENP-C motif. During the cell cycle the C-terminal motif might temporarily bind to an H3.3 placeholder nucleosome. The C-terminal Cupin-like domain promotes dimerization.

The N-Terminus of CENP-C contains a 20-residue motif which provides binding to the outer kinetochore MIS12 complex (Przewloka et al., 2011; Richter et al., 2016). Overexpression of a short N-terminal CENP-C construct reduces the outer kinetochore assembly in human cells through competition with endogenous CENP-C (Screpanti et al., 2011). Thus, CENP-C is the second CCAN component besides CENP-T that forms a link to the outer kinetochore. In contrast to CENP-T, which needs to be phosphorylated by CDK1 to bind MIS12, CENP-C binds MIS12 in a CDK1 independent manner. The *S. cerevisiae* CENP-C ortholog Mif2 also contains an N-terminal binding

site for the Mtw1 complex. Surprisingly, this motif is not essential for viability in contrast to the Mtw1 binding motif of the COMA complex member Ame1 (Hornung et al., 2014).

The N-terminal MIS12 binding site is followed by the so-called PEST-rich region, named after the abundance of the amino acids Proline, Glutamic acid, Serine and Threonine. PEST regions have been originally identified in proteins with a short intracellular half-life and have therefore been hypothesized to mediate protein degradation (Rogers et al., 1986). However, the presence of such a region in a centromere protein, that is structurally important for the assembly of the whole kinetochore, remains unclear. The PEST-rich region contains two distinct binding sites for CCAN subcomplexes. The first site provides binding to the CENP-HIKM complex, the second site promotes binding to CENP-LN (Klare et al., 2015; Pentakota et al., 2017). Although both sites are close together, point mutations within one of each side only abrogate the binding of one subcomplex, which indicates, that CENP-HIKM and CENP-LN bind CENP-C completely independent from each other. Disrupting the binding between CENP-C and CENP-HIKM also leads to reduced levels of CENP-T and thereby destabilizes the inner and outer kinetochore (Klare et al., 2015). Deletion of the PEST region in *S. cerevisiae* leads to slow growing and temperature sensitive cells (Cohen et al., 2008). This indicates, that the PEST domain is also important in budding yeast. Furthermore, the two hydrophobic motifs, that are present in CENP-C and necessary for CENP-HIKM binding in human, are also present in Mif2, although their relative position is inverted (Klare et al., 2015).

Human CENP-C has two nucleosome binding motifs, one is located in the central region of CENP-C, the second is located close to the C-Terminus. While the central motif is present almost exclusively in mammals, the C-terminal CENP-C motif is conserved from yeast to humans (Kral, 2015). The central motif has a higher affinity for CENP-A over H3 *in vitro* compared to the conserved C-terminal CENP-C motif, but CDK-mediated phosphorylation of the CENP-C motif has been recently shown to facilitate CENP-A binding in chickens (Kato et al., 2013; Watanabe et al., 2019). Furthermore, the central motif outcompetes the CENP-C motif bound to CENP-A nucleosomes (Ali-Ahmad et al., 2019). The different binding affinities can be explained by minor sequence differences in both motifs. However, the mechanism of CENP-A nucleosome recognition is conserved in both motifs. While several positively charged residues at the N-terminus of both motifs interact electrostatically with the acidic patch

formed by H2A/H2B, two aromatic residues at the C-Terminus interact with the hydrophobic tail of CENP-A (Kato et al., 2013). The central motif, and especially its arginine anchor Arg522, plays an important role in the retention of CENP-A nucleosomes at the centromere. It furthermore stabilizes, together with CENP-N, the overall CENP-A nucleosome structure (Cao et al., 2018; Guo et al., 2017; Melters et al., 2019). Whether CENP-C binds two adjacent nucleosomes with its two motifs and how the composition of this potential dinucleosome structure changes during the cell cycle, remains an unanswered question. Nevertheless, this question is of great importance, especially in regard to centromere propagation, which will be discussed in detail in the later part of this work.

The C-Terminus of CENP-C contains the only known structured part of the protein, the so-called "Cupin like" domain, named after its barrel- or cup-like appearance. In *S. cerevisiae*, the Cupin domain forms a dimeric, nine-stranded β-jelly roll. Deletion of the Mif2 Cupin domain results in viable cells showing a temperature-sensitive growth phenotype (Cohen et al., 2008). The CENP-C Cupin domains of organisms with regional centromeres, namely *Schizosaccharomyces pombe* (*S. pombe)* and *Drosophila melanogaster* (*D. melanogaster)*, share the central jelly roll architecture, but possess extra N-terminal secondary structure elements and a twice as large dimer interface compared to the Mif2 Cupin domain. Furthermore, the Cupin domain of the *S. pombe* CENP-C ortholog Cnp3 has an internal binding pocket for the Meiosis specific protein Moa1 (Chik et al., 2019). Thus, besides being a dimerization domain, the Cupin domain plays an important role during meiosis in that organism. A single point mutation in the Cupin domain of *Xenopus laevis* (*X. laevis*) CENP-C causes a drastic decrease in centromere localization suggesting that CENP-C dimerization is an important mechanism which promotes its centromere recruitment (Carroll et al., 2010). Human CENP-C has also been demonstrated to oligomerize *in vitro* and *in vivo* (Trazzi et al., 2009). However, additional functions of the CENP-C Cupin domain in humans have not been reported yet.

Localization studies in human cells revealed, that, in the presence of endogenous CENP-C, N-terminal or C-terminal CENP-C truncation mutants containing only the first or the second motif, respectively, show centromere localization (Song et al., 2002; Suzuki et al., 2004; Trazzi et al., 2002; Trazzi et al., 2009). In chicken cells, an N-terminal CENP-C fragment can localize in interphase, whereas a C-terminal fragment

localizes only in mitosis. Since chicken CENP-C has only one nucleosome binding motif, the centromere localization seems to be CENP-A dependent only in mitosis, whereas in interphase it is probably recruited by other CCAN members (Nagpal et al., 2015). In human cells, a CENP-C truncation mutant lacking the first nucleosome binding motif showed a 40 % reduction in centromere localization in CENP-C depleted cells, whereas the deletion of the C-terminal CENP-C motif did not have any effect. (Guo et al., 2017). Similar to chicken CENP-C, a C-terminal CENP-C fragment could only localize during mitosis in CENP-C depleted human cells. Although a CENP-C mutant lacking both nucleosome binding motifs is able to localize at centromeres, this mutant is not able to suppress growth defects in CENP-C depleted RPE1 cells (Watanabe et al., 2019). This finding demonstrates, that a physical interaction between CENP-C and CENP-A is indeed necessary for the long-time survival of human cells. However, the determinants for CENP-C centromere localization have not been completely investigated so far. Since centromeric CENP-C levels are severely reduced in CENP-N and CENP-M depleted cells, the centromere localization of CENP-C might not solely depend on direct CENP-A recognition, but also on interactions with further CCAN members (McKinley et al., 2015; Weir et al., 2016).

Thus, CENP-C is the fundamental structural component of the kinetochore, that directly binds centromeric nucleosomes and forms the seed for the assembly of all other inner and outer kinetochore members. The centromere recruitment of CENP-C, that does not solely depend on its physical interactions with CENP-A nucleosomes, is only incompletely understood. Furthermore, full-length CENP-C has not been purified yet and most of the studies investigating the interactions between CENP-C and CENP-A are based on relatively short truncation mutants that harbour the individual CENP-C motif sequences. Therefore, the purification and characterisation of full-length recombinant CENP-C is one of the aims I want to achieve in this work.

1.5 The outer kinetochore

The outer kinetochore is the binding platform for microtubules and furthermore generates the MCC, the major SAC effector. It is recruited by the inner kinetochore members CENP-C and CENP-T specifically during mitosis (Huis In 't Veld et al., 2016; Malvezzi et al., 2013; Rago et al., 2015; Screpanti et al., 2011). The core of the outer kinetochore consists of the 10 subunit KMN network, including the KNL1 complex, the MIS12 complex and the NDC80 complex (Figure 1-6).

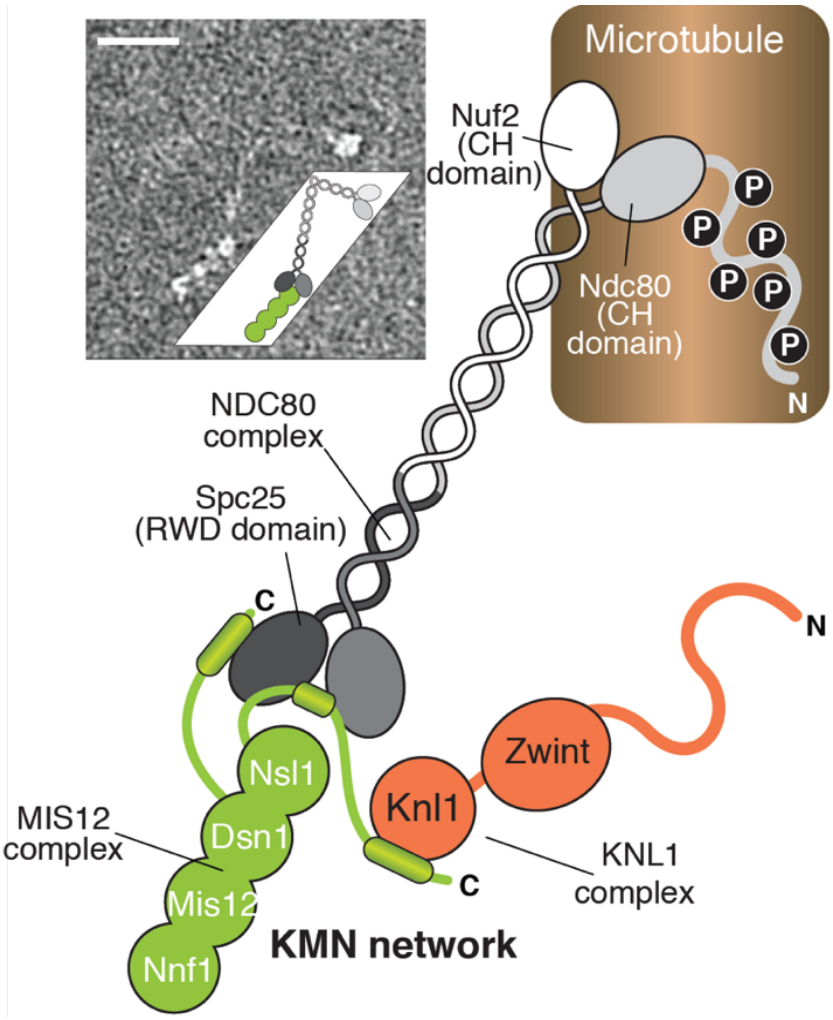

Figure 1-6 Molecular organization of the KMN network

The MIS12 complex is the central hub of the outer kinetochore providing binding sites for the KNL1 complex and the NDC80 complex. The NDC80 complex is the main microtubule receptor of the whole kinetochore. EM images reveal that the NDC80 complex and the MIS12 complex bind in series. KNL1 is the largest member of the core kinetochore and plays an important role in the formation of the MCC during mitosis. Figure adapted from (Pesenti et al., 2016)

1.5.1 The NDC80 complex

The NDC80 complex is the main microtubule receptor at the kinetochore and consists of the four subunits NDC80 (also known as HEC1), NUF2, SPC24 and SPC25. The dumbbell shaped NDC80 complex is highly elongated and contains large coiled coil segments in the middle which are flanked by two globular domains at both ends (Ciferri et al., 2008; Wei et al., 2006; Wei et al., 2005). The N-terminal globular domains of NDC80 and NUF2 fold into a calponin-homology (CH) domain and bind to the plus-ends of microtubules. The CH domain of the NDC80 subunit specifically recognizes a site between two tubulin monomers, that is present at both intra- and inter- tubulin dimer interfaces. This "toe" of NDC80 acts as a conformational sensor of tubulin and preferentially binds to straight protofilaments (Alushin et al., 2010). Furthermore, NDC80 possesses an N-terminal disordered and positively charged tail. This tail has been shown to promote microtubule binding by interacting electrostatically with so called "E-hooks", the negatively charged C-terminal tails of the individual tubulin monomers (Alushin et al., 2012). Nine Aurora B phosphorylation sites have been identified in the N-terminal NDC80 tail. Phosphorylation by Aurora B neutralizes the positive charges of the tail and thereby greatly decreases the binding affinity of NDC80 to microtubules *in vitro* (Cheeseman et al., 2006; Ciferri et al., 2008; DeLuca et al., 2011). The C-terminal regions of SPC24 and SPC25 fold into RWD domains and are crucial for the kinetochore targeting of the NDC80 complex. Two distinct competitive NDC80 recruiters have been shown to target the same binding site on SPC24-25. The first recruiter is CENP-T that binds up to two SPC24-25 in a CDK1 dependent manner in humans (Huis In 't Veld et al., 2016; Nishino et al., 2013; Rago et al., 2015). The second kinetochore receptor for the NDC80 complex is formed by DSN1-NSL1, two subunits of the MIS12 complex (Malvezzi et al., 2013; Petrovic et al., 2010).

1.5.2 The MIS12 complex

The MIS12 complex contains the four subunits MIS12, NNF1, DSN1 and NSL1. Within the KMN network, the MIS12 complex functions as a central interaction hub (Petrovic et al., 2010). The crystal structure of the MIS12 complex revealed, that the helical proteins DSN1-NSL1 and MIS12-NNF1 form pairs that meet in a central stark domain. The motifs providing the binding to SPC24-25 are located close to the C-Termini of DSN1-NSL1 (Petrovic et al., 2016). In metal-shadowed NDC80:MIS12 complexes, the

MIS12 complex appears as a rod-like 18 nm extension on the 60 nm NDC80 complex (Huis In 't Veld et al., 2016). The stalk region provides a binding site for the C-Terminus of KNL1. As already discussed in the previous section, MIS12 recruitment to the kinetochore is promoted by two CCAN members, CENP-C and CENP-T. While CENP-C itself, in contrast to CENP-T, does not need to be phosphorylated by CDK1 to bind to the MIS12 complex, phosphorylation of Ser100 and Ser109 of human DSN1 by Aurora B enhances the CENP-C:MIS12 interaction by releasing the CENP-C binding region of NNF1 from an autoinhibitory inhibition mediated by unphosphorylated DSN1 (Kim and Yu, 2015; Petrovic et al., 2016). In this way, a strong interaction between CENP-C and MIS12 is limited exclusively to the kinetochore. The reason for two independent linkages between the inner and outer kinetochore remains unclear. Furthermore, the importance of the CENP-T-MIS12 pathway varies in different species. In chicken cells, disruption of the CENP-C-MIS12 pathway reduces the centromeric MIS12 signal by 40 % but does not affect NDC80 levels in mitosis and results in viable cells. However, the interaction between CENP-T and MIS12 is crucial in that organism and manipulations lead to cell death (Hara et al., 2018). Contrarily, the *S. cerevisiae* CENP-T ortholog is not essential for cell viability (Malvezzi et al., 2013; Schleiffer et al., 2012).

1.5.3 The KNL1 complex

The KNL1 complex consists of the two subunits KNL1 and Zwint. KNL1 is the largest core kinetochore component having 2316 residues. Most of the sequence, except the C-terminal 500 residues, is largely intrinsically disordered. The C-terminal region consists of a predicted coiled-coil followed by tandem RWD domains, which mediate the binding between KNL1 and the NSL1 subunit of the MIS12 complex (Petrovic et al., 2014). Furthermore, the C-Terminus binds Zwint, which recruits ZW10, a member of the Rod-Zwilch-ZW10 (RZZ) complex, that is involved in SAC regulation during mitosis (Kiyomitsu et al., 2011; Wang et al., 2004). The unstructured N-Terminus of KNL1 contains a canonical binding site for the phosphatase PP1 as well as multiple Met-Glu-Leu-Thr (MELT) repeats. Phosphorylation of these MELT repeats by the MPS1 kinase is a key step for the recruitment of BUB1/BUB3 and further SAC components that are crucial for MCC generation (Yamagishi et al., 2012).

In conclusion, the human kinetochore is composed of 26 core subunits, of which 16 form the CCAN and further 10 form the KMN network. The CCAN directly spans the centromeric chromatin mediated through direct interactions of CENP-C and CENP-N with CENP-A nucleosomes, the epigenetic marks of each centromere. CENP-C plays a key role in kinetochore assembly, since it recruits, directly or indirectly, all other CCAN members. Furthermore, CENP-C provides a link to the outer kinetochore, together with CENP-T. The outer kinetochore mediates the binding to spindle microtubules, which is fine-tuned by error-correcting phosphorylations. Unattached outer kinetochores additionally create inhibitory signals in form of MCC complexes, that retard the onset of mitosis until all chromosomes are bioriented.

1.6 The Propagation of CENP-A chromatin

The epigenetic specification of the centromere by CENP-A necessitates a conservation of the centromeric CENP-A pool during the cell cycle. During DNA replication, the CENP-A nucleosomes are distributed between the two sister chromatids, resulting in a halved CENP-A concentration (Jansen et al., 2007; Schuh et al., 2007). The resulting gaps are most likely filled with histone H3.3 containing nucleosomes, serving as a placeholder (Dunleavy et al., 2011). To remain the centromere identity, the original CENP-A concentration has to be restored (Figure 1-7). Once the number of CENP-A nucleosomes falls below a critical quantity, the chance of centromere loss increases dramatically (Bodor et al., 2014) with severe consequences on the genomic stability of the cell. On the other hand, incorporation of CENP-A at non-centromeric sites has to be minimized to prevent the formation of ectopic kinetochores causing chromosomal segregation aberrations and genomic instability (Sharma et al., 2019). This spatial regulation of CENP-A inheritance is mediated by the pool of pre-existing CENP-A nucleosomes recruiting, most probably mediated by the CCAN, a specialized loading machinery. CENP-A replenishment is uncoupled from DNA replication and happens in early G1 phase (Jansen et al., 2007; Schuh et al., 2007; Shelby et al., 2000).

The CENP-A replenishment process can be divided into three main steps, that will be discussed in detail in the following sections. First, the Mis18 complex localizes at the centromere directly after mitotic exit. This step has been originally understood as a

priming event, which modifies the chromatin to a permissive state for CENP-A deposition (Fujita et al., 2007; Stellfox et al., 2013). In a second step, the CENP-A specific chaperone Holliday Junction Recognition Protein (HJURP) binds to the Mis18 complex and recruits prenucleosomal CENP-A to the centromere (Dunleavy et al., 2009; Foltz et al., 2009). After CENP-A has been deposited and incorporated into the final nucleosome structure, these nascent CENP-A nucleosomes have to be stabilized or maintained, which is considered the last step of the replenishment process (Lagana et al., 2010; Perpelescu et al., 2009; Stellfox et al., 2013).

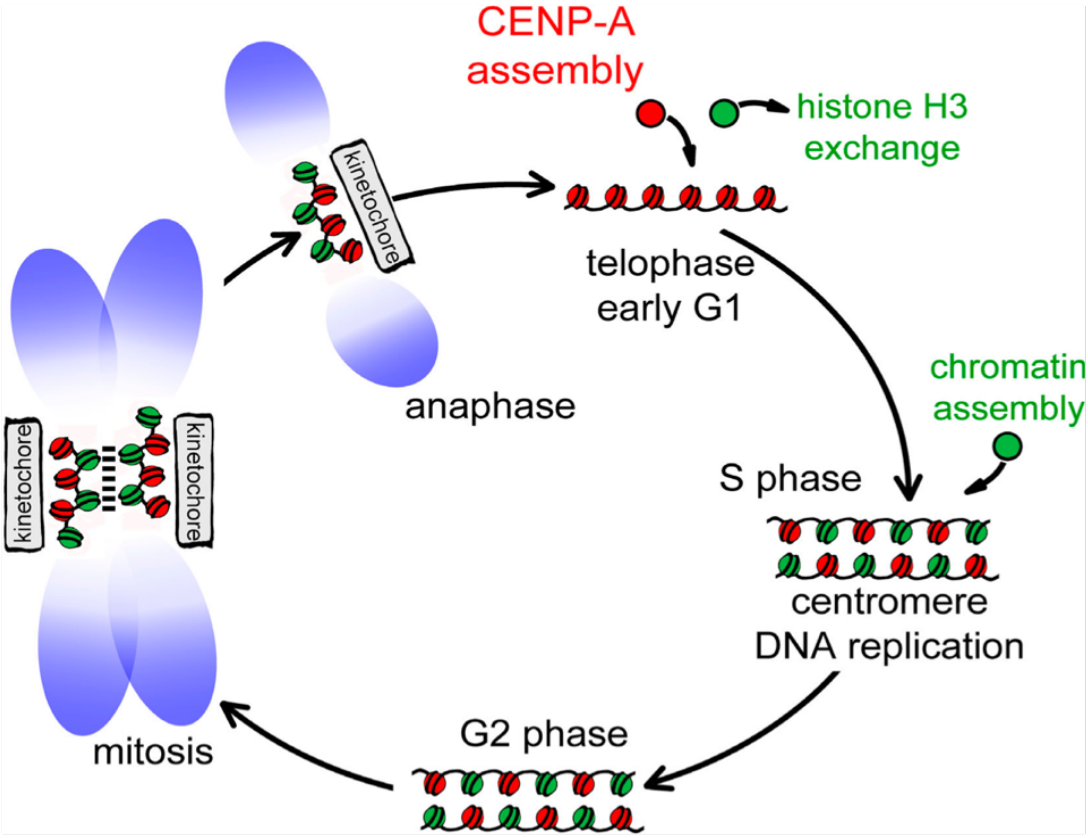

Figure 1-7 CENP-A deposition is uncoupled from DNA replication and takes place in early G1 phase

During DNA replication CENP-A nucleosomes (red) are distributed to the arising sister chromatid resulting in a halved CENP-A concentration per centromere. H3 nucleosomes (green) temporarily fill the resulting gaps and are exchanged against CENP-A in early G1 phase after mitotic exit. Figure adapted from (Jansen et al., 2007)

1.6.1 The Mis18 complex

Mis18 was initially discovered by screening *S. pombe* for temperature sensitive kinetochore mutants. Along with Mis16 mutants (homolog of the human Retinoblastoma protein associated proteins (RbAp) 46 and 48), the Mis18 mutants caused a reduction of the fission yeast CENP-A homolog Cnp1 and chromosomal mis-segregation. Furthermore, Mis16 and Mis18 have been shown to form a complex, and co-depletion of RbAp46 and RbAp48 in human cells resulted in a strong reduction of centromeric CENP-A (Hayashi et al., 2004). RbAp46/48 have been shown to acetylate pre-nucleosomal H4 on Lys5 and Lys12, which is crucial for the CENP-A replenishment reaction (Shang et al., 2016). In a later study, the human homologs Mis18α and Mis18β have been identified, together with an uncharacterized third protein, called Mis18 Binding Protein 1 (M18BP1), which is widely conserved across different species *(French et al., 2017; Fujita et al., 2007; Hori et al., 2017; Kral, 2015; Maddox et al., 2007; Sandmann et al., 2017)*. M18BP1 is a large, intrinsically disordered protein containing a 50-residue SANT (Swi3, Ada2, N-CoR, TFIIIB) domain and a twice as large SANTA (SANT associated) domain (Fujita et al., 2007; Maddox et al., 2007) (Figure 1-8). *S. pombe* Mis18 forms a homotetramer, whereas human Mis18α/Mis18β forms a hexamer with an unusual 4:2 stoichiometry of Mis18α:Mis18β (Pan et al., 2017; Spiller et al., 2017; Subramanian et al., 2016). The Mis18α:β hexamer binds to the N-Terminus of M18BP1 and promotes its dimerization, which is crucial for the centromere localization of the Mis18 complex and the subsequent CENP-A loading reaction (Pan et al., 2017).

M18BP1, Mis18α and Mis18β co-localize at the centromere in telophase and early G1 phase. Depletion of any Mis18 complex member causes severe CENP-A loading defects (Fujita et al., 2007; McKinley and Cheeseman, 2014; Pan et al., 2017). M18BP1 harbours numerous CDK consensus sites and is phosphorylated by CDK1 and CDK2 during S phase, G2 phase and mitosis (Silva et al., 2012; Stankovic et al., 2017). CDK inhibition enables localization of the Mis18 complex and CENP-A loading both in S phase and G2 phase (Silva et al., 2012). Among all the CDK consensus sites of M18BP1, three particularly important phosphorylation sites have been identified. CDK phosphorylation of two N-terminal residues, Thr40 and Ser110, prevents the binding of Mis18α and Mis18β to M18BP1 (Pan et al., 2017). A central residue, Thr653,

controls the centromere localization of the Mis18 complex, and an Alanine mutant is able to localize in G2 phase (Stankovic et al., 2017).

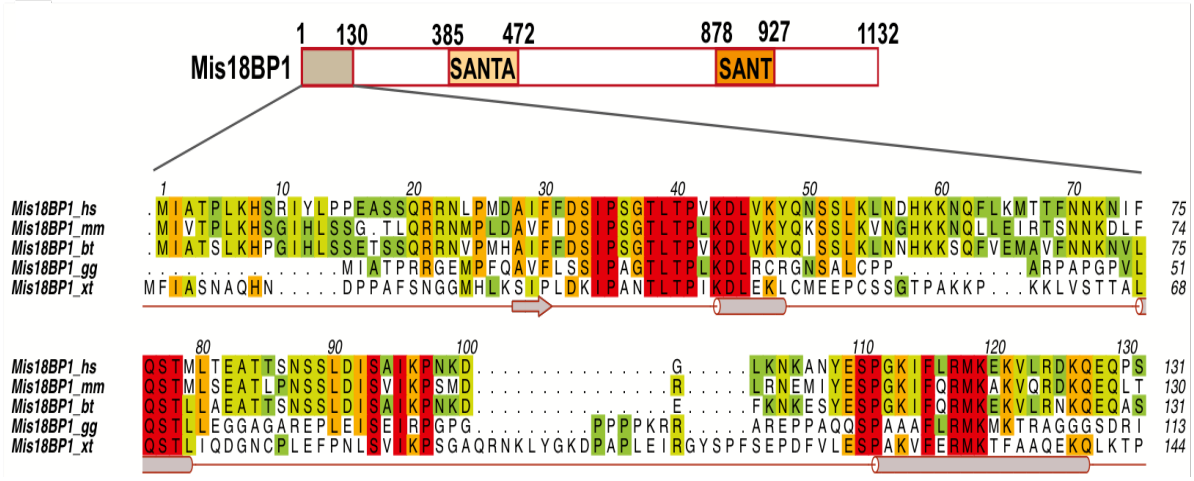

Figure 1-8 Organization of human M18BP1 protein

The N-Terminus of M18BP1 contains two crucial CDK sites, Thr40 and Ser110. CDK1 phosphorylation inhibits the binding of Mis18α and Mis18β and thereby prevents the premature formation of the Mis18 complex. M18BP1 further contains a SANT domain in the C-terminal part and a SANTA domain. Figure adapted from (Spiller et al., 2017).

The recruitment of the Mis18 complex to the centromere remains poorly understood. CENP-C and CENP-I have been shown to induce *de novo* CENP-A deposition when tethered to alphoid HAC centromeres by recruiting M18BP1 (Shono et al., 2015). Furthermore, Mis18β has been proposed to bind to CENP-C (Stellfox et al., 2016). An interaction between the C-terminal portion of CENP-C and M18BP1 was also reported in mouse and *X. laevis* (Barnhart et al., 2011; Dambacher et al., 2012; Moree et al., 2011). Depletion of CENP-C in *Xenopus* extracts specifically prevents the localization of M18BP1 isoform 1, that localizes at the centromere in metaphase and interphase, but not of isoform 2, that localizes exclusively in interphase. Furthermore, CENP-A assembly on sperm chromatin is severely reduced under CENP-C depleted conditions (Moree et al., 2011). The CENP-C dependent localization of M18BP1 isoform 1 during metaphase is mediated by the SANTA domain and a conserved CDK phosphorylation site.

Strikingly, when the metaphase interaction between M18BP1 and CENP-C is disrupted in *X. laevis*, this isoform of M18BP1 also fails to localize in interphase, which results in CENP-A assembly defects (French and Straight, 2019). In contrast to this, only M18BP1 isoform 2, but not isoform 1, is able to substantially rescue CENP-A assembly

on artificial chromatin arrays (Westhorpe et al., 2015). Interestingly, M18BP1 in non-mammalian vertebrates contains the CENP-C motif (Kral, 2015). Studies in *G. gallus* and *X. laevis* M18BP1 demonstrated, that in these organisms M18BP1 directly interacts with CENP-A nucleosomes (French et al., 2017; Hori et al., 2017). In humans, CENP-C seems to be the most probable centromere receptor, but the concrete binding site has not been identified. Since CENP-C has two nucleosome binding motifs, the conserved C-terminal CENP-C motif, that has a lower binding affinity towards CENP-A than the central motif, might be temporarily occupied by the H3.3 placeholder nucleosome, which is recognized by the Mis18 complex and exchanged against CENP-A in early G1. However, the concrete molecular details remain to be investigated and the chromatin remodelling complexes, that promote the nucleosome exchange reaction, have not been identified yet.

1.6.2 Centromere Licensing

The discovery of the Mis18 complex led to the hypothesis that CENP-A deposition requires certain chromatin modifications, which license the centromere for the CENP-A loading reaction (Stellfox et al., 2013). M18BP1 contains a SANTA and a SANT domain, the latter being found in chromatin remodelling complexes like SWI/SNF and the SAGA histone acetyltransferase complex (Boyer et al., 2002). The SANTA domain, which has been identified *in silico* as a SANT associated domain, might furthermore promote protein-protein interactions with its conserved hydrophobic residues and might also be involved in chromatin remodelling activities (Zhang et al., 2006).

RbAp46 and RbAp48, which have been identified as interactors of the Mis18 complex, are histone binding proteins and components of protein complexes that are involved in chromatin remodelling and histone deacetylation (Knoepfler and Eisenman, 1999). It was therefore speculated, that the Mis18 complex recruits histone modifying complexes to the centromere. Confusingly, Mis16 and Mis18 inhibit histone acetylation in *S. pombe*, whereas RbAp46/48 and the Mis18 complex promote histone acetylation in humans and chicken (Fujita et al., 2007; Hayashi et al., 2004; Shang et al., 2016). Treatment of Mis18α depleted HeLa cells with a histone deacetylase inhibitor could furthermore partially rescue CENP-A deposition defects (Fujita et al., 2007). Subsequent studies revealed that tethering of the histone acetyltransferase (HAT)

domains of p300 or PCAF protein to alphoid^{TetO} sequences allowed *de novo* CENP-A deposition in HeLa cells. Furthermore, the acetyltransferase KAT7/HBO1/MYST2 has been shown to interact with M18BP1 when tethered to alphoid^{TetO} DNA repeats and has been proposed to antagonize heterochromatin invasion which is mediated by the H3K9me3 activity of the histone methyltransferase Suv39h1 (Ohzeki et al., 2012; Ohzeki et al., 2016).

In conditional knockout mice, Mis18α deficiency leads to embryonic lethality caused by CENP-A mis-localization and chromosomal segregation errors (Kim et al., 2012). Furthermore, crucial histone modifications like H3K9 and H3K4 methylation are reduced, whereas histone acetylation levels and transcription levels of centromeric DNA are increased in the absence of Mis18α. Mis18α also interacts with the DNA methylases DNMT3A/3B, and a Mis18α mutant, that localizes at the centromere, but cannot bind to DNMT3A/B, fails to rescue CENP-A deposition (Kim et al., 2012). In addition, di-methylation of H3K4 in centromeric H3 nucleosomes has been demonstrated to be crucial for HJURP targeting to the centromere (Bergmann et al., 2011). The transcription elongation-associated chromatin remodelling factor CHD1 binds to these H3K4me2 marks and its knockdown leads to reduced centromeric CENP-A levels (Okada et al., 2009). Transcription of centromeric DNA by RNA Polymerase II (RNAPII) is important for centromere function in general and also plays a particular role in the deposition of new CENP-A in G1 phase (Bobkov et al., 2018). The Facilitates Chromatin Transcription (FACT) remodelling complex disassembles nucleosomes in front of progressing RNAPII and is also able to re-assemble nucleosomes after RNAPII has passed (Kulaeva et al., 2013). FACT interacts with SPT6, a histone chaperone, that assembles histones into nucleosomes and is also able to increase the RNAPII elongation rate (Jeronimo et al., 2019; McDonald et al., 2010). SPT6 can interact with H3 and CENP-A, but the binding to CENP-A is much stronger *in vitro* (Bobkov et al., 2020). In *D. melanogaster* FACT is a binding partner of the CENP-A loading factor CAL1 and its activity is necessary for the incorporation of new CENP-A nucleosomes both at endogenous centromeres and ectopic sites (Chen et al., 2015).

Another licensing factor, that has been identified by mass spectrometry analysis of Mis18α immunoprecipitations, is Polo-like kinase 1 (PLK1). PLK1 colocalizes with the Mis18 complex in early G1 phase, and inhibition of PLK1 prevents the localization of

both PLK1 and the Mis18 complex (McKinley and Cheeseman, 2014). Furthermore, PLK1 inhibition leads to severe CENP-A deposition defects. Creation of an M18BP1 mutant, that lacks all potential PLK1 phosphorylation sites, also abolishes localization of the Mis18 complex and CENP-A loading (McKinley and Cheeseman, 2014). However, it remains unclear how PLK1 phosphorylation promotes the centromere targeting of M18BP1. The Polo box domain of PLK1 has been proposed to bind to the Mis18 complex in a PLK1 phosphorylation dependent manner, but the concrete binding site has not been detected yet (McKinley and Cheeseman, 2014).

1.6.3 Deposition of CENP-A

HJURP is the CENP-A specific chaperone that localizes at the centromere in a Mis18 complex dependent manner and loads new CENP-A onto centromeric chromatin (Dunleavy et al., 2009; Foltz et al., 2009). HJURP and CENP-A form a soluble prenucleosomal complex with one copy of HJURP binding to a CENP-A/H4 heterodimer (Cho and Harrison, 2011; Hu et al., 2011; Mizuguchi et al., 2007). A short N-terminal region of HJURP shows nearly 70 % sequence homology to the yeast homologue Scm3 (Figure 1-9), which is crucial for the deposition of centromeric Cse4 nucleosomes in that organism (Camahort et al., 2007; Mizuguchi et al., 2007; Sanchez-Pulido et al., 2009; Shuaib et al., 2010). The Scm3 homology domain of HJURP has been shown to be necessary and sufficient to deposit CENP-A *in vivo* and to assemble CENP-A nucleosomes *in vitro*. Furthermore, tethering of the HJURP Scm3 homology domain to a LacO array in M18BP1 depleted cells still permits efficient CENP-A deposition at the ectopic site (Barnhart et al., 2011). This demonstrates, that even though HJURP depends on the Mis18 complex for its centromere recruitment, it can independently deposit CENP-A. CENP-A seeding by tethering HJURP to alphoid DNA is sufficient for centromere formation and inheritance on human artificial chromosomes even in the absence of CENP-B (Logsdon et al., 2019), a process, that had previously depended on a high density of CENP-B boxes (Ohzeki, 2002; Okada et al., 2007). The HJURP mid-domain binds to DNA and is required for CENP-A deposition, but not for the centromere targeting of HJURP (Muller et al., 2014). The C-terminal portion of HJURP contains two sequence-related domains, which promote the centromere recruitment of HJURP (Pan et al., 2019; Zasadzinska et al., 2013). Additionally, the C-

Terminus has been proposed to interact with the Condensin II complex during G1 phase (Barnhart-Dailey et al., 2017).

HJURP harbours, similar to M18BP1, several CDK consensus sites. Furthermore, the mid-domain of HJURP contains a Cyclin A binding site. Alanine substitutions of three CDK phosphorylation sites uncouple HJURP localization from G1 phase and a Cyclin A binding mutant is able to deposit CENP-A in G2 phase (Muller et al., 2014; Stankovic et al., 2017). Since the efficient deposition of CENP-A in G2 phase additionally requires the expression of an M18BP1 mutant, that is able to colocalize with HJURP in G2 phase, HJURP seems to depend on the Mis18 complex also in other cell cycle phases than G1 (Stankovic et al., 2017). The second C-terminal HJURP domain has been proposed to dimerize and thereby allow the HJURP dimer to simultaneously incorporate two CENP-A/H4 heterodimers into the final octameric nucleosome structure (Bodor and Jansen, 2013; Zasadzinska et al., 2013). However, *in vitro* studies revealed, that HJURP is a monomer (Pan et al., 2019). Strikingly, exchanging the second C-terminal HJURP domain against a LacI dimerization domain is compatible with HJURP centromere localization (Stankovic et al., 2017) in G1 and G2 phase, whereas the native HJURP protein strictly requires both C-terminal domains (Pan et al., 2019).

The removal of the Mis18 complex from the centromere has been proposed to be necessary for efficient CENP-A assembly, and HJURP has been hypothesized to induce the dissociation of the Mis18 complex by actively removing Mis18α from the

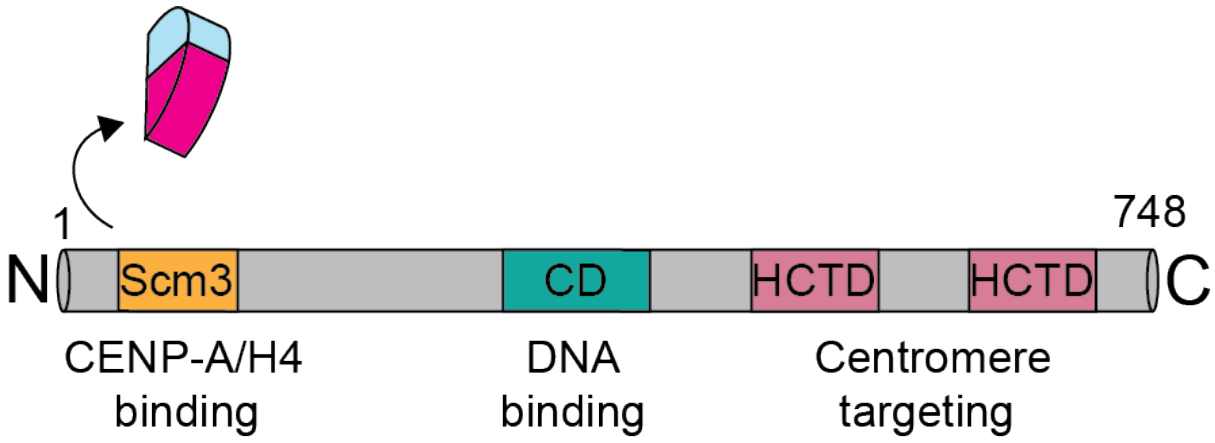

Figure 1-9 Organization of the CENP-A specific chaperone HJURP

HJURP contains an N-terminal Scm3 homology domain, that binds prenucleosomal CENP-A/H4 dimers. The central domain (CD) binds DNA and is also involved in CENP-A deposition. The centromere targeting of HJURP is mediated by two sequence related HJURP C-terminal domains (HCTDs)

centromere (Nardi et al., 2016; Stankovic et al., 2017). However, analytical ultracentrifugation experiments demonstrated that the octameric Mis18 complex is not disrupted upon binding of an HJURP monomer (Pan et al., 2019). Another plausible hypothesis proposed the CENP-A replenishment reaction to be an enzymatic reaction, in which the substrate, a CENP-A-H3 dinucleosome, is converted into the product, a CENP-A-CENP-A dinucleosome (Pan et al., 2019). CCAN members like CENP-C and CENP-T could bridge this dinucleosome structure (Thakur and Henikoff, 2016), recruit the loading machinery to the substrate and subsequently release it after the H3 nucleosome has been exchanged against a CENP-A nucleosome.

1.6.4 Maintenance of CENP-A nucleosomes

After their initial deposition in early G1 phase, CENP-A nucleosomes require further stabilization to prevent their loss from the centromeric chromatin. Super-resolution microscopy analyses revealed, that newly incorporated CENP-A forms rosette-like clusters with HJURP being located in the center as a nucleation point. Interestingly, in late G1 these clusters have a shape similar to the clusters of pre-existing CENP-A due to a structural transition (Andronov et al., 2019). Several factors have been found to be involved in the maintenance process of newly incorporated CENP-A nucleosomes. MgcRacGAP, a Rho family GTPase activating protein, which localizes at the centromere in late G1 phase, has been identified as a potential M18BP1 interactor in a mass spectrometry IP approach (Lagana et al., 2010). MgcRacGAP depletion causes a reduction of newly incorporated CENP-A, whereas the old CENP-A pool remains unaltered. Furthermore, CDC42 has been proposed to be the responsible GTPase, that is recruited to the centromere in late G1 to finally preserve the newly incorporated CENP-A nucleosome. GTPase cycling mediated by MgcRacGAP and the antagonizing GEF ECT2 is necessary for this process (Lagana et al., 2010). The mammalian diaphanous-related formin 2 (mDia2) has been identified as a downstream effector of the MgcRacGAP pathway (Liu and Mao, 2016). Interestingly, depletion of mDia2 causes a prolonged HJURP localization at the centromere indicating a direct involvement in CENP-A deposition. A constitutively active mDia2 mutant could restore centromeric CENP-A levels in MgcRacGAP depleted cells proposing mDia2 as the main effector of that pathway (Liu and Mao, 2016). Another identified CENP-A maintenance factor is the remodelling and spacing factor (RSF) complex, which

localizes at the centromere in mid G1 phase (Perpelescu et al., 2009). Depletion of RSF1, an RSF complex subunit, induces loss of centromeric CENP-A over time. How the RSF complex is targeted to the centromere specifically in mid G1 phase, remains unclear. A recent study identified SPT6 as a further CENP-A maintenance factor (Bobkov et al., 2020). SPT6 interacts with RNAPII and the FACT remodelling complex and has been shown to protect the old CENP-A pool from being lost during centromere transcription in G1, while it permits the active removal of H3.3 placeholder nucleosomes (Bobkov et al., 2020).

HJURP has been shown to be bound to CENP-A during S phase. Thus, besides its crucial role in CENP-A deposition, HJURP has been proposed to be also involved in CENP-A retention during DNA replication (Zasadzinska et al., 2018). According to the hypothesized model, an intermediate complex comprising CENP-A bound to HJURP and the MCM2-7 DNA helicase complex could protect the CENP-A/H4 heterodimer after disassembly of the CENP-A nucleosome from the parental DNA until it is incorporated again into a nucleosome on the nascent sister chromatids (Zasadzinska et al., 2018). A recent genetic screening approach identified SENP6, a SUMO-protease, as a further important CENP-A maintenance factor during the cell cycle. Depletion of SENP6 leads to a hyper-SUMOylation and destabilization of several core CCAN components like CENP-C, CENP-I and CENP-T. As a consequence, CENP-A retention and deposition are negatively affected upon SENP6 depletion, most probably due to an overall destabilization of the kinetochore (Mitra et al., 2020).

1.7 Objectives

The kinetochore is a complex multi-protein assembly, which is of great importance for the maintenance of the genetic stability in all eukaryotes. For this reason, the kinetochore has been the focus of intensive research during the past three decades to understand its molecular architecture and its functioning. Recent biochemical reconstitution and structural studies revealed detailed insights into the complex architecture of the human and budding yeast kinetochore (Allu et al., 2019; Hinshaw and Harrison, 2019; Pesenti et al., 2018; Weir et al., 2016; Yan et al., 2019). However, these studies either omitted CENP-C, a key CCAN component, or used N-terminal, monomeric truncation mutants. In my PhD thesis, I want to gain further insights into the organization of the human kinetochore.

By reconstituting the full-length CENP-C protein, I want to answer the question, if CENP-C interacts with two nucleosomes and thereby structurally links the human kinetochore to a dinucleosome structure. Using biochemical reconstitution, I want to investigate the interactions of CENP-C with centromere specific and canonical nucleosomes as well as other CCAN members. Combining the CENP-C and CENP-T pathway, I want to extend the kinetochore reconstitution of previous studies. Using electroporation as a tool to deliver purified fluorescently tagged protein variants into living cells, I want to further investigate, which are the determinants for the centromere recruitment of CENP-C.

Last, I want to gain further insights into the poorly understood mechanism of CENP-A replenishment. Using an immunoprecipitation mass spectrometry approach, I want to identify interactors of the CENP-A loading machinery and want to further characterize their contribution to the maintenance of the centromere identity.

2 Materials and Methods

2.1 Materials

2.1.1 Affinity Matrices

Table 2–1 Affinity matrices

Affinity matrix	Company
Amylose resin	New England Biolabs
cOmplete His-Tag purification resin	Roche
GFP-Trap magnetic agarose	ChromoTek
RFP-Trap magnetic agarose	ChromoTek

2.1.2 Chromatography columns

Table 2–2 Chromatography columns

Column	Type	Company
Superose 6 Increase 5/150 GL	size-exclusion	GE Healthcare
Superose 6 Increase 10/300 GL	size-exclusion	GE Healthcare
Superdex 200 10/300 GL	size-exclusion	GE Healthcare
Superdex 200 HiLoad 16/60	size-exclusion	GE Healthcare
HiTrap SP FF	cation-exchange	GE Healthcare

2.1.3 Devices

Table 2–3 Devices

Device name	Company
ÄKTA micro/Purifier chromatography systems	GE Healthcare
Bioruptor sonication device	Diagenode
Centrifuge 5418 R	Eppendorf
Centrifuge Allegra X-14	Beckman Coulter
Centrifuge Sorvall Lynx 6000	Thermo Scientific
Centrifuge Sorvall RC 3BP+	Thermo Scientific
ChemiDoc MP Gel Imaging System	Bio-Rad
CLARIOstar Plus microplate reader	BMG Labtech
Class II Biosafety Cabinet NU 437-400 E	NuAire
Fusion FX Gel Imaging System	Vilber Lourmat
Incubator with natural convection BD-53	Binder GmbH
Labgard Class II Laminar Flow Biological Safety Cabinet NU 437-400 E	NuAire
Mini Prep Cell electrophoresis device	Bio-Rad
Multitron incubator shaker	Infors HT
Nanodrop2000 Spectrophotometer	Thermo Fisher Scientific
pH-meter	Sartorius AG
Pipettes Research Plus series	Eppendorf AG
Platform shaker Duomax	Heidolph Instruments

Professional Trio Thermocycler	Analytik Jena AG
Sonifier cell Disruptor	Branson Ultrasonics
Thermomixer R, dry block heating and cooling shaker	Eppendorf
Tube roller	Starlab
Ultracentrifuge ProteomLab XLA	Beckman Coulter
Vortex mixer Genie 2	Carl Roth

2.1.4 Consumables

Table 2–4 Consumables

Consumable	**Company**
Pipette tips	Sarstedt
Test tubes (0.5 ml, 1.5 ml, 2 ml)	Sarstedt
Cell culture dishes (6 cm, 10 cm, 15 cm)	Sarstedt
Cell culture flasks (T-175)	Sarstedt
Cell culture plates (6 well, 12 well, 24 well)	Sarstedt
Nitrocellulose membrane	GE Healthcare
Polyvinylidenfluorid (PVDF) membrane	GE Healthcare
TG PRIME Vertical Tris-Glycine gels 4-12 %	SERVA Electrophoresis GmbH
Filtropur S 0.45	Sarstedt

2.1.5 Buffers

Table 2–5 Buffers

Buffer	Ingredients
Western Blot transfer buffer	25 mM Tris, 192 mM glycine, 10 % methanol
PBS (pH 7.4)	137 mM NaCl, 2.7 mM KCl, 10 mM Na_2HPO_4, 1.8 mM KH_2HPO_4
TBS (pH 7.6)	50 mM Tris, 150 mM NaCl
TBST	TBS pH 7.6 + 0.1 % Tween-20
PBST	PBS + 0.5 % Triton X-100
Lysis buffer A	30 mM HEPES pH 7.5, 500 mM NaCl, 10 % glycerol (w/v), 1 mM TCEP
Lysis buffer B	75 mM HEPES pH 7.5, 20mM KCl, 0.5 mM EGTA, 0.5 mM DTE, 1x Protease inhibitor mix
SEC buffer	10 mM HEPES pH7.5, 300 mM NaCl, 2.5 % glycerol, 1 mM TCEP
Binding buffer A	10 mM HEPES pH7.5, 200 mM NaCl, 1 mM TCEP
SDS anode buffer (10x)	2 M Tris pH 8.9, 225 mM HCl
SDS cathode buffer (10x)	1 M Tris pH 8.25, 1 M Tricine, 1% SDS
SDS gel buffer	3 M Tris, 1 M HCl, 0.3% SDS pH 8.45
SDS sample loading buffer (5x)	5 mM EDTA pH 6.8, 60 mM Tris-HCl, 250 mM DTT, 15% SDS, 30% glycerol, 0.1 % Bromophenolblue

2.1.6 Chemicals

Table 2–6 Chemicals

Chemical	Company
4-(2-hydroxyethyl)-1-piperazineethanesulfonic acid(HEPES)	Carl Roth
4′,6-diamidino-2-phenylindole **(**DAPI)	Serva
Acetic Acid	AppliChem
Acrylamide solution 30 %	AppliChem GmbH
Agarose powder	Invitrogen
Ammonium persulfate (APS)	Serva
Bradford solution (5x)	Carl Roth
Bromophenolblue	Sigma-Aldrich
Coomassie G250/R250	Serva
Dimethyl sulfoxide (DMSO)	Serva
Dithioerythritol (DTE)	Carl Roth
Egtazic acid (EGTA)	VWR Life Science
Ethanol	Fisher Scientific
Ethylenediaminetetraacetic acid (EDTA)	Merck/Sigma-Aldrich
Glycerol	Gerbu Biotechnik
Glycine	Carl Roth
Isopropyl β-D-1-thiogalactopyranoside (IPTG)	Carl Roth
Magnesium chloride ($MgCl_2$)	AppliChem

Methanol	Sigma-Aldrich
Milk powder	Carl Roth
Mowiol	Calbiochem
Nonidet P-40 (NP-40)	Fluka
Orange loading dye (6x)	Thermo Scientific
p-Benzoylphenylalanine (Bpa)	Bachem
Paraformaldehyde (PFA) 16 %	Alfa Aesar GmbH
Phenylmethylsulfonyl fluoride (PMSF)	Serva
Potassium chloride (KCl)	Merck
Sodium chloride (NaCl)	Carl Roth
Sodium dodecyl sulfate (SDS) pellets	Carl Roth
Tetramethylethylenediamine (TEMED)	Carl Roth
Tris	Carl Roth
Tris(2-carboxyethyl)phosphine **(**TCEP)	Biosynth AG
Triton X-100	Sigma-Aldrich
Tween-20	VWR Chemicals
WesternBright ECL Spray Detection Reagent	Advansta Inc.

2.1.7 Antibiotics

The following antibiotics were used for bacterial culture and mammalian cell culture.

Table 2–7 Antibiotics

Antibiotic	Concentration	Company
Ampicillin	100 µg/ml	Gerbu Biotechnik
Blasticidin	5 µg/mL	Invitrogen
Chloramphenicol	25 µg/ml	Sigma-Aldrich
Hygromycin	250 µg/mL	Carl Roth
Penicillin	100 U/mL	Carl Roth
Streptomycin	0.1 mg/mL	Carl Roth
Zeocin	50 µg/mL	Invitrogen

2.1.8 Mammalian cell culture reagents

Table 2–8 Mammalian cell culture reagents

Reagent	Company
BI2536	Selleck Chemicals Llc
Doxycycline	Sigma-Aldrich
Dulbecco's modified eagle medium (DMEM)	Thermo Fisher Scientific
Fetal bovine serum (FBS, Tetracycline-free)	Thermo Fisher Scientific
Lipofectamine RNAiMAX	Thermo Fisher Scientific
MG132	Merck
Opti-MEM	Thermo Fisher Scientific

Poly-L-Lysine	Sigma-Aldrich
Protease Inhibitor mix (500x)	Serva
Reversine	Cayman Chemical
RO3306	Merck
Roscovitine	Sigma-Aldrich
SNAP-Cell 647 SiR	New England Biolabs
SNAP-Cell Block	New England Biolabs
STLC	Sigma-Aldrich
Thymidine	Sigma-Aldrich
Trypan blue solution (0.4 %)	Thermo Fisher Scientific
Trypsin	Pan Biotech
X-tremeGENE 9 DNA Transfection Reagent	Merck

2.1.9 Media

All bacterial culture media used in this work were produced in-house.

Table 2–9 Media

Media	**Formulation (per litre)**
2x Yeast Extract Tryptone **(**YT)	16 g tryptone, 10 g yeast extract,5 g sodium chloride
Lysogeny Broth **(**LB)	10 g tryptone, 5 g yeast extract,10 g sodium chloride
Terrific Broth (TB)	12 g tryptone, 24 g yeast extract, 4 ml glycerol, 100 ml phosphate buffer

HeLa cells and DLD-1 cells were cultured in Dulbecco's modified eagle medium (DMEM) obtained from Thermo Fisher Scientific.

2.1.10 Kits

Table 2–10 Kits

Kit	Company
GeneJET Plasmid Miniprep Kit	Thermo Fisher Scientific
Monarch DNA gel extraction kit	New England BioLabs
NucleoBond PC 10000 Giga kit	Macherey-Nagel
PureLink PCR purification kit	Thermo Fisher Scientific

2.1.11 Enzymes

Table 2–11 Enzymes

Enzyme	Company
Benzonase nuclease	Sigma-Aldrich
DNase I	Roche
Fast Digest Restriction Enzymes	Thermo Fisher Scientific
Gibson Assembly Master Mix	New England BioLabs
Pfu Turbo Polymerase	Agilent Technologies
preScission protease	produced in-house
Q5 polymerase 2 x Master Mix	New England BioLabs
T4 Ligase	New England BioLabs
Taq DNA ligase	New England BioLabs

TEV protease	produced in-house

2.1.12 Antibodies

2.1.12.1 Primary Antibodies

Table 2–12 Primary Antibodies

Antibody	Origin	Dilution	Company
anti-CENP-A	Rabbit	1:1000	Cell Signaling
anti-CENP-C	Rabbit	1:1000 (IF) 1:2000 (WB)	produced in-house
anti-CENP-HK	Rabbit	1:500	produced in-house
anti-GFP	Rabbit	1:1000	produced in-house
anti-M18BP1	Rabbit	1:600 (IF) 1:1000(WB)	Bethyl Laboratories
anti-M18BP1 pT702	Rabbit	1:400 (IF) 1:1000(WB)	EMD Millipore
anti-mCherry	Mouse	1:2000	Novus Biologicals
anti-PLK1	Mouse	1:300 (IF) 1:1000(WB)	Abcam
anti-Tubulin	Mouse	1:10,000	Sigma Aldrich Corp.
anti-Vinculin	Mouse	1:15,000	Sigma Aldrich Corp.
CREST sera	Human	1:200	Antibodies Inc.

2.1.12.2 Secondary Antibodies

Table 2–13 Secondary Antibodies

Against	Coupled	Origin	Dilution	Company
Human	Alexa Fluor 488	Goat	1:200	Jackson ImmunoResearch
Human	Alexa Fluor 647	Goat	1:200	Jackson ImmunoResearch
Human	DyeLight 405	Donkey	1:200	Jackson ImmunoResearch
Human	Rhodamine Red	Goat	1:200	Jackson ImmunoResearch
Mouse	Alexa Fluor 647	Donkey	1:200	Invitrogen
Mouse	Alexa Fluor 488	Goat	1:200	Invitrogen
Mouse	Rhodamine Red	Goat	1:200	Jackson ImmunoResearch
Mouse	HRP	Sheep	1:10,000	GE Healthcare
Rabbit	Alexa Fluor 488	Donkey	1:200	Invitrogen
Rabbit	Alexa Fluor 647	Donkey	1:200	Invitrogen
Rabbit	Rhodamine Red	Goat	1:200	Jackson ImmunoResearch
Rabbit	HRP	Donkey	1:10,000	GE Healthcare

2.1.13 2.1.13 Software

Table 2–14 Software

Software	Version	Company
Adobe Illustrator CS5.1	15.1.0	Adobe Inc.
Adobe Photoshop CS5	12.1	Adobe Inc.
Excel	16.30	Microsoft Corp.

FIJI	2.0.0-rc-69	National Institutes of Health
GraphPad Prism	7.0	GraphPad Software Inc.
ImageLab	5.1	Bio-Rad Laboratories GmbH
SEDFIT	14.4d	National Institutes of Health, USA
SEDNTERP	1.10	National Institutes of Health, USA
softWoRx	7.0	GE Healthcare
Word	16.30	Microsoft Corp.

2.1.14 Oligonucleotides

The following oligonucleotides have been used for PCR and were produced by Sigma-Aldrich or Eurofins MWG Synthesis GmbH.

Table 2–15 Oligonucleotides

Name	**Sequence (5' to 3')**
CENPC_742RA_751WA	ACCCCGAACGTGCGTCGCACGAAAGCGACCCGCCTGAAACCGCTGGAATATGCGCGTGGCGAACGCATTGATTACCG
CENPC_773_NheI_F	GATCGCTAGCTCCCCGGACACCATCTC
CENPC_BamHI_F	CATGGGATCCATGGCTGCTAGTGGTCTGG
CENPC_d426-537	AAACAGAAACAACGTCGCAAATTTAGCCCGGTCTATTCTAATAGCTCT
CENPC_d736-758	CTGGTCCTGCCGAGCAATACCCCGCAGGGTCGTCCGAGCGGCGGTTTT
CENPC_G601_BamF	CATGGGATCCGGCGGTATTGTCGGTCATG

CENPC_G760_BamHI_F	ACTCGGATCCGGTCGTCCGAGCGG
CENPC_HindIII_F	CATGAAGCTTATGGCTGCTAGTGGTCTGG
CENPC_K721_Nhe1F	CATGGCTAGCGGTAGTAAAAACCGCATCCATCACAAAC
CENPC_L772_XhoI_TAAR	CATCCTCGAGTTACAGAACGCCACTAATCAC
CENPC_Nhe1_F	CATGGCTAGCATGGCTGCTAGTGGTCTGG
CENPC_NheI_R TAA	CATGGCTAGCTTAGCGTTTGATTTGGGTGAAC
CENPC_R522A_W531A	ACCAGCACGGTCACCAAATCCCGTGCCATTTCACGTCGCCCGTCGGATTGGGCGGTCGTGAAATCGGAAGAAAGCCCG
CENPC_S600_KpnI_R	CATGGGTACCTGAGCCTTCAGCGTTCAG
CENPC_S600_XhoR	CATGCTCGAGTGAGCCTTCAGCGTTCAG
CENPC_XhoXma_R	CATGCCCGGGCTCGAGGCGTTTGATTTGGGTGAAC
CENPC_Y541_TAG	GAAGAAAGCCCGGTCTAGTCTAATAGCTCTGTGC
CENPC_Y758TAGqF	GTGGCGAACGCATTGATTAGCAGGGTCGTCCGAGCGGCGG
CENPT_KpnIL_F	GTACCATGGCTGACCACAACC
CENPT_KpnIS_F	CATGGCTGACCACAACC
CENPT_TAA_XhoI_R	ACTGCTCGAGTTATTACTGCGCCGGGAAC
CENPW_BamHI_F	CATGGGATCCGGAATGGCGCTGTCGACCATAG

CENPW_NotI_TAA_R	ACTGGCGGCCGCTTATTAACCACGGCTTTTCTTCAG
DmCupin_BamHI_F	ACTGGGATCCAATGAACTGATTTTTTGTCAGGTTGATGGC
DmCupin_NotI_XhoI_TAA_R	ACTGCTCGAGGCGGCCGCTTAGCTGCGAATACACATCAGC
EGmCh_Sal1F	CATGGTCGACATGGTGAGCAAGGGCGAG
EGmCh_XhoXma_R	CATGCCCGGGTTATTACTCGAGCTTGTACAGCTCGTCCATGC
GST_NheI_F	CTAGGCTAGCATGTCCCCTATACTAGGTGATTGG
GST_XmaI_TAA_R	ACTGCCCGGGTTATTTTGGAGGATGGTCGCC
HumCupin_BamHI_NheI_F	ACTGGGATCCGCTAGCAAACATGGCGAACTGAAAGTC
HumCupin_XhoI_R_TAA	CATGCTCGAGTTAGCGTTTGATTTGGGTGAAC
LacI_338_XmaI_TAAR	ACTGCCCGGGTTAAGAGGCGGTTTGCGTATTGG
LacI_57_NheI_F	ATGCGCTAGCGCGGGCAAACAGTCGTTG
Mif2Cupin_BamHI_F	CATGGGATCCGAGAATTTTGCCCTTGAGATAATGTTCG
Mif2Cupin_NotI_XhoI_TAA_R	ACTGCTCGAGGCGGCCGCTTAAACGGTCACTTGAACGAAG
SpyCatcher_Bam_F	CATGGGATCCTTTAGTTGCTTTGCCATTTACAG

SpyCatcher_SalI1R	CATGGTCGACTTATTAAATATGAGCGTCACCTTTAGTTGC
SpyTag_Bgl2BamF	CATGAGATCTGCCCACATCGTGATGGTGGACGCCTACAAGCCGACGAAGGGATCCGGCGGTGGCGACGAC

2.1.15 Cell lines

Table 2–16 Cell lines

Cell line name	Transfected plasmid	Origin
Flp-In T-REx HeLa	-	human
Flp-In T-REx DLD-1 CENP-C-AID-EYFP	-	human
Flp-In T-TREx HeLa CENP-A-SNAP	-	human
Flp-In T-TREx HeLa CENP-A-SNAP	pcDNA5-EGFPN-M18BP1-PT-mCherry-Mis18α	human
Flp-In T-TREx HeLa CENP-A-SNAP	pcDNA5-GST-EGFPN-M18BP1-PT-mCherry-Mis18α	human
Flp-In T-REx HeLa CENP-A-SNAP	pcDNA5-EGFPN-M18BP1(S93A)-PT-mCherry-Mis18α	human
Flp-In T-REx HeLa	pcDNA5-CENP-C1-600-EGFP-CENP-C601-772-Mif2_321-529	human
Flp-In T-REx HeLa	pcDNA5-CENP-C1-600-EGFP-CENP-C601-772-DmCENP-C1127-1410	human

Flp-In T-REx HeLa	pcDNA5-CENP-C 1-600-EGFP-CENP-C 601-772-LacI-DimDomain	human
Flp-In T-REx HeLa	pdDNA5-CENP-C1-600-EGFP-601-772	human
Flp-In T-REx HeLa	pdDNA5-CENP-C1-600-EGFP-601-943	human
Flp-In T-REx HeLa	pcDNA5-EGFP-CENP-C721-943	human
Flp-In T-REx HeLa	pcDNA5-EGFP-CENP-C760-943	human

2.2 Methods

2.2.1 Molecular biological methods

2.2.1.1 Agarose gel electrophoresis

Agarose gel electrophoresis was used to separate DNA molecules by size. Usually, agarose concentrations between 0.9 % and 1 % were used. The agarose was dissolved in Tris-acetate-Ethylenediaminetetraacetic acid (EDTA) buffer. To detect the separated DNA by UV-light, Midori green advance was added in a 1:25,000 dilution to the liquid agarose. The electrophoresis was usually performed at 140 V for 20-30 min. To estimate the size of the separated DNA bands, the molecular-weight size marker GeneRuler 1 kb Plus DNA ladder (Thermo Fisher Scientific) was used.

2.2.1.2 Polymerase chain reaction

The polymerase chain reaction (PCR) is a commonly used method to amplify specific DNA sequences (Mullis et al., 1986). In this work, the Q5 high-fidelity polymerase (New England BioLabs) was used to amplify the DNA fragments which were subsequently digested by restriction enzymes and ligated with a plasmid backbone using T4 ligase. PCR reactions were prepared on ice and set up according to the manufacturer's protocol. Afterwards, the PCR products were purified using the PureLink PCR purification kit (Invitrogen) to remove the polymerase, the PCR primers and the buffer. The kit was used according to the manufacturer's protocol.

2.2.1.3 Restriction digestion

Restriction digestions were performed using FastDigest restriction enzymes (Thermo Fisher Scientific). The purified PCR products or 1 µg of plasmid DNA were digested using 0.5 µl of each restriction enzyme in a total volume of 30 µl for 2-4 hours at 37 °C. After the restriction digestion, the digested DNA fragments were separated on a 1 % agarose gel and subsequently purified using the Monarch DNA gel extraction kit (New England BioLabs) following the protocol provided by the manufacturer.

2.2.1.4 DNA ligation

To ligate the restriction digested plasmid DNA with the insert DNA, 10-20 ng of plasmid backbone and a threefold molar excess of insert DNA were mixed with 1 µl of 5 x Rapid Ligation buffer (Thermo Fisher Scientific) and 1 U T4 DNA ligase (New England BioLabs) in a total volume of 5 µl. The reaction mixture was incubated for 15 min at 22 °C.

2.2.1.5 Transformation of ligation reactions into competent bacterial cells

Chemically competent *Escherichia coli* (*E. coli*) OmniMax cells (Invitrogen) were used for the transformation of ligation reactions. The cells were thawed on ice, subsequently the ligation mixture was added to the cell suspension and mixed gently. The cells were incubated on ice for 30 min and additional 45 s at 42 °C. Afterwards, 50 µl cell suspension was plated on a Lysogeny Broth (LB)-agar plate containing 100 µg/mL ampicillin and incubated at 37 °C for 16 h.

2.2.1.6 Isolation of plasmid DNA from bacterial cells

Single colonies were picked from the LB-agar plate and transferred into 4 mL LB medium containing 100 µg/mL ampicillin. The inoculated culture was incubated for 16 h at 37 °C and 130 rpm. Subsequently, the bacterial culture was centrifuged at 18,000 g for 1 min and the cell pellet was either frozen at -20 °C or directly processed to isolate the plasmid DNA using the GeneJET Plasmid-Miniprep kit (Thermo Fisher Scientific) following the manufacturer's protocol. The purified plasmids were checked by analytical restriction digestion and the nucleotide sequence was confirmed by Sanger sequencing (Microsynth Seqlab GmbH).

2.2.1.7 Site-directed mutagenesis

Site-directed mutagenesis was used in this work to create point mutants, deletion mutants and to replace a specific codon by the amber stop codon TAG. First, a primer containing the desired mutations was annealed to the template DNA and extended using the *PfuTurbo* DNA polymerase (Agilent Technologies). This DNA polymerase does not displace the primer from the templates resulting in ds-DNA molecules, in

which the newly synthesized strand carries the desired mutations. The resulting nicks in the synthesized strand were ligated by the Taq ligase enzyme (New England Biolabs). After the polymerase chain reaction, the products were treated with the endonuclease DpnI, that will only digest the methylated template DNA, but not the synthesized DNA strand. The resulting ss-DNA molecules were finally transformed into competent OmniMax cells.

2.2.1.8 Gibson Assembly

As an alternative approach to the restriction enzyme-based cloning, some constructs were created using the Gibson assembly reaction (Gibson et al., 2009). In this approach, the DNA fragments to be joined contain a 25 base pair overlap, that was added by polymerase chain reaction to both ends of the insert DNA fragment. The Gibson assembly uses three different enzymes to join the DNA fragments. A DNA exonuclease cuts the DNA from the 5' end leading to single stranded 3' ends that can anneal to each other. Subsequently a DNA polymerase will fill the gaps and a DNA ligase will seal the resulting nicks. 10-20 ng of linearized plasmid backbone was mixed with a threefold molar excess of insert DNA. The mixture was added to the Gibson Assembly Master Mix (New England BioLabs) and incubated in a thermocycler for 1 h at 50 °C. The reaction mixture was transformed into competent OmniMax cells.

2.2.1.9 Purification of Cen1-like DNA fragments for nucleosome reconstitution

Eight tandem repeats of DNA fragment 1 harbouring a 189 bp Cen1-like sequence without CENP-B box or of DNA fragment 2 harbouring a 205 bp Cen1-like sequence with CENP-B box were cloned into a pUC18 plasmid using restriction enzyme-based cloning and Gibson assembly. Each copy of DNA fragment 1 is flanked by non-palindromic *BstX*I and *Bgl*I restriction sites, and each copy of DNA fragment 2 is flanked by non-palindromic *Bgl*I and *Dra*III restriction sites. The pUC18 plasmids were transformed into competent *E. coli* cells. Inoculated bacteria cultures were incubated overnight at 37°C in TB media supplemented with 100 µg/mL. Subsequently the plasmid DNA was purified using a Giga Purification Kit (Macherey-Nagel). After *EcoR*V digestion the insert DNA was separated from the backbone DNA by PEG precipitation. The isolated DNA fragments were digested with *BstX*I/*Bgl*I (DNA1) and *Bgl*I/*Dra*III

(DNA2). The digested DNA fragments were loaded on a HiTrap Q FF anion exchange column (GE Healthcare) and eluted with a linear gradient from 0-2000 mM NaCl in 20 bed volumes. Fractions containing the DNA fragments were precipitated with ethanol and dissolved in 2 M NaCl.

2.2.2 Biochemical methods

2.2.2.1 Analytical ultracentrifugation

Sedimentation velocity analytical ultracentrifugation (AUC) was performed at 42,000 rpm at 20 °C in a Beckman XL-A ultracentrifuge. The protein samples were incubated on ice for 1 h and loaded into standard double-sector centerpieces. The cells were scanned every minute at 260 nm wavelength. The software SEDFIT was used for data analysis and the continuous *c*(s) distribution model was applied. The software SEDNTERP was used for calculating the partial specific volumes (vbar) of the proteins, buffer density and buffer viscosity. Figures were generated using the software GUSSI.

2.2.2.2 Analytical size-exclusion chromatography

The analytical size-exclusion chromatography (SEC) is a method used to detect complex formation of proteins. The difference in elution time of the analytes solely depends on their different size, because the analytes do not interact with the polymer beads that are packed in a column. Smaller proteins can enter into pores between the polymer beads whereas larger proteins cannot enter into as many pores, leading to a faster elution of bigger proteins or protein complexes. In this work, a Superose 6 Increase 5/150 GL chromatography column (GE Healthcare) was used for all analytical size exclusion chromatography experiments. The column was installed in a ÄKTA micro chromatography system. The proteins were mixed and incubated on ice for 1 h in SEC buffer (10 mM HEPES pH 7.5, 300 mM sodium chloride (NaCl), 2.5 % glycerol, 1 mM Tris(2-carboxyethyl)phosphine (TCEP)) at 5-10 µM concentration in a total volume of 50 µl and centrifuged for 20 min at 18,000 g and 4 °C before injection. The flowrate was set to 0.2 mL/min and the eluted fractions were analyzed by SDS-PAGE and CBB staining.

2.2.2.3 Amylose-resin pull-down assay

The amylose-resin pull-down assay was performed to check the binding of nucleosomes and kinetochore components to MBP-tagged WT CENP-C or CENP-C mutants. The proteins were diluted with binding buffer A to 3 µM concentration in a total volume of 50 µl and mixed with 20 µl amylose beads (New England BioLabs). After mixing the proteins and the beads, 20 µl were taken as input. The rest of the solution was incubated at 4 °C for 1 h on a thermomixer (Eppendorf) set to 1000 rpm. To separate the proteins bound to the amylose beads from the unbound proteins, the samples were centrifuged at 800 g for 2 min at 4 °C. The supernatant was removed, and the beads were washed four times with 500 µl binding buffer A. After the last washing step, 20 µl 2 x SDS-PAGE sample loading buffer was added to the dry beads. The samples were boiled for 5 min at 95 °C and analyzed by SDS-PAGE and CBB staining.

2.2.2.4 Electromobility shift assays (EMSA)

EMSAs were performed using either Alexa-647-labelled $H3^{NCP}$ or Alexa-555-labelled CENP-A^{NCP} each at 10 nM concentration. CENP-C^{F} was added at the indicated concentrations in a buffer containing 10 mM HEPES, 100 mM NaCl, 1 mM TCEP, 2.5 % glycerol and 0.01 % Tween-20 in a total volume of 10 µL. Native PAGE was performed using 6 % polyacrylamide gels and 1× Tris borate (TB) running buffer. The gels were run at 10 mA constant current for 1 h at 4 °C. Gels were scanned for fluorescence using a ChemiDoc MP Gel Imaging System (Bio-Rad). Quantification was performed using FIJI, and the data were plotted and analyzed using Prism (Graphpad, La Jolla, California, USA). Binding curves were fit with a quadratic binding equation.

2.2.2.5 UV-cross-linking

The full-length CENP-C variants MBP-CENP-$C^{Y541Bpa}$ and MBP-CENP-$C^{Y758Bpa}$ were diluted in SEC buffer and incubated on ice with dinucleosomes in a total volume of 50 µl. LED ultraviolet (UV) light of 365 nm wavelength (Nichia, NCSU276A) was used to irradiate the protein samples for 15 min to induce the cross-linking reaction. Subsequently, 50 µl of 2 x SDS-PAGE sample loading buffer was added to the samples. SDS-PAGE was performed using 4-12 % gradient polyacrylamide gels

(SERVA Electrophoresis GmbH). Immunoblots against the histone variant CENP-A were performed to analyze the cross-linking between the CENP-C Bpa mutants and CENP-A.

2.2.2.6 Expression of MBP-CENP-C protein

pETDuet plasmids containing the CDS of 6His-TEV-MBP-CENP-C1-600-SpyCatcher, 6His-TEV-mCherry-CENP-C1-600-SpyCatcher and MBP-TEV-SpyTag-CENP-C601-943-8His were transformed into *E. coli* cells of BL21-CodonPlus (DE3)-RIL strain (Agilent Technologies, #230240). The bacterial culture was grown in Terrific Broth (TB) media supplemented with 100 µg/mL ampicillin and 25 µg/mL chloramphenicol at 37 °C and 130 rpm. Isopropyl-β-D-thiogalactopyranoside (IPTG) at 0.2 mM concentration was added after OD_{600} reached 0.6 and the culture was incubated at 20 °C for further 16 h. Subsequently, the culture was centrifuged for 20 min at 5000 g and the pellets were washed with phosphate-buffered saline (PBS) once. The dry pellets were stored at -20 °C.

2.2.2.7 Expression of CENP-T/-W/-S/-X protein

E. coli BL21(DE3) codon cells co-transformed with pETDuet-His-TEV-CENP-W-RBS-Halo-TEV-CENP-T and pSKB2LNB-CENP-X-RBS-CENP-S were grown in TB supplemented with Ampicillin (100µg/ml), Kanamycin (25µg/ml) and Chloramphenicol (37µg/ml) at 37°C. When OD_{600} reached 0.8, temperature was reduced to 20°C until OD_{600} reached 1.0. Subsequently, 0.2 mM IPTG was added and the culture was incubated at 20°C for further 16 hours.

2.2.2.8 Expression of Halo-CENP-T/MBP-W protein

pETDuet plasmids containing the coding sequences (CDS) of His-P-MBP-CENP-W-Halo-TEV-CENP-T or His-TEV-CENP-W-Halo-TEV-CENP-T were transformed into *E. coli* cells of BL21-CodonPlus (DE3)-RIL strain (Agilent Technologies, #230240). The proteins were expressed under the same conditions as CENP-C.

2.2.2.9 Expression of Bpa-incorporated MBP-CENP-C mutants

The Bpa-incorporated MBP-CENP-C variants were expressed in *E. coli* cells of BL21(DE3) strain (Agilent Technologies, catalog # 200131). pETDuet plasmids containing the CDS of MBP-CENP-C1-600-SpyCatcher-8His or MBP-TEV-SpyTag-CENP-C601-943-8His with the amber codon incorporated at the specific positions were used for transformation of *E. coli* cells together with the pEVOL-pBpF plasmid. The cells were cultured in 2 × Yeast Extract Tryptone (YT) media supplemented with 100 µg/mL ampicillin, 25 µg/mL chloramphenicol and 0.2% arabinose at 37 °C until OD_{600} reached 0.6. Protein expression was induced by the addition of 0.2 mM IPTG, additionally the unnatural amino-acid Bpa (Bachem) was added at 1 mM concentration to the bacterial culture. Subsequently, the temperature was reduced to 25 °C. After 16 h the culture was centrifuged for 20 min at 5000 g. The pellets were washed once with PBS, centrifuged again and frozen at -20 °C.

2.2.2.10 Tricine-sodium dodecyl sulfate polyacrylamide gel electrophoresis

Sodium dodecyl sulfate polyacrylamide gel elctrophoresis (SDS-PAGE) was performed using a TRIS-Tricine buffer system (Schagger and von Jagow, 1987). The SDS-PAGE separates proteins by their molecular masses in an electric field. SDS denatures the proteins and covers the proteins with a negative charge leading to similar charge-to-mass ratios. Once the proteins are loaded onto the polyacrylamide gel, a voltage is applied causing the negatively charged proteins to migrate through the gel towards the anode. Smaller proteins pass the gel faster than larger proteins which results in a separation of proteins by their molecular weight. In this work, Tricine polyacrylamide gels with an acrylamide concentration between 8-14 % were used depending on the average size of the proteins to be separated. Before running the SDS-PAGE, protein samples were mixed with SDS-PAGE sample loading buffer and boiled at 95 °C for 5 min. To estimate the molecular weight of the separated proteins, the Precision Plus Protein Unstained marker (Bio-Rad) was loaded on the gel. In case the polyacrylamide gel was used for a Western Blot, the Precision Plus Protein Dual Color (Bio-Rad) marker was used.

2.2.2.11 Coumassie Brilliant Blue staining

To visualize the protein bands after SDS-PAGE, the polyacrylamide gels were stained with Coumassie Brilliant Blue (CBB). First, the protein bands were fixed by incubating the polyacrylamide gel in a fixation solution containing 50 % Ethanol and 10 % acetic acid for 15 min under mild shaking. Subsequently, the polyacrylamide gel was incubated for 5 min with a staining solution (fixation solution + 0.1 % Coumassie Brilliant Blue R-250 + 0.1 % Coumassie Brilliant Blue G-250) and destained for 16 h in distilled water under mild shaking.

2.2.2.12 Immunoblotting

After Tricine-SDS-PAGE, the proteins were transferred onto a nitrocellulose membrane or polyvinylidene fluoride (PVDF) membrane (GE Healthcare) using a wet tank chamber system (Bio-Rad). The transfer was performed at 100 V for 100 min on ice. To check the transfer efficiency, the membrane was stained with Ponceau S (Bio-Rad). The Ponceau S solution was washed away by rinsing the membrane with tris-buffered saline (TBS) supplemented with 0.1 % Tween-20 (TBST) on a shaker. Subsequently, the membrane was blocked with TBST containing 5 % milk powder (Roth) for 60 min at room temperature. The primary antibodies were diluted in TBST containing 5 % milk powder as indicated in section 2.1.12.1. The membrane was incubated with the primary antibody solution overnight at 4 °C on a shaker. Subsequently, the membrane was washed three times with TBST for 5 min. Then, the membrane was incubated for 1 h at room temperature with the appropriate secondary horseradish peroxidase conjugated antibody diluted in TBST containing 5 % milk powder. The membrane was washed again three times with TBST for 5 min each and was finally incubated with the ECL Prime Western Blotting detection reagent (GE Healthcare) according to the manufacturer's instructions. Images were acquired using the ChemiDocTM MP System (Bio-Rad) using ImageLab 5.1 software.

2.2.2.13 *In vitro* protein phosphorylation

In some *in vitro* binding experiments, proteins were phosphorylated by the mitotic kinase CDK1:Cyclin B:CAK1 (CCC), which were purified in-house. Proteins were diluted to 3 µM in SEC buffer (+ 1 mM adenosine triphosphate (ATP) and 10 mM

calcium chloride ($CaCl_2$)) and kinases were added at a final concentration of 100 nM. The reaction mixture was incubated either 120 min at 30 °C or 16 h at 4 °C.

2.2.2.14 MBP-CENP-C protein purification

The bacterial cell pellets were resuspended in lysis buffer A and subsequently lysed by sonication. The crude lysate was cleared by centrifugation at 75.000 g for 30 min at 4 °C. The supernatant was passed through a 0.45 µm filter (Sarstedt) and incubated with cOmplete His-Tag purification resin (Roche) for 16 hours on a tube roller (Starlab) at 4 °C. After incubation, the resin was washed with 200 ml lysis buffer A supplemented with 10 mM imidazole. The bound protein was finally eluted in 15 ml lysis buffer supplemented with 400 mM imidazole. The samples were concentrated using centrifugal filters with a 30 kDa mass cut-off (Merck) and were subsequently applied to a Superose 6 10/300 size-exclusion column (GE healthcare) equilibrated in SEC buffer A. SEC was performed under isocratic conditions at a constant flow rate of 0.5 ml/min. 500 µl fractions were collected and relevant fractions were analyzed by SDS-PAGE, pooled, concentrated, flash-frozen and stored at -80 °C until used for further experiments.

2.2.2.15 SpyTag reaction for *in-vitro* reconstitution of full-length CENP-C protein

To reconstitute full-length CENP-C, the SpyTag reaction was used (Zakeri et al., 2012). MBP-TEV-SpyTag-CENP-C601-943-8His was incubated with Tobacco Etch Virus (TEV) protease for 8 h at 4 °C to cleave off the N-Terminal MBP tag. Subsequently, 6His-TEV-MBP-CENP-C1-600-SpyCatcher was added in 3-fold molar excess. After incubation at 4 °C for 16 h, the reconstituted MBP-CENP-C1-600-Spy-CENP-C601-943-8His protein was separated from unligated protein fragments on a Superose 6 10/300 size-exclusion column (GE Healthcare). Relevant fractions were pooled and concentrated using 50 kDa cut-off Amicon filters. The concentrated protein was flash frozen and stored at -80 °C.

2.2.2.16 MBP-CENP-W/Halo-CENP-T purification

The bacterial pellets were resuspended in lysis buffer (50 mM Tris pH 8.0, 1 M NaCl, 10 % glycerol, 1 mM TCEP) supplemented with 1 mM PMSF, lysed by sonication and cleared by centrifugation at 75,000 g at 4°C for 1 hour. The cleared lysate was applied to Complete nickel beads (Roche), pre-equilibrated in lysis buffer and incubated at 4°C for 6 h on a tube roller. The nickel beads were washed with lysis buffer supplemented with 10 mM of imidazole and Halo-CENP-T/His-MBP-CENP-W was eluted in lysis buffer supplemented with 400 mM imidazole. The samples were concentrated using centrifugal filters with a 30 kDa mass cut-off (Merck) and were subsequently applied to a Superdex 200 10/300 size-exclusion column (GE healthcare) equilibrated in SEC buffer (20 mM Tris pH 8.0, 300 mM NaCl, 5 % glycerol, 1 mM TCEP). SEC was performed under isocratic conditions at a constant flow rate of 0.5 ml/min. 500 µl fractions were collected and relevant fractions were analyzed by SDS-PAGE, pooled, concentrated, flash-frozen and stored at -80 °C until used for further experiments.

2.2.2.17 CENP-TWSX purification

The bacterial pellets were resuspended in lysis buffer (50 mM Tris pH 8.0, 1 M NaCl, 10 % glycerol, 1 mM EDTA, 5 mM 2-Mercaptoethanol,1 mM PMSF and 1 mM TCEP), lysed by sonication and cleared by centrifugation at 75,000 g at 4°C for 1 hour. The cleared lysate was applied to Complete nickel beads (Roche), pre-equilibrated in lysis buffer and incubated at 4°C for 6 h on a tube roller. The nickel beads were washed with lysis buffer supplemented with 10 mM of imidazole and an excess of CENP-XS was added to the beads. After 16 h incubation on a tube roller at 4°C, the beads were washed with lysis buffer supplemented with 10 mM imidazole. Subsequently, the CENP-TWSX complex was eluted in lysis buffer supplemented with 400 mM imidazole. His-TEV protease was added and the CENP-TWSX complex was dialysed three times against 2 L of lysis buffer containing 300 mM NaCl. After dialysis, the protein complex was loaded on a Hi Trap SP FF column, washed with 10 CV of 15 % Buffer B (50 mM Tris pH 7.4, 2M NaCl, 5 % glycerol, 1 mM EDTA, 5 mM 2-Mercaptoethanol, 1 mM TCEP) and eluted using a gradient of 300 - 2000 mM NaCl. The fractions containing CENP-TWSX were pooled, concentrated and loaded onto a Superdex 200 10/300 SEC column (GE Healthcare) pre-equilibrated in SEC buffer (50 mM Tris pH 8.0,

500 mM NaCl, 5 % glycerol, 1 mM TCEP). Fractions containing CENP-TWXS were pooled, concentrated, flash-frozen in liquid nitrogen and stored at -80°C.

2.2.2.18 CENP-HIKM purification

Recombinant CENP-HIKM protein complex was purified in-house as described previously (Weir et al., 2016).

2.2.2.19 CENP-LN purification

Recombinant CENP-LN protein complex was purified in-house as described previously (Pentakota et al., 2017; Weir et al., 2016).

2.2.2.20 CENP-OPQUR purification

Recombinant CENP-OPQUR protein complex was purified in-house as described previously (Pesenti et al., 2018).

2.2.2.21 MIS12(∆10) complex purification

Recombinant MIS12(∆10) protein complex was purified in-house as described previously (Petrovic et al., 2016).

2.2.2.22 NDC80 complex purification

Recombinant NDC80 protein complex was purified in-house as described previously. (Pesenti et al., 2018; Weir et al., 2016).

2.2.2.23 Nucleosome Reconstitution

CENP-A and H3 containing nucleosome core particles (NPCs) were purified in-house as described previously (Weir et al., 2016).

2.2.2.24 Reconstitution and purification of dinucleosome particles

NCPs were reconstituted using Cen-like DNA fragments. 1 µM of NCPs reconstituted on DNA fragment 1 and DNA fragment 2 were ligated to each other for 16 h at 4 °C using 8xHis-tagged T4 DNA ligase. The ligated NCPs were incubated with nickel beads (Roche) for 7 h at 4°C to remove the T4 DNA ligase. The ligated dinucleosomes were concentrated, and glycerol was added at a final concentration of 2 % (v/v). The mixture was loaded on a cylindrical gel containing 5 % reduced Bis-acrylamide. Native PAGE was carried out on a Mini Prep Cell apparatus (Bio-Rad) at 1 W constant power. Dinucleosomes were eluted at a constant flow rate of 0.1 mL/min overnight at 4°C into nucleosome buffer (50 mM NaCl, 10 mM triethanolamine, 1 mM EDTA) and collected in 250 µL fractions on 96-well-plates. The OD_{260} and OD_{280} of the individual fractions were measured using a CLARIOstar Plus plater reader (BMG Labtech). Fractions containing dinucleosomes were pooled, concentrated and stored at 4 °C.

2.2.2.25 Plasmids for bacterial expression

2.2.2.25.1 CENP-C

The codon optimized sequence of human CENP-C was purchased from GeneArt and subcloned into a pETDuet plasmid using restriction-enzyme-based cloning. The plasmid pETDuet-6His-TEV-MBP-CENP-C1-600-SpyCatcher was generated by inserting the PCR-amplified CDS of CENP-C1-600 using *Nhe*I and *Xho*I restriction sites. The plasmid pETDuet-His-TEV-mCherry-CENP-C1-600-SpyCatcher was generated by exchanging the CDS of maltose-binding protein (MBP) against the CDS of mCherry using the restriction sites *Bam*HI and *Nhe*I. The plasmid pETDuet-MBP-TEV-SpyTag-CENP-C601-943-8His was generated by inserting the CDS of CENP-C601-943 using the restriction sites *Bam*HI and *Xho*I. Point mutations and deletions were introduced by PCR-based site-directed mutagenesis.

2.2.2.25.2 Halo-CENP-T/-MPB-CENP-W

The codon optimized sequences of CENP-T and CENP-W were purchased from GeneArt and subcloned into a pETDuet plasmid using restriction-enzyme-based cloning and Gibson assembly. The plasmid pETDuet-His-P-MBP-TEV-CENP-W-Halo-TEV-CENP-T was generated by inserting the PCR-amplified CDS of CENP-W and

CENP-T using the restriction sites *Bam*HI/*Not*I and *Kpn*I/*Xho*I. The plasmid pETDuet-His-TEV-CENP-W-Halo-TEV-CENP-T was generated using Gibson Assembly.

2.2.2.25.3 CENP-SX

The cDNA segment encoding human CENP-X isoform1, was subcloned using Xba1/Sal1 into the first cassette of pSKB2LNB, a modified pET28 plasmid. The cDNA encoding human CENP-S was subcloned into the second cassette using Sal1/Not1.

2.2.2.25.4 tRNA synthetase/tRNA pair for incorporation of the photo crosslinker p-benzoyl-L-phenylalanine

The plasmid pEVOL-pBpF was created by the Schultz lab (Chin et al., 2002) and was ordered from Addgene (Catalog # 31190). This plasmid contains an orthogonal tRNA synthetase/tRNA pair for the *in vivo* incorporation of the photo crosslinker p-benzoyl-L-phenylalanine (Bpa) into proteins in *E. coli* in response to the TAG amber codon.

2.2.3 Cell biological methods

2.2.3.1 Cell culture

Human cancer cells were cultured in Dulbecco's Modified Eagle Medium (DMEM, PAN Biotech) supplemented with 10 % tetracycline-free fetal bovine serum (FBS, Thermo Fisher), 2 mM Pen/Strep (PAN Biotech) and 2 mM L-Glutamine (PAN Biotech) at 37 °C in a 5 % CO_2 humidified atmosphere. Cells were grown in cell culture dishes (Sarstedt) and were passaged when cell confluency reached 90 %. All experiments and cell treatments were performed under sterile conditions in laminar flow cabinets (NuAire).

2.2.3.2 Freezing and thawing of cells

Cells were frozen at a density of 2 x 10^6 cells/ml in tetracycline-free FBS supplemented with 10% DMSO as cryoprotective agent. The cryotubes (Greiner AG) were placed in isopropanol containing freezing containers (VWR International) and stored for at -80 °C for at least 24 h to gradually lower the temperature to -80 °C. For long-term storage, cells were transferred to a -150 °C freezer. Frozen aliquots were thawed rapidly in a water bath at 37 °C. The cell suspension was added to 5 ml warm DMEM

and centrifuged for 5 min at 500 g to remove remaining DMSO. The cell pellet was resuspended in DMEM and cells were seeded in a cell culture dish.

2.2.3.3 Human cell lines

Parental Flp-In T-REx HeLa cells were a gift from S. Taylor (University of Manchester, Manchester, England, UK). Flp-In T-REx DLD-1 CENP-C-AID-EYFP cells were a gift from D. Fachinetti (Institut Curie, Paris, France). These cells have both alleles of CENP-C tagged at the C-Terminus with an Auxin-inducible degron (AID)-EYFP fusion. Furthermore, a gene encoding the plant E3 ubiquitin ligase osTIR1 was stably integrated into the genome of the cells. (Hoffmann et al., 2016). The cell line Flp-In T-REx HeLa CENP-A-SNAP was generated in-house as previously described (Pan et al., 2017).

2.2.3.4 RNA interference

Gene expression of endogenous CENP-C was inhibited using small interfering RNA (siRNA) at 30 nM with the target sequence 5′-GGAUCAUCUCAGAAUAGAA-3′, which binds to the coding region of CENP-C mRNA. The expression of codon-optimized CENP-C rescue constructs was not affected by the siRNA treatment. Gene expression of endogenous M18BP1 was inhibited using siRNA at 30 nM with the target sequence 5’-GAAG UCUGGUGUUAGGAAA-3'. Lipofectamine RNAiMax (ThermoFisher) was used for siRNA transfection. While seeding the cells at a density of 1.3 x 10^5 cells/mL, 3 µl/ml RNAiMax transfection reagent and 30 nM CENP-C siRNA was added. To induce the expression of GFP-tagged CENP-C or M18BP1 rescue constructs, 50 ng/ml Doxycycline (Sigma) was added to the cells at the time of siRNA transfection. Phenotypes were analyzed 60 hours after transfection by immunofluorescence (IF) microscopy or immunoblotting analysis.

2.2.3.5 Fixation of cells

Cells grown on a coverslip were fixated for 10 min at room temperature using a freshly prepared 4 % paraformaldehyde (PFA) solution in PBS. After removing the PFA

solution, the fixated cells were washed three times with PBS. The fixated cells were stored at 4 °C for up to 1 month.

2.2.3.6 Expression plasmids for mammalian cells

All plasmids used in this work were derived from the pcDNA5/FRT/TO plasmid (Thermo Fisher). The CDS of enhanced green fluorescent protein (EGFP) was inserted using the restriction sites *Kpn*I and *Bam*HI. The CDS of CENP-C 1-600 was inserted using the restriction sites *Hind*III and *Kpn*I, the CDS of CENP-C 601-943 was inserted using the restriction sites *Bam*HI and *Nhe*I. Point mutants and deletion mutants were created using PCR-based site-specific mutagenesis. The plasmid pcDNA5-GST-EGFP-M18BP1-P2AT2A-mCherry-Mis18a contains a tandem of two 2A peptide sequences both causing ribosome skipping and thereby allowing the co-expression of two proteins from one transcript. The plasmid was cloned as previously described (Pan et al., 2017). The plasmid pcDNA5-mCherry-P2AT2A-IRESv12-SNAP-M18BP1 for co-expression of mCherry-tagged CENP-C variants and SNAP-CENP-A was constructed by Gibson cloning. The CDSs of CENP-C 1-600 and CENP-C 601-943 were inserted into that plasmid using restriction enzyme-based cloning.

2.2.3.7 Generation of stable cell lines

Stable Flp-In T-REx HeLa cell lines were generated by Flp/FRT recombination. The CDS of the protein to be expressed was cloned into a pcDNA5/FRT plasmid and co-transfected with pOG44 (Invitrogen), a plasmid expressing the Flp recombinase, into Flp-In T-REx HeLa cells using the transfection reagent X-tremeGENE (Roche) according to manufacturer's instructions. Following 2 weeks of selection in 250 µg/mL Hygromycin B (Thermo Fisher) and 4 µg mL Blasticidin (Thermo Fisher), single cell colonies were collected and subsequently expanded. Expression of the transgenes was checked by immunofluorescence microscopy and Western Blot analysis.

2.2.3.8 Preparation of nuclear extracts from HeLa cells

For the pull-down of EGFP-tagged M18BP1 and mCherry-tagged Mis18α, the nuclear fraction of the HeLa cell lysates was purified. The cell pellets were resuspended in

5 pellet volumes of lysis buffer B (20 mM Hepes pH 7.7, 20 mM potassium chloride (KCl), 0.5 mM egtazic acid (EGTA), 0.5 mM Dithioerythritol (DTE), 1 mM phenylmethylsulfonyl fluoride (PMSF), 1x protease inhibitor cocktail). The samples were incubated for 10 min on ice, subsequently Nonidet P-40 (NP-40) at a final concentration of 0.1 % was added and the samples were mixed by inverting the tube gently. The samples were centrifuged at 500 g for 10 min. The supernatant was discarded, and 10 pellet volumes of washing buffer were added to the pellet. The samples were centrifuged as before. This washing step was repeated twice. Subsequently, the cell pellets were resuspended in 5 pellet volumes of washing buffer. The samples were subjected to sonication treatment for 5 cycles in the Bioruptor device (Diagenode). 10 U/ml benzonase and 5 mM magnesium chloride ($MgCl_2$) was added to the samples followed by 2 h incubation on ice under mild shaking. Subsequently, 420 mM NaCl was added to the samples followed by 60 min incubation on ice. The samples were centrifuged at 18,000 g and 4 °C for 30 min and the supernatant was used for subsequent pull-down assays.

2.2.3.9 Immunoprecipitation of GFP- and mCherry-tagged proteins from HeLa cell lysates

Purified nuclear extracts from HeLa Flp-In T-REx cells co-expressing GST-EGFP-M18BP1 and mCherry-Mis18α were used for co-immunoprecipitation (IP) experiments and subsequent mass spectrometry analysis. 4 mg lysate were incubated with 15 µl GFP-Trap or RFP-Trap magnetic agarose beads (Chromotek) for 3 h at 4 h on a tube roller. Subsequently, the beads were washed three times with 500 µl of washing buffer. Afterwards, the samples were processed for mass spectrometry analysis. To apply statistical tests on the obtained data, all IPs were performed in technical triplicates.

2.2.3.10 Electroporation of recombinant mCherry-CENP-C into DLD-1 cells

To electroporate recombinant mCherry-CENP-C protein into DLD-1 cells, the Neon Transfection System Kit (Thermo Fisher) was used. 3 x 10^6 cells were trypsinized, washed with PBS and resuspended in electroporation Buffer R (Thermo Fisher) to a final volume of 90 µl. Recombinant mCherry-CENP-C protein was diluted 1:2 in buffer R to 15 µM and 30 µl of the mixture was added to the 90 µl cell suspension.

After mixing the sample, 100 µl of the mixture was loaded into a Neon Pipette Tip (Thermo Fisher) and electroporated by applying two consecutive 35 ms pulses with an amplitude of 800 V. The sample was subsequently added to 50 ml of pre-warmed PBS, centrifuged at 500 g for 3 min and trypsinized for 7 min to remove non-internalized extracellular protein. After one additional PBS washing step and centrifugation, the cell pellet was resuspended in DMEM without antibiotics and transferred to a 12 well plate containing poly-L-Lysine coated coverslips.

2.2.3.11 Synchronization of cells

In some experiments, cells were synchronized in different phases of the cell cycle. To synchronize cells at the G1/S-phase border, cells were treated for 16 h with 2 mM thymidine (Sigma-Aldrich). A prometaphase arrest was induced by treating cells with 5 µM of the Eg5 inhibitor S-trityl-L-cysteine (STLC) for 12-15 h. By washing out STLC three times with DMEM, cells were released from the prometaphase arrest and were let to enter G1 phase before being harvested after 3-4 h. Alternatively, 500 nM Reversine, 9 µM RO3306 and 10 µM Roscovitine was added to the STLC arrested cells to induce a rapid mitotic exit.

2.2.3.12 Immunofluorescence

The PFA fixated cells were permeabilized with PBST for 10 min. Afterwards, the cells were blocked using a PBST solution supplemented with 4 % BSA for 40 min. The coverslips were incubated with 20 µl of the corresponding primary antibody solution (see table 2-12). After the incubation, the coverslips were washed three times with 500 µl PBST. Subsequently, the secondary antibody solution (see table 2-13) was added for 45 min to the samples. The DNA was optionally stained with 0.5 µg/ml 4′,6-diamidino-2-phenylindole (DAPI) for 3 min. Afterwards, the coverslips were washed thrice with PBS and once with ultrapure water and were mounted with Mowiol (Calbiochem). The samples were let dry at room temperature for at least 16 h and subsequently stored at 4 °C protected from light.

2.2.3.13 Chromosome congression assay

Cells were treated for 15 h with 10 µM STLC. After washing out STLC using warm DMEM, 10 µM of the proteasome inhibitor MG132 was added to the cells. After 3 h, cells were fixated using a 4 % paraformaldehyde solution in PBS. After the immunofluorescence staining of CREST and DNA staining by DAPI, the chromosome alignment of the cells was analyzed using the DeltaVision widefield microscope.

2.2.3.14 Image acquisition

Cells were imaged using a Deltavision Elite System (GE Healthcare) equipped with an IX-71 inverted microscope (Olympus), a PLAPON 60x/1.42NA objective and a pco.edge sCMOS camera (PCO-TECH Inc.). For each image, a z-stack containing 16 layers with a distance of 200 nm was acquired using the software softWoRx (GE Healthcare). The raw data were deconvolved and converted into average intensity projections for illustrative and quantification purposes. The images were edited and analyzed using the software FIJI. For the quantification of centromere signals, an adapted version of the published FIJI plugin "Centromere recognition and quantification (CRaQ)" was used (Bodor et al., 2012). In brief, centromere signals were chosen based on their size, shape and intensity using the CREST channel as the reference channel. The positions of the centromere signals were recorded and the mean intensity value of adjacent pixels of a centromere spot was subtracted as background intensity from the mean intensity value of the centromere spot.

3 Results

3.1 Biochemical and in-cell investigation of the human kinetochore architecture

In the first part of my PhD thesis, I will focus on the biochemical reconstitution of the human kinetochore. CENP-C is a core component of the inner kinetochore and structurally provides a linearly organized set of binding sites for the outer kinetochore MIS12 complex, the inner kinetochore CENP-HIKM and CENP-LN complexes as well as two sequence-related nucleosomes binding motifs. The predominant part of the CENP-C sequence is predicted to be intrinsically disordered, impeding the purification of the full-length protein. In previous reconstitution studies, a CENP-C truncation mutant has been used that comprises the N-terminal 544 residues and therefore lacks the C-terminal CENP-C motif as well as the Cupin domain (Klare et al., 2015; Pentakota et al., 2017; Pesenti et al., 2018; Weir et al., 2016). To overcome the limitations of a truncated CENP-C variant, my first aim was to reconstitute the full-length CENP-C protein that comprises the complete set of binding sites and the C-terminal dimerization domain.

3.1.1 Purification of full-length CENP-C

To reconstitute full-length CENP-C, two individual CENP-C truncation mutants were purified from *E. coli*, namely CENP-C$^{1\text{-}600}$ and CENP-C$^{601\text{-}943}$. The CENP-C$^{1\text{-}600}$ truncation mutant was tagged with a SpyCatcher at the C-Terminus, whereas the CENP-C$^{601\text{-}943}$ truncation mutant was fused with a SpyTag at the N-Terminus (Figure 3-1). SpyCatcher and SpyTag are engineered tags created by splitting a domain of the *Streptococcus pyogenes* fibronectin-binding protein FbaB that forms a spontaneous

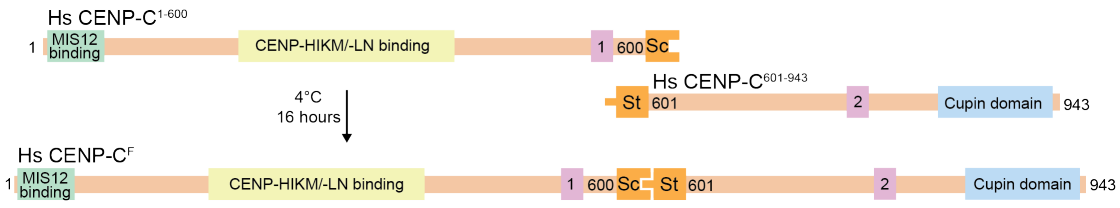

Figure 3-1 Schematic of the CENP-C purification procedure

The individual CENP-C fragments carried a SpyCatcher or a SpyTag, respectively. Important regions of CENP-C are highlighted. Sc: SpyCatcher Sp: SpyTag 1: Central CENP-C motif 2: Conserved CENP-C motif

isopeptide bond (Zakeri et al., 2012). The resulting binding partners SpyCatcher and SpyTag fused to the individual CENP-C fragments form a covalent peptide bond upon mixing and thereby generate a fusion protein containing the complete CENP-C sequence with a 13 kD SpyCatcher-SpyTag sequence between residues Ser600 and Gly601.

Two variants of the N-terminal CENP-C$^{1\text{-}600}$-SpyCatcher fusion protein were purified carrying either an MBP tag (Figure 3-2 A) or an mCherry tag (Figure 3-2 B). The MBP-tagged variant has a size of 123 kD, whereas the mCherry-tagged variant is 110 kD in size. In preparative SEC both variants of CENP-C$^{1\text{-}600}$-SpyCatcher co-eluted with a significant amount of smaller protein species, most likely reflecting significant susceptibility to proteolytic degradation due to the disordered structure of CENP-C. The typical yield of the N-terminal CENP-C constructs ranged between 8-12 mg protein per 1 L *E. coli* culture.

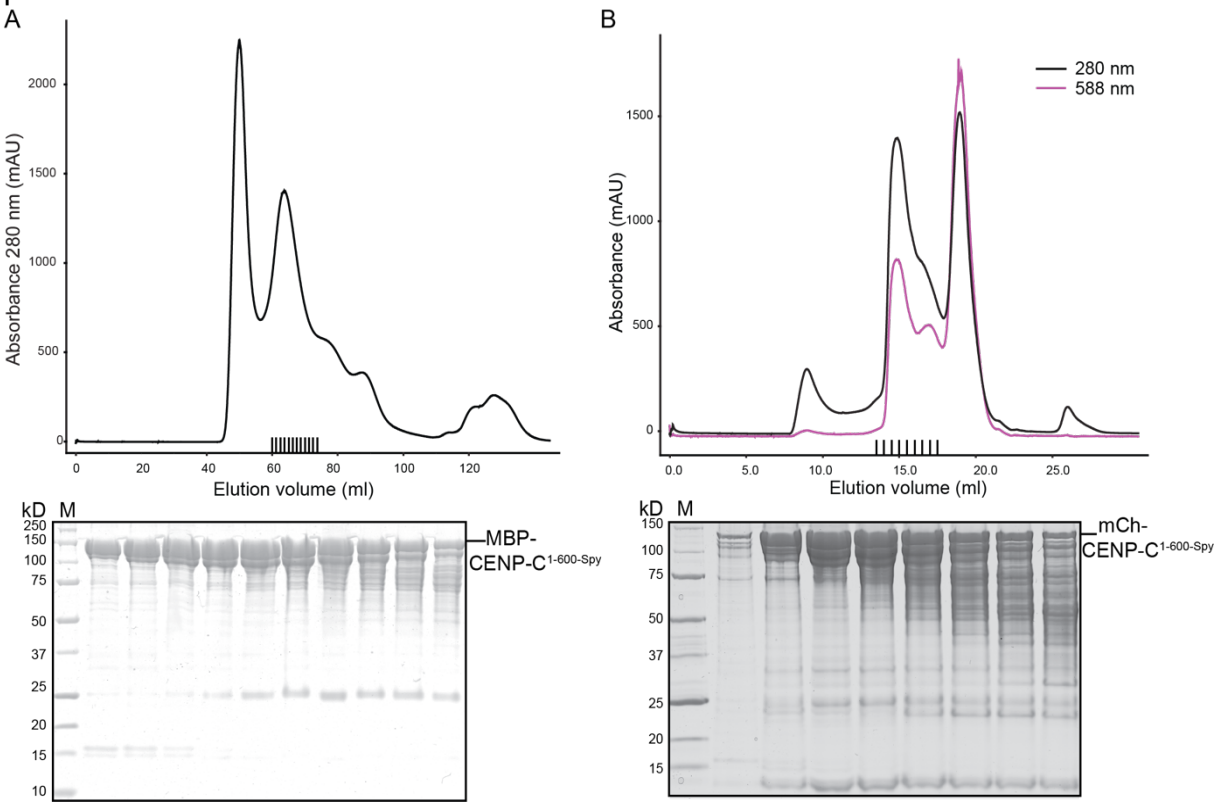

Figure 3-2 Purification of MBP-CENP-C$^{1\text{-}600}$-SpyCatcher and mCherry-CENP-C$^{1\text{-}600}$-SpyCatcher

(A) SEC elution profile (S200 HiLoad 16/60 pg) of MBP-CENP-C$^{1\text{-}600}$ after affinity purification. Black lines indicate collected fractions for Tricine-SDS-PAGE analysis. The gel was stained with CBB. (B) SEC elution profile (S6 10/300 Increase) of mCherry-CENP-C$^{1\text{-}600}$ after affinity purification. The absorbance was monitored at 280 nm (black curve) and 588 nm (magenta curve). Black lines indicate collected fractions for Tricine-SDS-PAGE. The gel was stained with CBB.

In contrast to the N-terminal CENP-C constructs, MBP-SpyTag-CENP-C$^{601-943}$ eluted in a monodisperse, sharp peak and appeared as one prominent band of 83 kD size in the Tricine-SDS-PAGE analysis (Figure 3-3). Thus, the C-Terminus of CENP-C containing the structured Cupin domain is more stable than the N-terminal portion of CENP-C which is largely intrinsically disordered. The typical yield of that construct ranged between 15-20 mg protein per 1 L *E. coli* culture. Both the N-terminal and C-terminal CENP-C constructs could be stored at -80 °C and thawed again without precipitation.

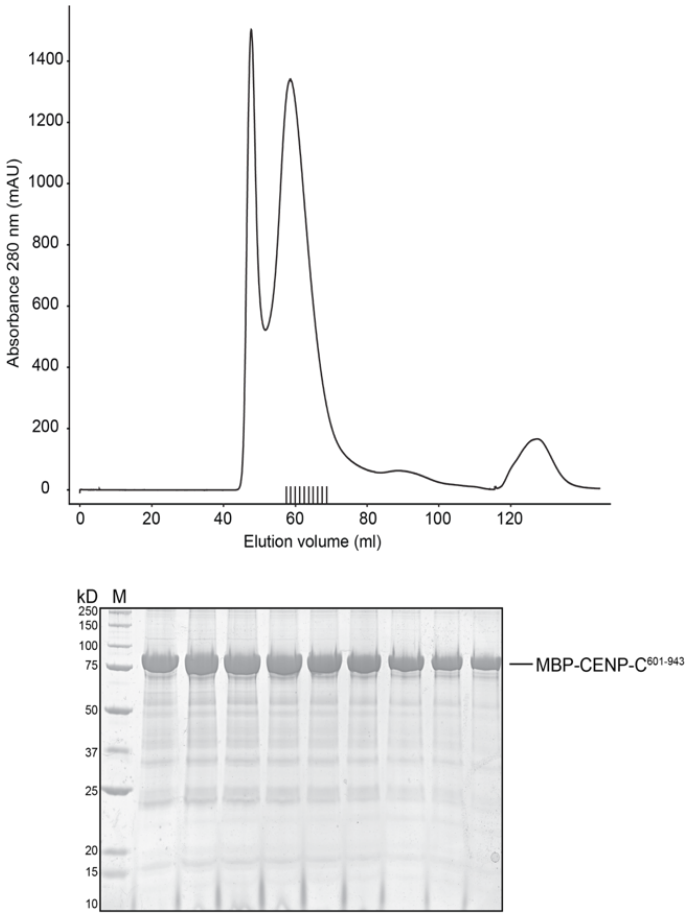

Figure 3-3 Purification of MBP-SpyTag-CENP-C$^{601-943}$

SEC elution profile (S200 HiLoad 16/60 pg) of MBP-SpyTag-CENP-C$^{601-943}$ after affinity purification. Black lines indicate collected fractions for Tricine-SDS-PAGE analysis. The gel was stained with CBB.

To determine the optimal ratio between the N-terminal and C-terminal CENP-C fragments for the SpyCatcher-SpyTag ligation reaction, an increasing amount of MBP-CENP$^{1-600}$-SpyCatcher was added to MBP-SpyTag-CENP-C$^{601-943}$ (Figure 3-4 A). TEV protease was used to cut off the MBP tag from SpyTag-CENP-C$^{601-943}$. The molar ratio of CENP-C$^{601-943}$ to CENP-C$^{1-600}$ was varied between 1:1 and 1:5. After mixing the different reactions, the samples were incubated for 16 h at 4°C and subsequently analysed by SDS-PAGE (Figure 3-4 B). With increasing amounts of CENP-C$^{1-600}$, the CENP-C$^{601-943}$ band weakened and an additional 163 kD band appeared representing the MBP-CENP-C$^{1-600}$-Spy-Catcher-Spy-Tag-CENP-C$^{601-943}$ ligation product (from now on referred to as CENP-C^{F}). The intensity of the CENP-C^{F} band plateaued between a molar ratio of 1:3 and 1:4. Therefore, a ratio of 1:3.5 was used for the SpyCatcher-SpyTag ligation.

To separate CENP-C^{F} from the excess of MBP-CENP-C$^{1-600}$-SpyCatcher, the reaction mixture was subjected to SEC. MBP-CENP-C^{F} and MBP-CENP-C$^{1-600}$-SpyCatcher eluted in two separated peaks (Figure 3-4 C). The majority of MBP-CENP-C^{F} eluted between 10.5-13.5 ml, and the corresponding fractions were pooled and concentrated. mCherry-CENP-C^{F} was purified accordingly (Figure 3-4 D). The two CENP-C^{F} variants were concentrated to at least 5 mg/ml and stored at -80 °C until further use. MBP-CENP-C^{F} was used for all *in vitro* reconstitution experiments presented in this thesis, whereas mCherry-CENP-C^{F} was used in electroporation experiments.

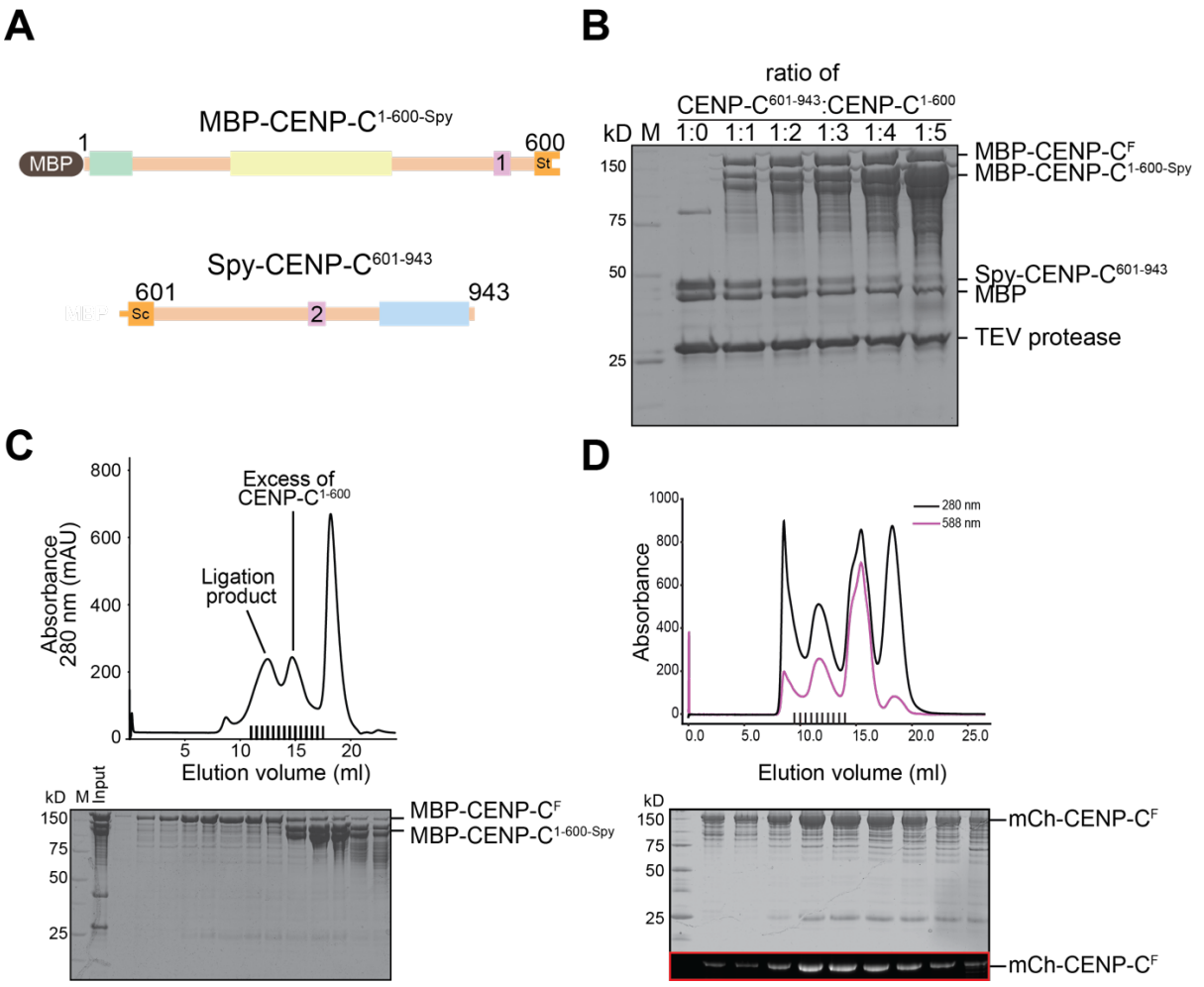

Figure 3-4 Ligation and purification of full-length CENP-C

(A) Schematic showing the individual CENP-C fragments used for the Spy ligation shown in B. (B) Titration of MBP-CENP-C$^{1-600}$ against CENP-C$^{601-943}$. The molar ratio between both CENP-C fragments is indicated above each lane. The Tricine-SDS gel was stained with CBB. (C) SEC elution profile (S6 10/300 Increase) of full-length MBP-CENP-C after Spy ligation. Black lines indicate collected fractions for Tricine-SDS-PAGE analysis. The gel was stained with CBB. (D) SEC elution profile (S6 10/300 Increase) of full-length mCherry-CENP-C after Spy ligation. The absorbance was monitored at 280 nm (black curve) and 588 nm (magenta curve). Black lines indicate collected fractions for Tricine-SDS-PAGE analysis. The CENP-C protein band was analysed by CBB staining or in gel fluorescence detection.

3.1.2 CENP-C^{F} preferentially binds CENP-A nucleosomes

Numerous previous studies demonstrated that CENP-C interacts with CENP-A nucleosomes *in vitro* (Allu et al., 2019; Carroll et al., 2010; Falk et al., 2015; Kato et al., 2013; Watanabe et al., 2019; Weir et al., 2016; Xiao et al., 2017). However, all of these studies used either CENP-C truncation mutants, short peptides or *in vitro* translated protein. Having reconstituted the full-length CENP-C protein I wanted to investigate if CENP-C^{F} binds exclusively to CENP-A^{NCP} or if the conserved motif also provides some affinity for H3^{NCP}. To test the binding between CENP-C^{F} and the different types of mononucleosomes, analytical SEC experiments were performed. Since CENP-C^{F} contains two nucleosome binding motifs, 5 µM CENP-C^{F} dimer were incubated with 10 µM of CENP-A^{NCP} or H3^{NCP}. The mixtures as well as the individual

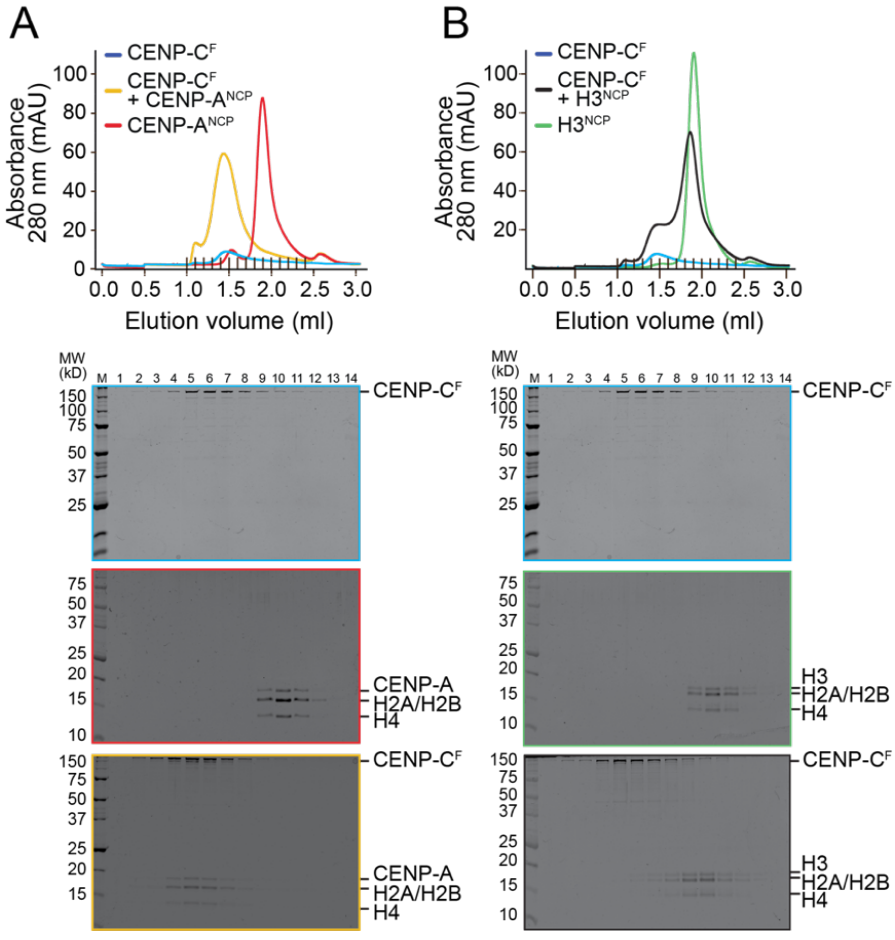

Figure 3-5 CENP-C binds preferentially to CENP-A nucleosomes

(A) Analytical SEC results (Superose 5/150 Increase) of CENP-C^{F} (blue), CENP-A^{NCP} (red) and CENP-C^{F}+CENP-A^{NCP} (yellow). Black lines indicate collected fractions for Tricine-SDS-PAGE analysis. Gels were stained with CBB. (B) Analytical SEC results (Superose 5/150 Increase) of CENP-C^{F} (blue), H3^{NCP} (green) and CENP-C^{F}+H3^{NCP} (black). Black lines indicate collected fractions for Tricine-SDS-PAGE analysis. Gels were stained with CBB.

components were incubated on ice for 30 min und subsequently subjected to analytical SEC (Figure 3-5).

CENP-A^{NCP} and H3^{NCP} appeared as sharp peaks and both eluted at 1.9 ml, whereas the CENP-C^{F} peak was broader due its disordered, elongated structure. CENP-C^{F} formed a stoichiometric complex with CENP-A^{NCP} and both components co-eluted at 1.4 ml (Figure 3-5 A). A modest, incomplete shift of the H3^{NCP} could also be detected upon incubation with CENP-C^{F} (Figure 3-5 B). This result clearly demonstrates, that the interaction between CENP-C^{F} and H3^{NCP} is not sufficiently strong to co-elute stoichiometrically and that CENP-C^{F} possesses a much stronger binding affinity to CENP-A^{NCP} than to H3^{NCP}. However, due to technical reasons, the analytical SEC experiments were performed at 300 mM NaCl concentration. Thus, under these conditions the interaction between CENP-C^{F} and H3^{NCP} might be significantly weaker than under physiological conditions.

Next, we performed competitive electrophoretic mobility shift assays (EMSA). To perform these assays at low nanomolar concentrations, we created Alexa-555 labelled CENP-A nucleosomes and Alexa-647 labelled H3 nucleosomes. The fluorophores were incorporated into the DNA of the NCPs by PCR using fluorophore-coupled oligonucleotides. Mixtures containing equimolar amounts of CENP-A^{NCP} and H3^{NCP} were incubated with increasing amounts of CENP-C^{F}. The complexes were subjected to native PAGE and the gel was subsequently scanned for two-colour fluorescence. Unbound NCPs appear at the bottom of the gel, whereas CENP-C^{F}-NCP complexes run as a higher molecular weight species causing a shift of the nucleosome band towards the upper part of the gel. The performed EMSA confirmed that CENP-C^{F} selectively binds to CENP-A^{NCP}. In the CENP-C^{F} concentration range between 0-15 nM, 80 % of CENP-A^{NCP} formed a complex with CENP-C, whereas most of the H3^{NCP} remained unbound (Figure 3-6 A). However, at higher concentrations CENP-C^{F} also bound H3^{NCP}. This demonstrates, that CENP-C^{F} can interact with H3^{NCP}, but preferentially binds to CENP-A^{NCP} with a 10-fold higher affinity (Figure 3-6 B).

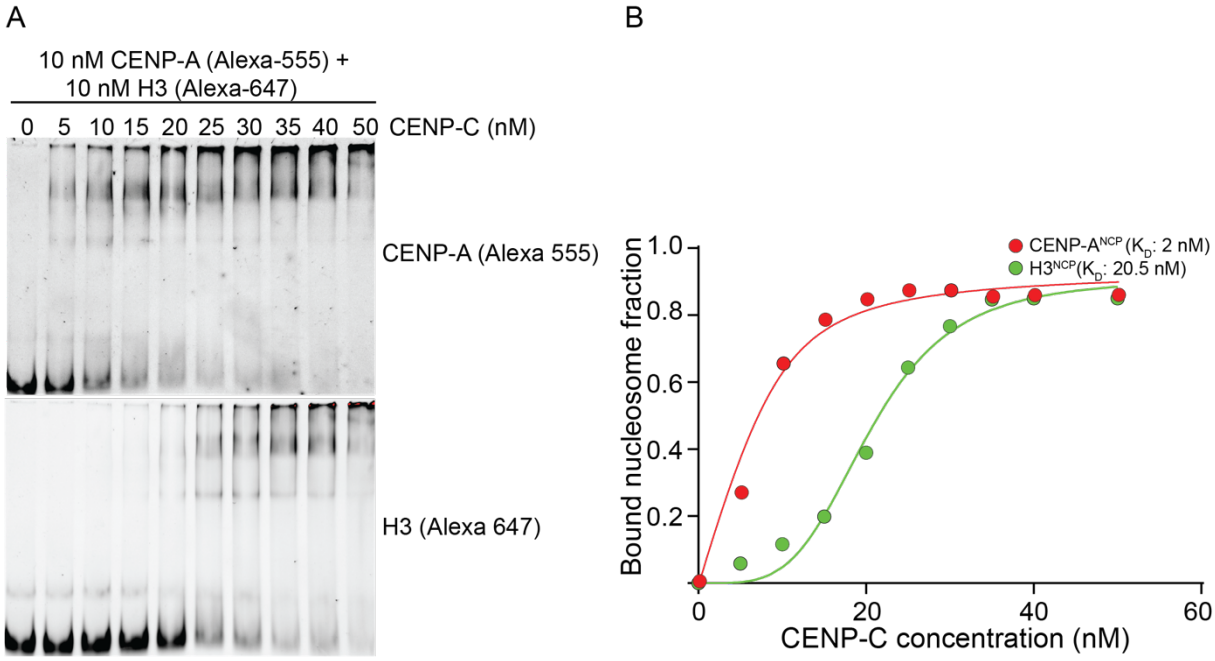

Figure 3-6 CENP-C selectively binds to CENP-A nucleosomes

(A) Representative gel scan images of EMSA using constant equimolar amounts of Alexa-555 labelled CENP-A^{NCP} and Alexa-647 labelled H3^{NCP} and increasing amounts of CENP-C^{F}. The mixtures were incubated on ice for 30 min and subsequently resolved on a 6 % native polyacrylamide gel. The gel was scanned using a ChemiDoc MP Gel Imaging System to detect the fluorescent signals of the different NCPs. (B) Data graph of EMSA shown in A. The fluorescent intensities were measured using the software FIJI. The obtained data were plotted and analyzed using the software GraphPad Prism.

3.1.3 CENP-C^{F} binds two CENP-A^{NCP}

We used analytical SEC as a reliable assay to further characterize the interaction between CENP-C^{F} and CENP-A^{NCP}. A C-terminal homodimer of the CENP-C orthologue Mif2 harbouring the conserved CENP-C motif has been shown to form a 1:1 complex with one Cse4 nucleosome (Xiao et al., 2017). Consistently, one CENP-A nucleosome binds two copies of the monomeric central CENP-C motif (Allu et al., 2019). Having reconstituted the CENP-C^{F} homodimer, we therefore hypothesized that two CENP-A^{NCP} can be bound by CENP-C^{F}. To test this hypothesis, we first created individual CENP-C motif mutants predicted to impair CENP-A binding. We substituted two critical, conserved residues present in both CENP-C motifs, namely Arg522/742 and Trp531/751, by alanine (Figure 3-7 A). Arg522/742 mediates electrostatic interactions with the acidic patch region of the CENP-A nucleosome, whereas Trp531/751 recognizes the hydrophobic tail of the CENP-A histone.

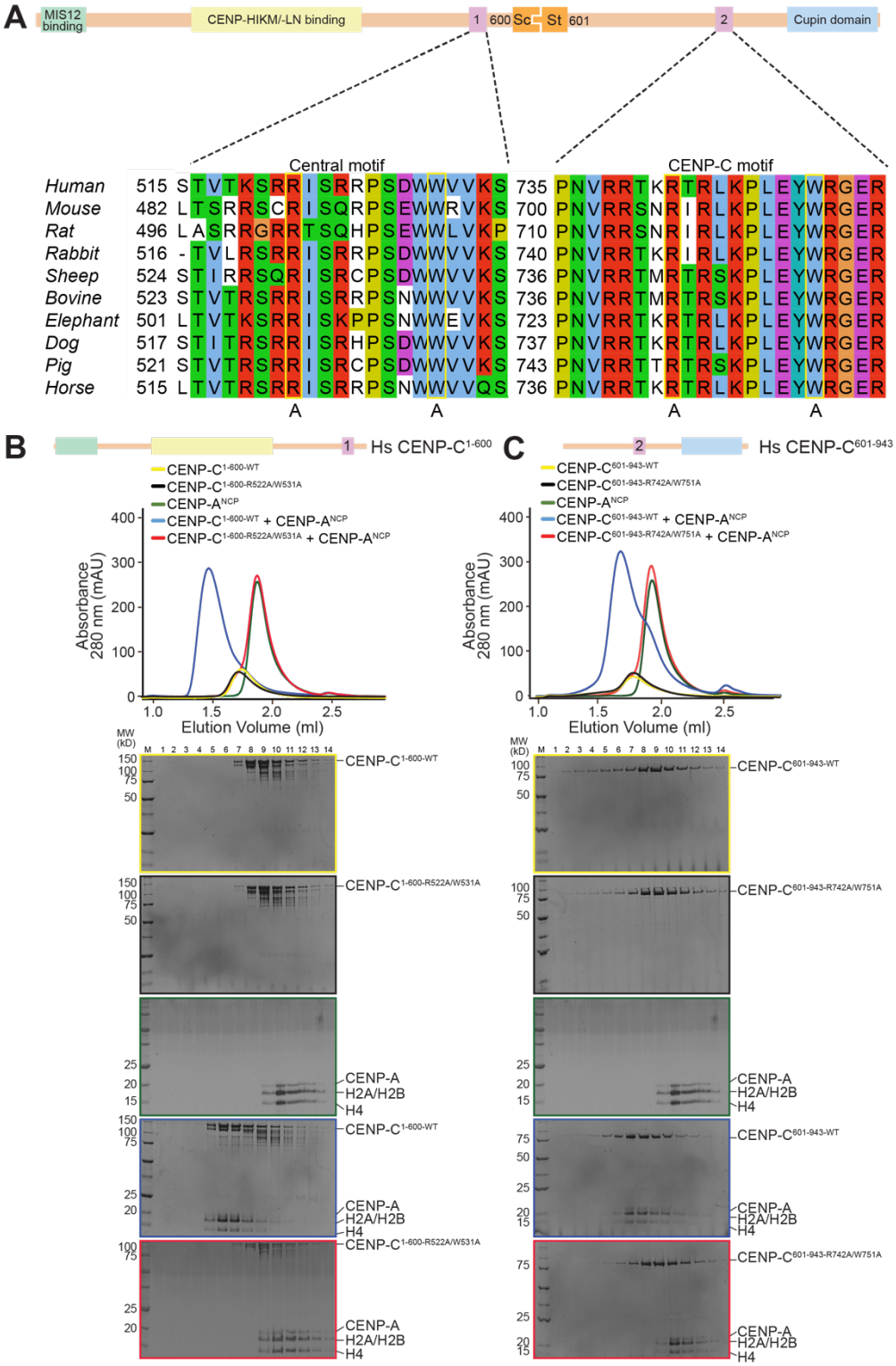

Figure 3-7 Mutation of two critical residues within the CENP-C motif abolishes the interaction between CENP-C and CENP-A^{NCP}

(A) Schematic of CENP-C and sequence alignment of the central and the conserved CENP-C motif. The two residues in each motif which were substituted by alanine are highlighted in yellow boxes. (B) Analytical SEC results (Superose 6 5/150 Increase) of CENP-C$^{1\text{-}600\ WT}$, CENP-C$^{1\text{-}600\ R522A/W531A}$ and CENP-A^{NCP}. The fractions that eluted between 1 ml and 2.4 ml were analysed by Tricine-SDS-PAGE. Gels were stained by CBB. (C) Analytical SEC results (Superose 6 5/150 Increase) of CENP-C$^{601\text{-}943\ WT}$, CENP-C$^{601\text{-}943\ R742A/W751A}$ and CENP-A^{NCP}. The fractions that eluted between 1 ml and 2.4 ml were analysed by Tricine-SDS-PAGE. Gels were stained by CBB.

Substitution of either Arg522 or Trp531 prevented the interaction between CENP-C and CENP-A nucleosomes in a previous study (Kato et al., 2013). First, we tested in analytical SEC experiments, whether the substitution of the mentioned residues in the individual CENP-C fragments, CENP-C^{1-600} and CENP-$C^{601-943}$, abolished the binding of the respective CENP-C fragments to CENP-A^{NCP}. We could confirm for both WT fragments an interaction with CENP-A^{NCP} (Figure 3-7 B and C, blue curves and gels). The Ala substitutions completely disrupted the binding between CENP-C and CENP-A^{NCP} (Figure 3-7 B and C, red curves and gels). Next, we created four different CENP-C^{F} variants, possessing either two functional CENP-C motifs (CENP-$C^{F\text{-}WT\text{-}WT}$), one functional CENP-C motif (CENP-$C^{F\text{-}WT1\text{-}M2}$ and CENP-$C^{F\text{-}M1\text{-}WT2}$) or two unfunctional motifs (CENP-$C^{F\text{-}M1\text{-}M2}$). Like in the previous SEC experiment, 5 µM CENP-C^{F} dimer of all four variants were incubated with 10 µM CENP-A^{NCP}. CENP-$C^{F\text{-}WT\text{-}WT}$, like demonstrated before, co-eluted with CENP-A^{NCP} at 1.4 ml (Figure 3-8 A). Strikingly, using the same molar CENP-C^{F}:CENP-A^{NCP} ratio, the CENP-C variants CENP-$C^{F\text{-}WT1\text{-}M2}$ and CENP-$C^{F\text{-}M1\text{-}WT2}$ could not induce a complete shift of the CENP-A^{NCP} peak (Figure 3-8 B and C). Approximately half of the CENP-A^{NCP} co-eluted with both CENP-C^{F} variants at 1.4 ml, whereas the other half remained unbound and eluted at 1.9 ml. The double mutant CENP-$C^{F\text{-}M1\text{-}M2}$ did not co-elute with CENP-A^{NCP} at all (Figure 3-8 D). The indicated peak fractions at 1.4 ml elution volume of the four performed SEC experiments were compared side-by-side by SDS-PAGE (Figure 3-8 E). The intensities of the single histone bands confirmed, that the amount of CENP-A^{NCP} bound by CENP-$C^{F\text{-}WT1\text{-}M2}$ and CENP-$C^{F\text{-}M1\text{-}WT2}$ was approximately halved compared to CENP-$C^{WT\text{-}WT}$. Thus, one molar equivalent of CENP-$C^{F\text{-}WT\text{-}WT}$ dimer binds two molar equivalents of CENP-A^{NCP}. In case one of two CENP-C motifs has been unfunctionalized, only one molar equivalent of CENP-A^{NCP} can be bound by CENP-C^{F}.

To confirm these results in a quantitative experiment, we used sedimentation-velocity analytical ultracentrifugation (AUC) as a tool to determine the molecular weight of two different CENP-C^{F}:CENP-A^{NCP} complexes that would further allow us to deduce the stoichiometry of the complexes. First, we analysed CENP-A^{NCP} alone (Figure 3-9 A). Measuring the absorbance at 260 nm, we obtained a molecular weight of 196 kD for the CENP-A^{NCP}, which comes very close to the actual molecular weight of 199 kD (Figure 3-9 D). To determine the stoichiometry of the WT CENP-C^{F}:CENP-A^{NCP} complex, we mixed 0.5 µM CENP-C^{F} dimer with 1 µM CENP-A^{NCP} (Figure 3-9 C). For

this sample, we obtained a molecular weight of 715 kD. This result strongly supports the proposed stoichiometry of one CENP-C^{F} dimer bound to two CENP-A^{NCP}.

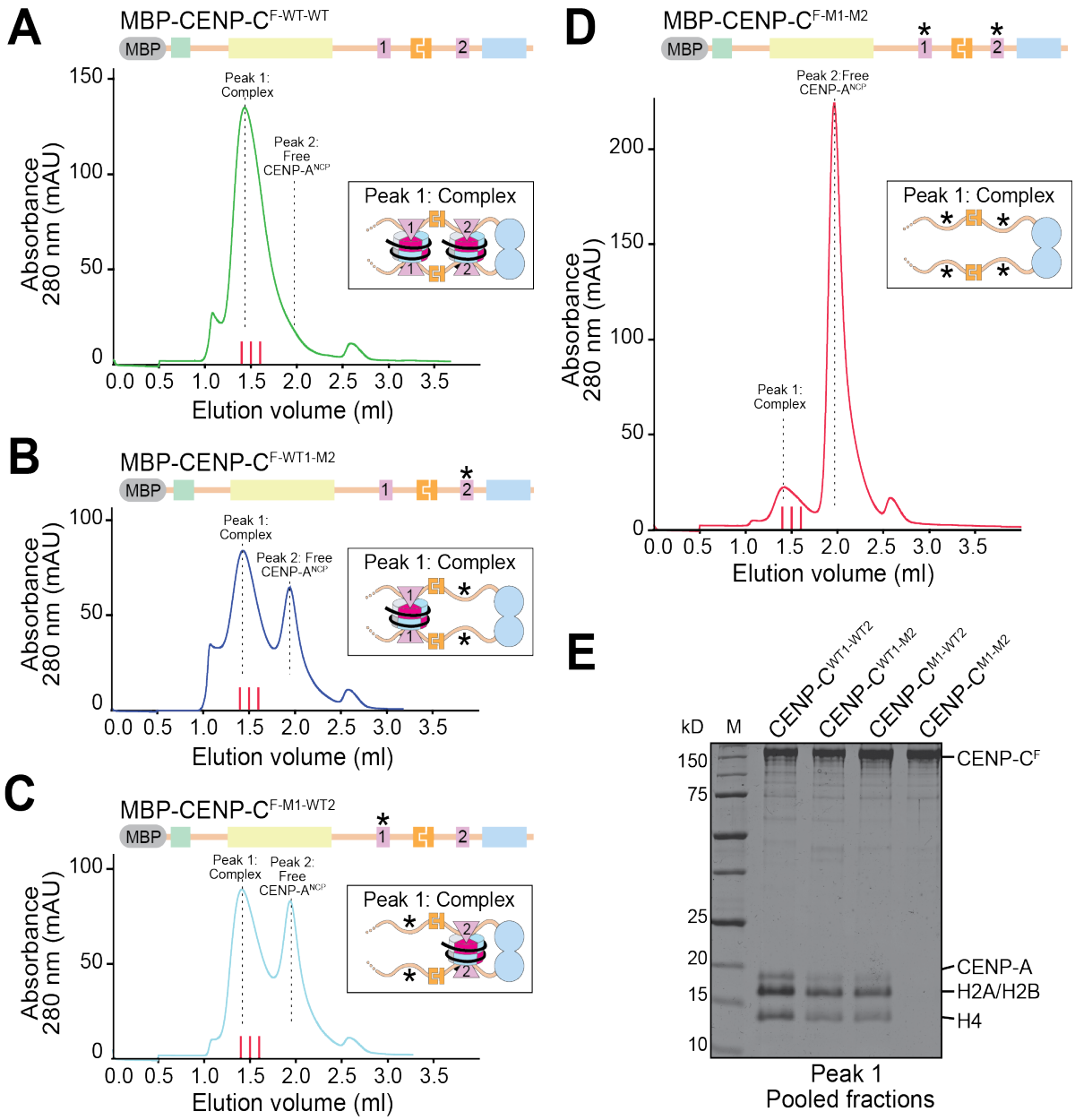

Figure 3-8 Mutation of each individual CENP-C motif reduces the amount of bound CENP-A^{NCP} by half

(A) Analytical SEC results (Superose 5/150 Increase) of CENP-C$^{F\text{-}WT\text{-}WT}$ and CENP-A^{NCP}. Red lines indicate the collected fractions for Tricine-SDS-PAGE analysis. (B) Analytical SEC results of CENP-C$^{F\text{-}WT1\text{-}M2}$ and CENP-A^{NCP}. (C) Analytical SEC results of CENP-C$^{F\text{-}M1\text{-}WT2}$ and CENP-A^{NCP}. (D) Analytical SEC results of CENP-C$^{F\text{-}M1\text{-}M2}$ and CENP-A^{NCP}. (E) Tricine-SDS-PAGE analysis of the collected peak fractions from the analytical SEC experiments shown in (A)-(D). The gel was stained with CBB.

To further validate, that each CENP-C motif binds one CENP-A^{NCP}, we analysed a third sample (Figure 3-9 C). Since the AUC experiments were performed at 150 mM NaCl concentration, we purified a CENP-C$^{F\text{-}\Delta motif2}$ mutant that lacks the C-terminal CENP-C motif instead of using the Ala mutant to prevent any residual binding between the CENP-C motif and CENP-A^{NCP}. We mixed equimolar amounts of CENP-C$^{F\text{-}\Delta motif2}$ dimer and CENP-A^{NCP} and obtained a molecular weight of 489 kD, which strongly supports the predicted stoichiometry of one CENP-C$^{F\text{-}\Delta motif2}$ dimer bound to one CENP-A^{NCP}. Thus, the AUC experiments confirmed that each CENP-C motif of the CENP-C^{F} dimer binds one CENP-A^{NCP}.

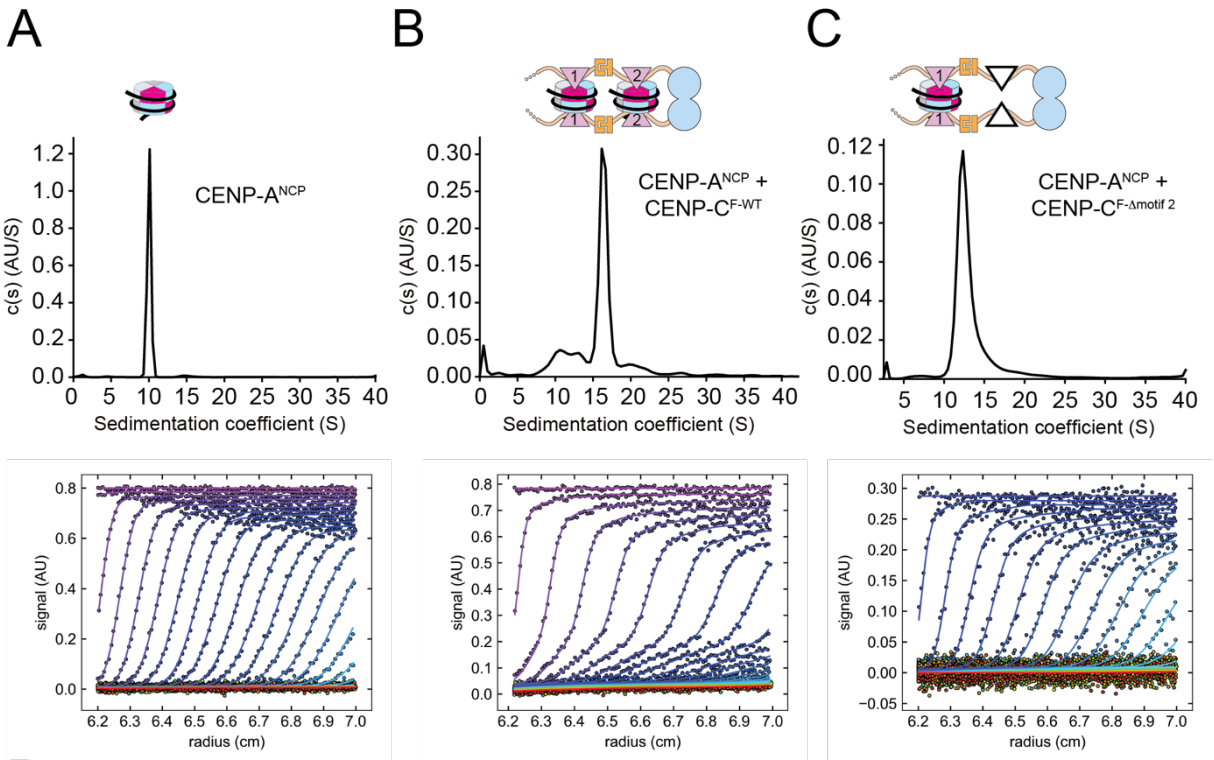

D

	CENP-A^{NCP}	CENP-A^{NCP} + CENP-C$^{F\text{-}WT}$	CENP-A^{NCP} + CENP-C$^{F\text{-}\Delta motif\ 2}$
Frictional ratio	1.483	1.884	1.749
Sedimentation coeff. (S)	9.997	16.92	13.282
Predicted stoichiometry	-	1 $(CENP\text{-}C)_2$ + 2 CENP-A^{NCP}	1 $(CENP\text{-}C)_2$ + 1 CENP-A^{NCP}
Theoretical MW (kD)	199	726	520
Observed MW (kD)	196	715	489

Figure 3-9 The full-length CENP-C dimer binds two CENP-A^{NCP}

(A) Sedimentation velocity AUC result showing the best-fit size distribution of CENP-A^{NCP} (B) Sedimentation velocity AUC result showing the best-fit size distribution of CENP-A^{NCP}+CENP-C$^{F\text{-}WT}$ (C) Sedimentation velocity AUC result showing the best-fit size distribution of CENP-A^{NCP}+CENP-C$^{F\text{-}\Delta motif2}$ (D) Summary table showing the results obtained in the sedimentation velocity AUC experiments shown in A-C

3.1.4 The central motif of CENP-C^F preferentially binds to the CENP-A portion of a CENP-A/H3 dinucleosome

Having demonstrated, that CENP-C^F binds two CENP-A mononucleosomes, we asked if CENP-C^F binds to CENP-A/H3 dinucleosomes in a specific orientation. Previous studies showed, that the central motif competes out the conserved CENP-C motif bound to CENP-A, whereas the C-terminal CENP-C motif cannot outcompete the central CENP-C motif (Ali-Ahmad et al., 2019; Watanabe et al., 2019). Furthermore, the central motif has been shown to have a much higher selectivity for CENP-A, relative to H3, compared to the conserved CENP-C motif, which instead binds CENP-A and H3 with similar affinity (Kato et al., 2013). Taking these findings into account, we speculated, that the CENP-A portion of a CENP-A/H3 dinucleosome would be preferentially oriented towards the central motif and the H3 portion accordingly to the conserved motif. To test this hypothesis, we created CENP-A and H3 containing mononucleosomes, which were assembled on centromeric alpha satellite DNA. Using non-palindromic restriction sites flanking both DNA sequences, we ligated the mononucleosomes using T4 ligase to obtain dinucleosomes of specific composition.

To monitor the binding between the two motifs of CENP-C and the dinucleosomes, we substituted by using amber codon suppression one Tyr residue adjacent to the central or the conserved CENP-C motif, namely Tyr541 and Tyr758 (Figure 3-10 A), by the unnatural amino acid p-benzoyl-L-phenylalanine (Bpa), which carries a photo-activatable crosslinking group. Using the SpyCatcher ligation approach, we created two full-length CENP-C Bpa mutants, CENP-C$^{F\text{-}541Bpa}$ and CENP-C$^{F\text{-}758Bpa}$ (Figure 3-10 B). First, we tested if the incorporated Bpa residue forms any crosslinks upon activation with 365 nm UV light. For this purpose, we incubated 250 nM CENP-C^F dimer with 500 nM CENP-A/H3 dinucleosomes for 15 min. Subsequently we treated the mixture with UV light for up to 30 min and analyzed the complexes at the indicated time points by SDS-PAGE (Figure 3-10 C). Remarkably, a crosslinked species could be detected even after 1 min of UV irradiation. The intensity of the CENP-C^F band decreased over time while the crosslinked adduct became stronger, particularly between 10 and 15 minutes. In contrast, we could not detect a visible decrease of the histone bands, most likely because of the excess of dinucleosomes used in this

experiment. We fixed the UV treatment to 15 min for all upcoming experiments, since the crosslinking reaction plateaus within this time range.

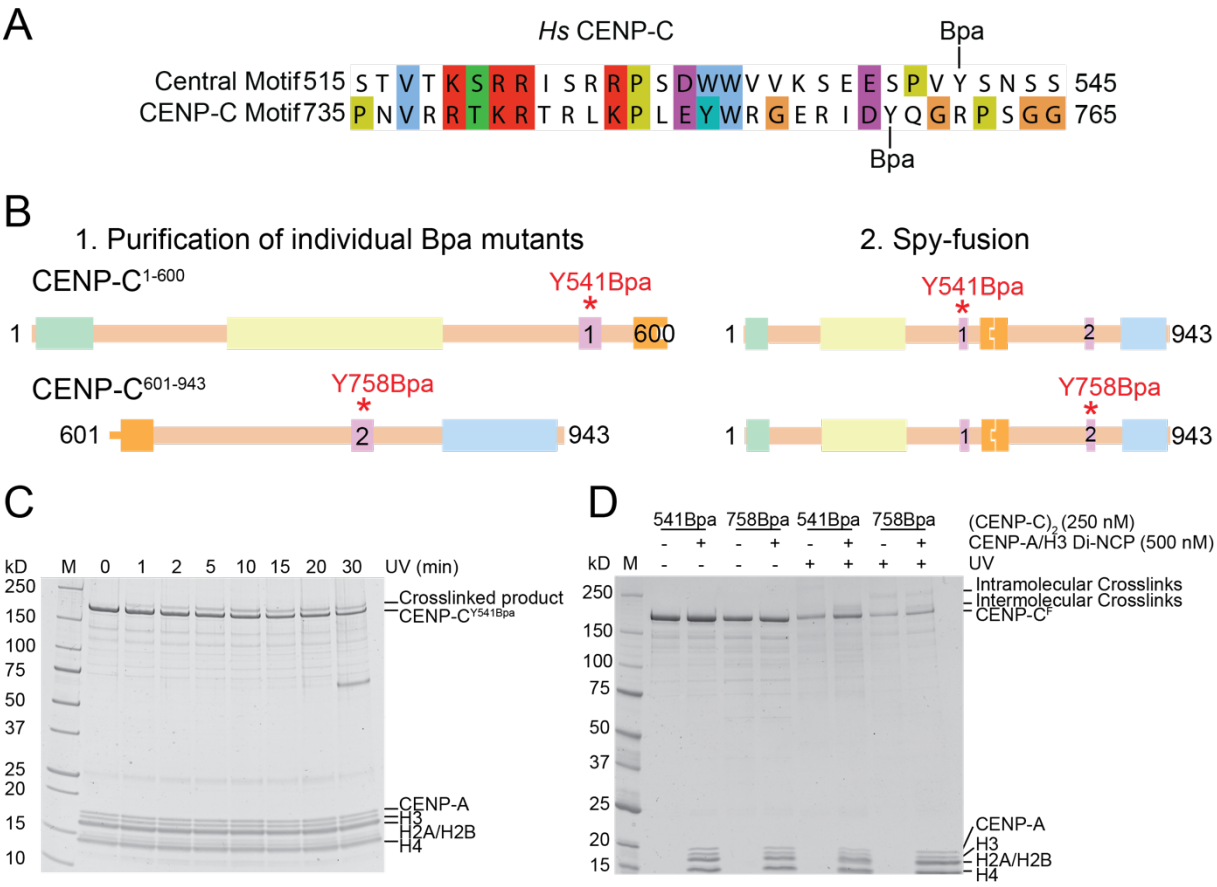

Figure 3-10 Generation of photo-crosslinkable CENP-C Bpa mutants

(A) Sequence alignment of the central motif and the conserved motif of human CENP-C. Bpa was incorporated at the indicated positions (B) Schematic showing the two full-length CENP-C Bpa mutants. (C) SDS gel showing the results of the crosslinking experiment. The duration of UV treatment is indicated above each lane. The gel was stained with CBB. (D) SDS gel showing the result of the crosslinking experiment. The gel was stained with CBB.

To test, whether the two CENP-C^F Bpa mutants form intramolecular crosslinks in the absence of dinucleosomes, we treated both mutants with UV light in the presence and absence of dinucleosomes (Figure 3-11 D). We observed a strong decrease of the CENP-C^F band of both individual Bpa mutants in the absence of dinucleosomes indicating that both mutants form intramolecular crosslinks. Addition of dinucleosomes in excess caused a less extensive decrease of the CENP-C^F bands implying that the intermolecular crosslinks are created less efficiently. In the SDS-PAGE, we could clearly distinguish between two kinds of crosslinked species. The intermolecular crosslinked species appeared closely above the CENP-C^F bands, most likely representing a CENP-C^F-histone adduct. The intramolecular crosslinked species had

a significantly higher molecular weight close to 250 kD. Remarkably, the CENP-$C^{F\text{-}758Bpa}$ mutant tended to form intramolecular crosslinks even in the presence of CENP-A/H3 dinucleosomes at saturating concentrations, possibly due to the close vicinity of the incorporated Bpa residue to the Cupin dimerization domain.

Next, we incubated both CENP-C^F Bpa mutants with equimolar and sub-equimolar concentrations of CENP-A/CENP-A dinucleosomes and CENP-A/H3 dinucleosomes (Figure 3-11 A). We analyzed the non-crosslinked (Figure 3-11 B) and UV crosslinked samples (Figure 3-11 C) both by SDS-PAGE and by Western Blot analysis of CENP-A and histone H3. Using equimolar ("High") concentrations of CENP-C^F dimer and dinucleosomes, we could detect crosslinks between CENP-A and both CENP-C^F Bpa mutants. In case we used CENP-A/CENP-A dinucleosomes at equimolar concentrations, we observed a stronger crosslinked CENP-A band in combination with the CENP-$C^{F\text{-}Y758Bpa}$ mutant, whereas we observed more CENP-A crosslinked to CENP-$C^{F\text{-}Y541Bpa}$ in case we incubated this mutant with CENP-A/H3 dinucleosomes. This result indicated, that the CENP-A/H3 dinucleosome might have a preferred orientation. However, using equimolar concentrations, we hypothesized that we start to oversaturate CENP-C with dinucleosomes which could eventually result in the binding of two dinucleosomes per CENP-C dimer (Figure 3-11 D).

Thus, we expected a potential dinucleosome orientation to become more evident at sub-saturating ("Low") dinucleosome concentrations. When we used sub-equimolar concentrations, the CENP-A/CENP-A dinucleosome crosslinked more efficiently to the CENP-$C^{F\text{-}Y541Bpa}$ mutant; however, we also detected CENP-A crosslinked to CENP-$C^{F\text{-}Y758Bpa}$. In contrast, when we used CENP-A/H3 dinucleosome at low concentrations, we only detected CENP-A crosslinked to the CENP-$C^{F\text{-}Y541Bpa}$ mutant, but not to CENP-$C^{F\text{-}Y758Bpa}$. Unfortunately, we were not able to detect any crosslinked species in the histone H3 Western blots. Nevertheless, the crosslinking experiments suggested, that the central motif of CENP-C^F preferentially binds to the CENP-A portion of CENP-A/H3 dinucleosomes at equimolar and sub-equimolar dinucleosome concentrations.

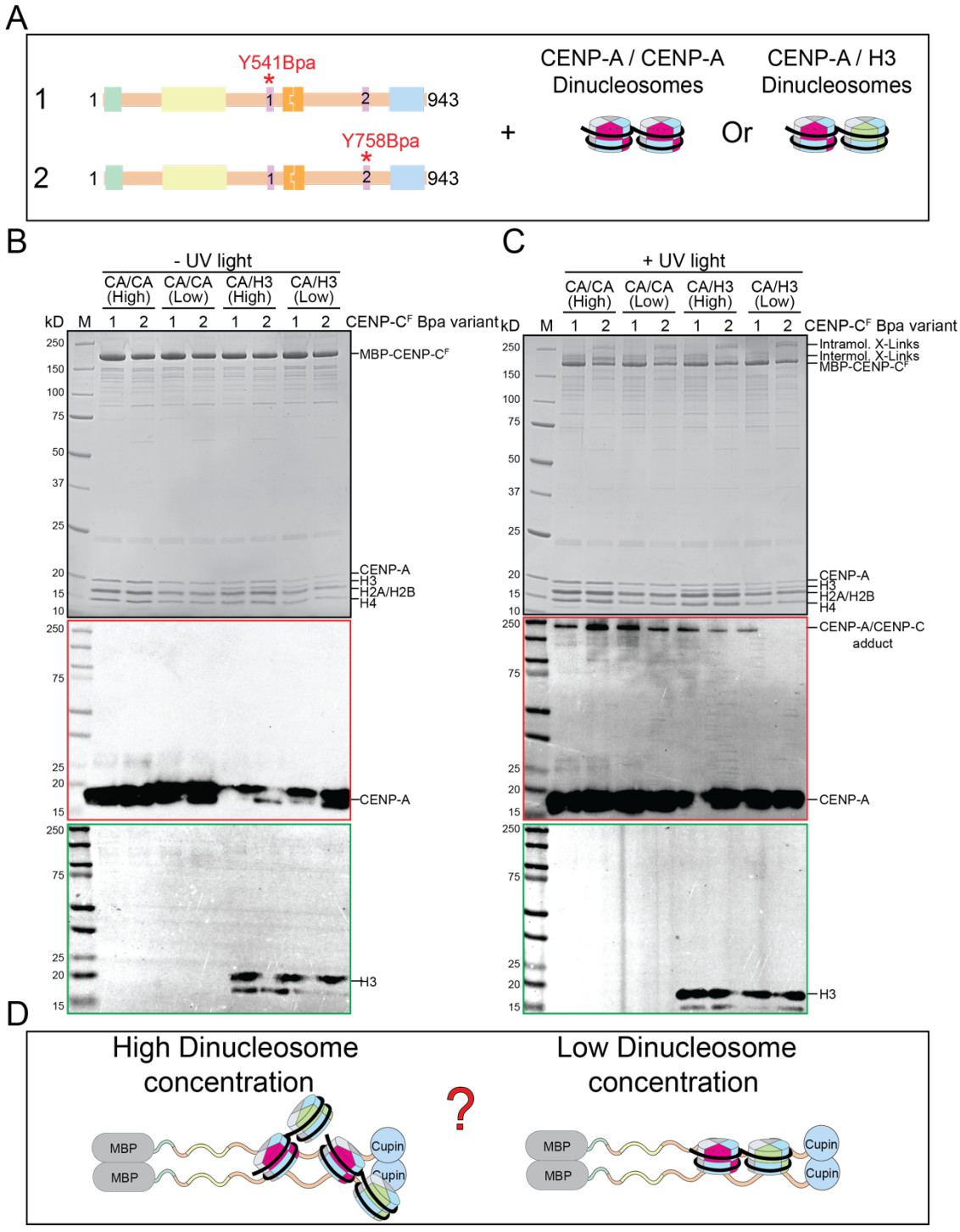

Figure 3-11 The central motif of CENP-C crosslinks to CENP-A at high and low dinucleosome concentrations

(A) Schematic showing the two CENP-C^F Bpa mutants used in this experiment. Each individual mutant was incubated with high and low concentrations of either CENP-A/CENP-A dinucleosomes or CENP-A/H3 dinucleosomes and crosslinked by UV light. (B) Representative SDS-PAGE (top), CENP-A immunoblot (middle) and H3 immunoblot (bottom) showing the non-crosslinked samples. The used CENP-C^F Bpa mutant is indicated above each lane. High and low concentrations of dinucleosomes were used. (C) Representative SDS-PAGE (top), CENP-A immunoblot (middle) and H3 immunoblot (bottom) of the UV-light induced crosslinked CENP-C^F Bpa mutants. In the gel inter- and intramolecular crosslinks could be detected. The CENP-A immunoblot shows a CENP-C/CENP-A adduct appearing at the top of the membrane. (D) Possible model summarizing the results obtained in B and C.

3.1.5 Reconstituted CENP-C^{F} localizes at the centromere and compensates the loss of endogenous CENP-C during mitosis

To test, if reconstituted CENP-C^{F} localizes at the centromere and allows cells to achieve faithful chromosome congression during mitosis, we used electroporation (EP) as a tool to deliver CENP-C into living human cells, which is a suitable approach even for the delivery of large protein assemblies like the NDC80 or the MIS12 complexes (Alex et al., 2019). We introduced mCherry-tagged CENP-C^{F} into a pseudo-diploid colorectal human cancer DLD-1 cell line, that was created and kindly provided by Dr. Daniele Fachinetti. The cell line has both CENP-C alleles tagged with a tandem of yellow fluorescent protein (YFP) and an Auxin-inducible degron (AID) (Hoffmann et al., 2016). Furthermore, the E3 ubiquitin TIR1 ligase of *Oryza sativa* was stably incorporated into the genome to enable rapid degradation of CENP-C$^{YFP\text{-}AID}$ upon addition of the synthetic auxin variant indole-3-acetic acid (IAA) (Nishimura et al., 2009).

Upon addition of 500 µM IAA, the signal of endogenous CENP-C$^{YFP\text{-}AID}$ was significantly decreased after 15 min and completely abolished after 30 min (Figure 3-12 A and B). Next, we electroporated mCherry-CENP-C^{F} into the cell line and additionally treated cells with 500 µM IAA after the electroporation procedure. After 12 hours, we fixed the cells and checked the centromere localization of the electroporated mCherry-CENP-C^{F} protein. While we could not detect endogenous CENP-C$^{YFP\text{-}AID}$ at the centromeres, mCherry-CENP-C^{F} strongly localized at the centromeres (Figure 3-12 C). Next, we asked if CENP-C^{F} could furthermore functionally rescue the loss of endogenous CENP-C$^{YFP\text{-}AID}$. We therefore electroporated either mCherry or mCherry-CENP-C^{F} into the DLD-1 cell line and monitored mitotic cells for chromosome congression. Like in the previous experiment, we treated cells with 500 µM IAA directly after electroporating the proteins. As a control, mCherry electroporated cells were not treated with IAA, but with the equivalent volume of DMSO. After 24 hours recovery time, cells were treated with 10 µM STLC for 15 hours to arrest them in prometaphase (Figure 3-13 A). Cells were fixed 3 hours after washout of STLC and screened for chromosome congression. To prevent mitotic exit, cells were treated with 10 µM of the proteasome inhibitor MG132.

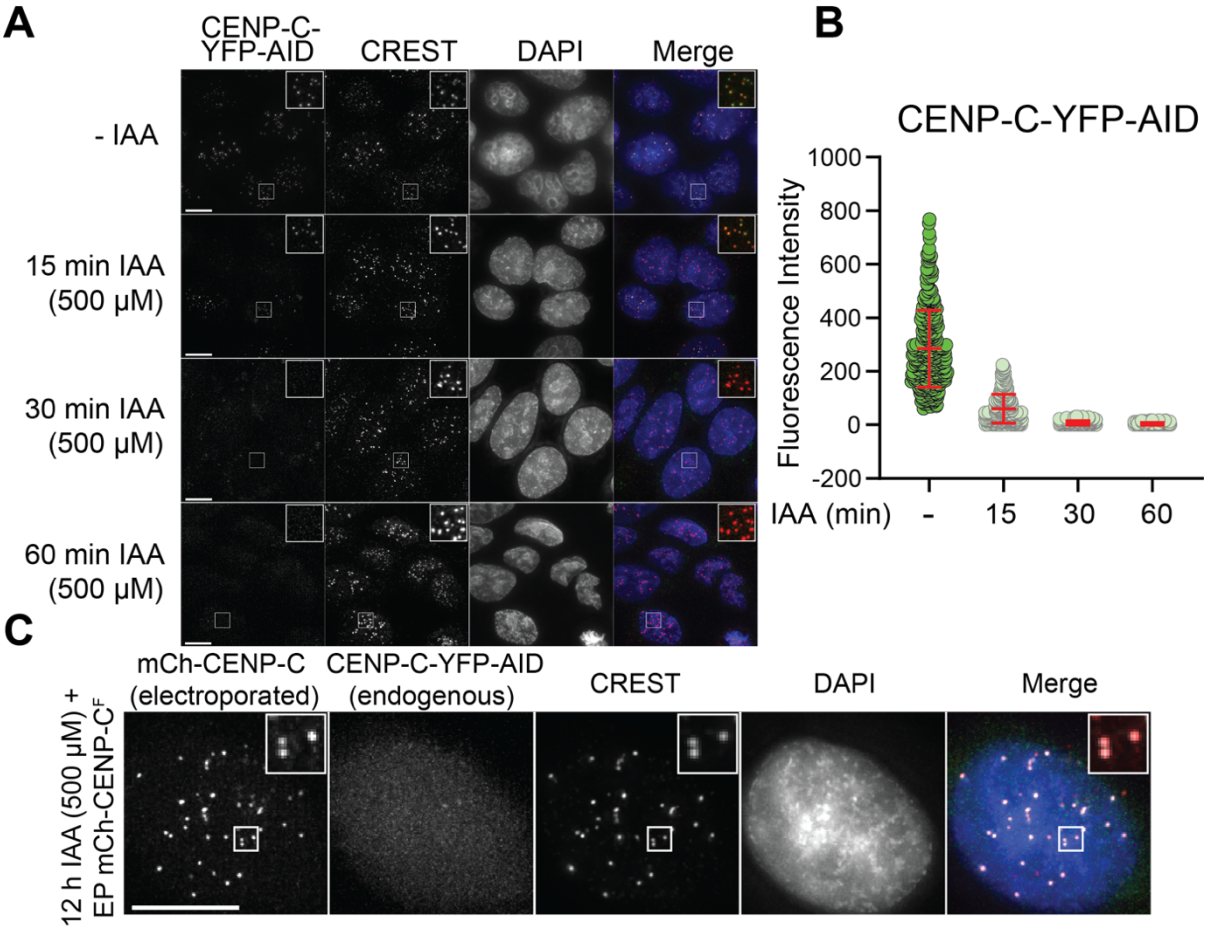

Figure 3-12: Electroporated recombinant mCherry-CENP-C localizes at centromeres in DLD-1 cells depleted of endogenous CENP-C

(A) Representative IF images showing the fluorescence of endogenous CENP-C-YFP-AID upon addition of IAA in fixated DLD-1 cells. Cells were fixed at the indicated time points. Centromeres were visualized by CREST sera and DNA was stained with DAPI. Scale bars represent 10 µm. (B) Quantification of the CENP-C-YFP-AID fluorescence of the experiment shown in B. (C) Representative IF image showing the fluorescence of electroporated recombinant mCherry-CENP-C^F and endogenous CENP-C-YFP-AID. Cells were treated with IAA as indicated. Centromeres were visualized by CREST sera and DNA was stained with DAPI. Scale bars represent 10 µm.

Like before, mCherry-CENP-C^F efficiently localized at centromeres in the absence of endogenous CENP-C, whereas mCherry gave a diffused signal throughout the cytoplasm (Figure 3-13 B). 60 % of the cells, that were electroporated with mCherry, but not treated with IAA, showed a metaphase plate without lagging chromosomes. The majority of the other 40 % also showed a metaphase plate but still had 1-5 unaligned chromosomes. One reason for the relatively high basal error rate in chromosome congression of this cell line could be the incorporation of the bulky YFP-AID tag at the C-Terminus of CENP-C. However, IAA treatment of the cells electroporated with mCherry prevented chromosome congression in nearly all observed cells. Most of the cells were in an early prometaphase-like state or had more

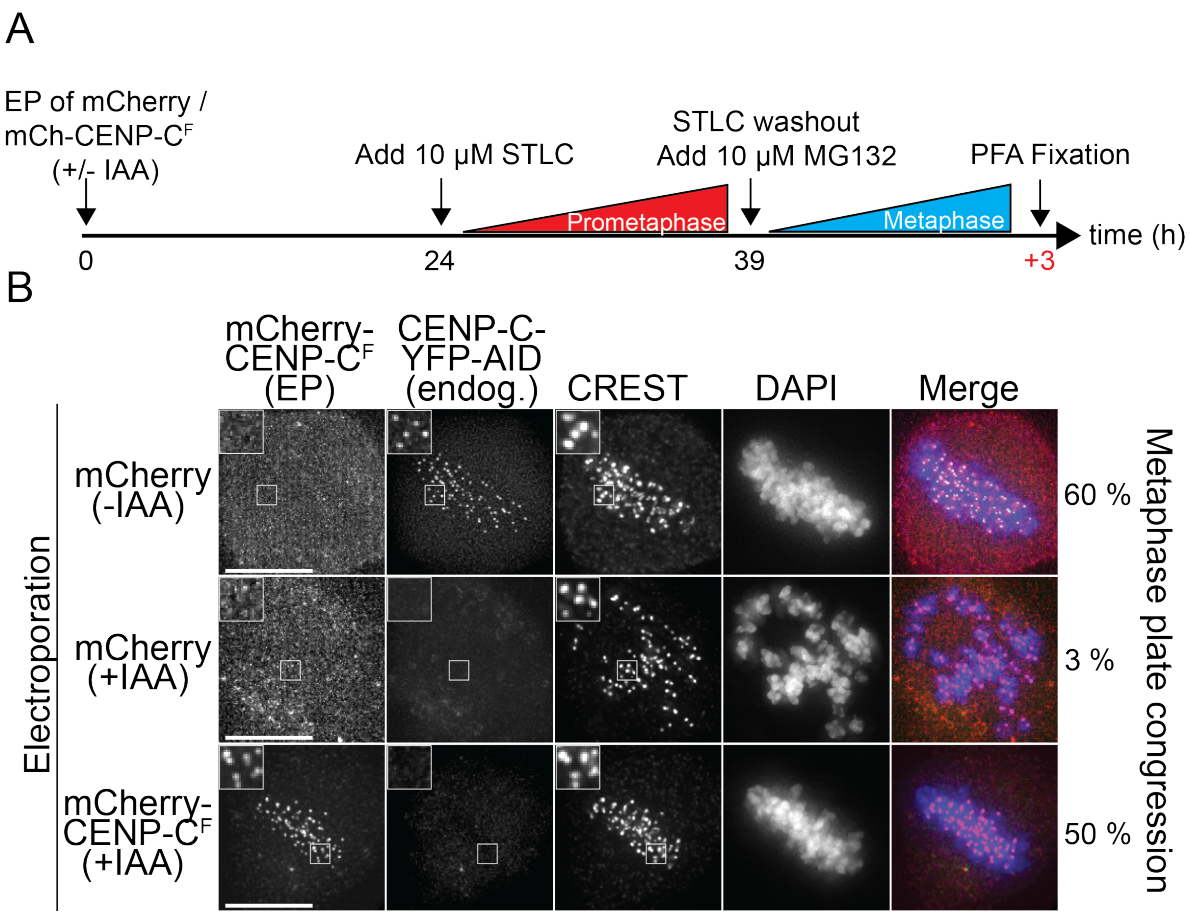

Figure 3-13 Electroporated mCherry-CENP-C compensates the loss of endogenous CENP-C in mitotic cells

(A) Schematic showing the experimental procedure for testing the ability of electroporated mCherry-CENP-C to complement the loss of endogenous CENP-C regarding chromosome congression in mitotic cells. Cells were fixed three hours after STLC washout and addition of MG132 and were screened for metaphase plate congression. (B) Representative IF images showing fluorescence of electroporated mCherry-CENP-C^F and endogenous CENP-C-YFP-AID in fixed DLD-1 cells. Centromeres were visualized using CREST sera, and DNA was stained with DAPI. Control cells were not treated with IAA and electroporated with mCherry. Scale bars represent 10 µm.

than five unaligned chromosomes. The observed phenotype clearly indicates, that CENP-C is a crucial component necessary for chromosome congression. While mCherry did not rescue the loss of endogenous CENP-C, mCherry-CENP-C^F restored the metaphase plate congression in 50 % of the observed cells, representing a recovery rate of 83 % compared to the control cells, which were not treated with IAA. Thus, mCherry-CENP-C^F electroporated into human cells is able to localize at the centromere in interphase and mitotic cells and furthermore forms the seed of a functional kinetochore that interacts with the mitotic spindle and enables chromosome congression.

3.1.6 The centromere recruitment of CENP-C^F is promoted by interactions with CENP-A and the CCAN

The centromere recruitment of CENP-C has been shown to be only partly dependent on the CENP-C motifs. While N-terminal CENP-C truncation mutants need a functional central motif for centromere localization, deletion of even both CENP-C motifs in the full-length protein still allows CENP-C to localize at the centromere, albeit to a lesser extent (Guo et al., 2017; Kato et al., 2013; Song et al., 2002; Watanabe et al., 2019). Furthermore, depletion of the CENP-HIKM and CENP-LN subcomplexes significantly reduced the centromere localization especially in interphase cells (McKinley et al., 2015). To test the dependence of CENP-C on CENP-A, CENP-HIKM and CENP-LN for its centromere recruitment, we purified four different mCherry-CENP-C^F variants (Figure 3-14 A), which we electroporated into DLD-1 cells, depleted of endogenous CENP-C.

The WT variant of mCherry-CENP-C^F could efficiently localize, as demonstrated before, at centromeres in the absence of endogenous CENP-C (Figure 3-14 B and C). The CENP-A binding mutant, which cannot interact with CENP-A nucleosomes *in vitro*, could also localize, but the measured fluorescence intensities were significantly lower compared to the WT CENP-C variant. The third CENP-C variant contained in sum eight Ala substitutions within the PEST region that abolish the binding of CENP-C to CENP-HIKM and CENP-LN (Klare et al., 2015; Pentakota et al., 2017). Compared to the CENP-A binding mutant, the CENP-HIKM/-LN binding mutant was only visible at a fraction of centromeres and created a diffuse signal in the nucleus of the cells, indicative of partly impaired kinetochore binding. Combining the mutations that disrupt the binding to CENP-A, CENP-HIKM and CENP-LN completely prevented CENP-C from localizing at the centromere. This experiment demonstrates, that the localization of CENP-C at the centromere indeed does not solely depend on direct interactions with centromeric CENP-A nucleosomes, but even more requires interactions with the other CCAN members. Since CENP-HIKM and CENP-LN bind to CENP-A nucleosomes and CENP-C *in vitro* (Weir et al., 2016), they could mediate an indirect interaction between CENP-A and the CENP-C mutant unable to bind CENP-A on its own.

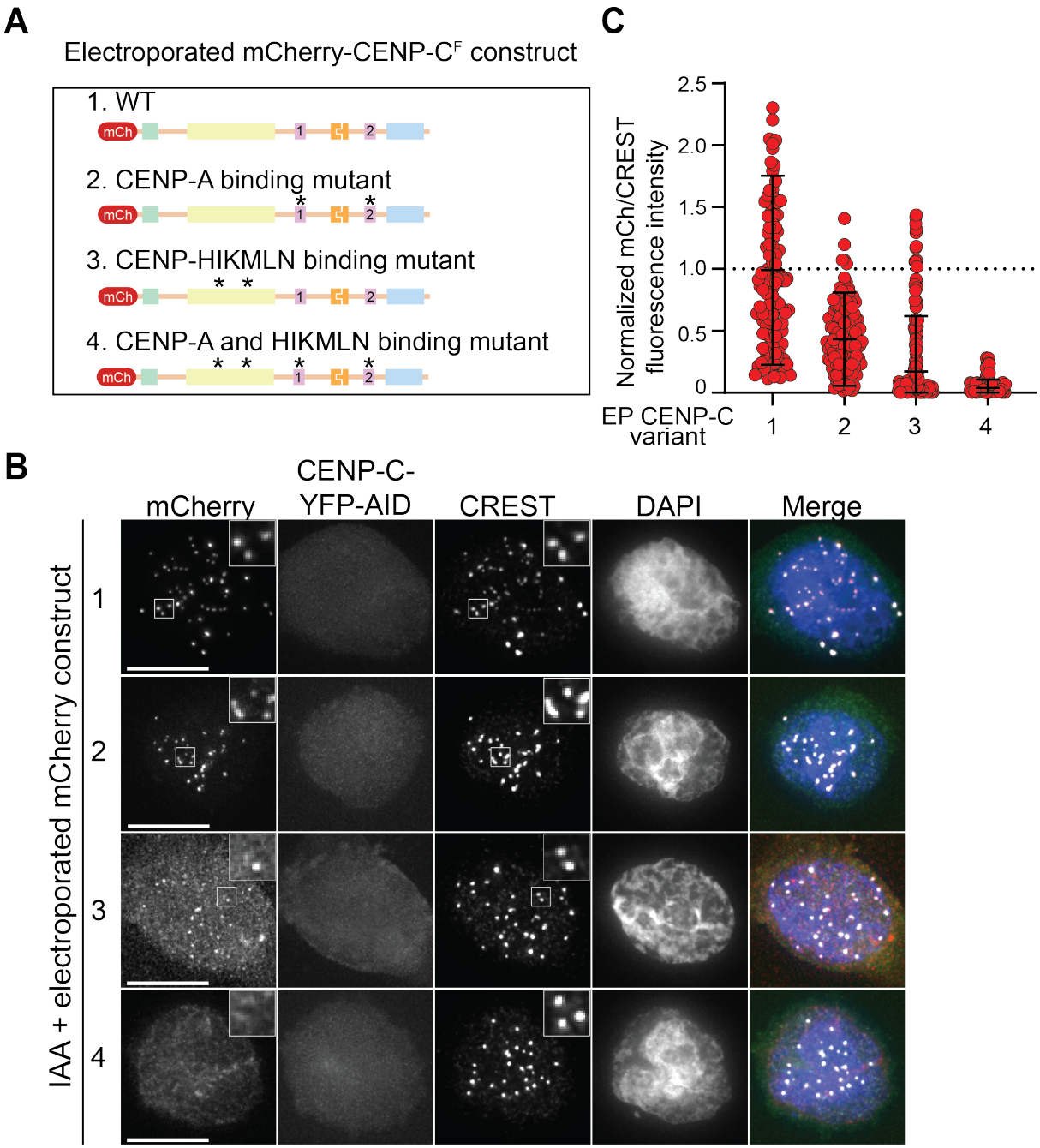

Figure 3-14 The centromere localization of CENP-C depends on the interactions with nucleosomes and the CCAN.

(A) Schematic representation of the electroporated mCherry-CENP-C variants. (B) Representative IF images of DLD-1 cells showing the centromere localization of the four electroporated CENP-C variants. All cells were treated with 500 µM IAA to rapidly deplete endogenous CENP-C carrying an Auxin-inducible degron. CREST sera were used to visualize the centromere, and DNA was stained with DAPI. Scale bars represent 10 µm (C) Quantification of the results shown in B. Each individual point represents a centromere intensity. Black bars represent the mean value +/- standard deviation. All quantified intensities were normalized to the mCherry/CREST ratio of the WT mCherry-CENP-C protein.

Using MBP-tagged variants of WT CENP-C^{F}, the CENP-A binding mutant and the CENP-A/-HIKM/-LN binding mutant as bait immobilized on amylose resin, we tried to recapitulate this possible scenario *in vitro*. As prey, we added either CENP-A^{NCP}, CENP-HIKM/-LN or both in combination (Figure 3-15 A). After a 1-hour incubation, we washed away the unbound prey and analysed the bound proteins by SDS-PAGE (Figure 3-15 B). WT MBP-CENP-C^{F} bound CENP-A^{NCP} and CENP-HIKM/-LN both in isolation and together. In contrast, the MBP-CENP-C^{F} CENP-A binding mutant was unable to directly interact with CENP-A^{NCP}, but it retained its ability to interact with CENP-HIKM/-LN. Remarkably, addition of CENP-A^{NCP} and CENP-HIKM/-LN together caused that CENP-A^{NCP} could be detected in the bound fraction. Compared to the

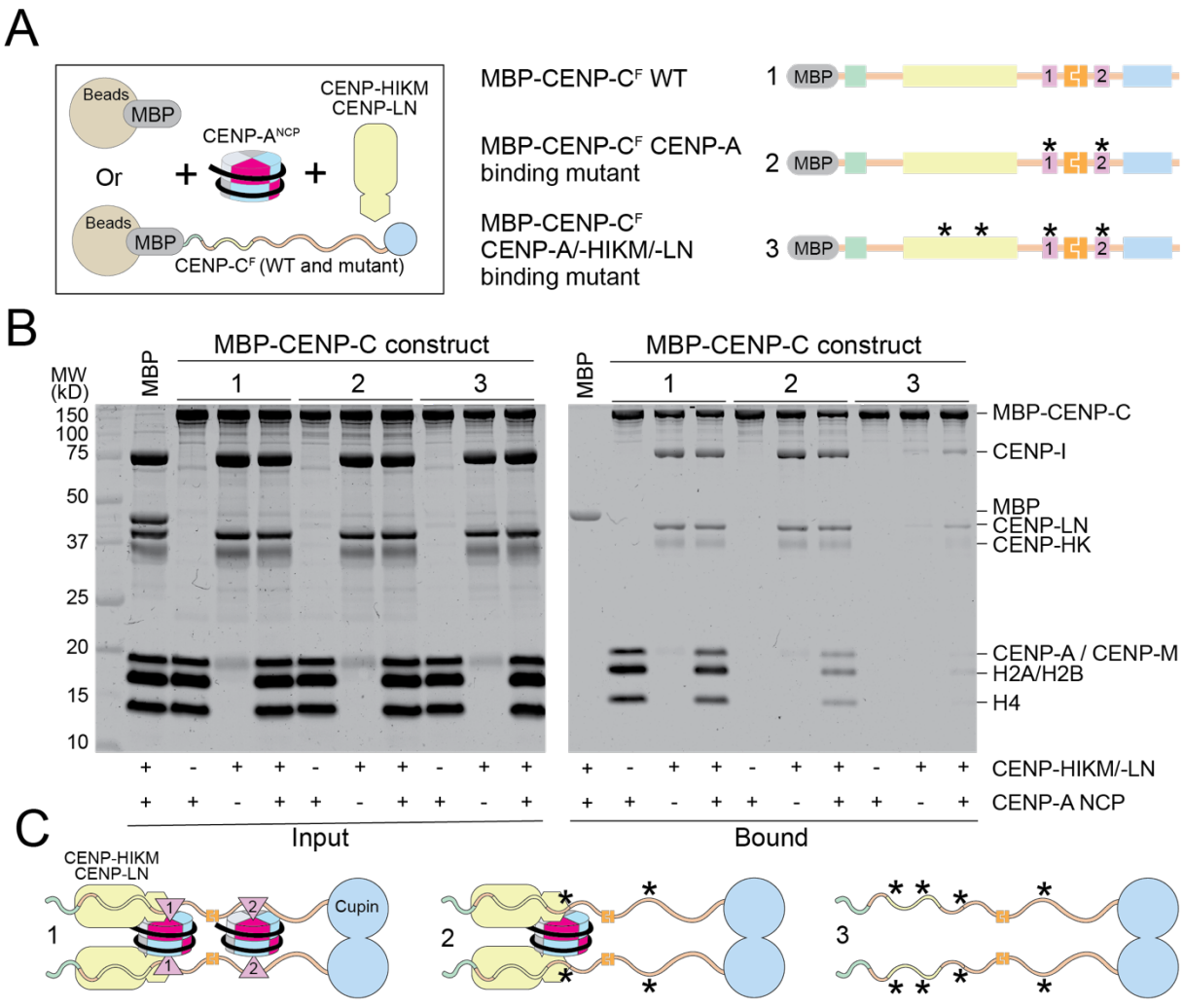

Figure 3-15 CENP-HIKM/-LN are able to recruit CENP-A^{NCP} to CENP-C

(A) Schematic representation of the amylose-resin pull-down assay to determine the interaction between three CENP-C variants, CENP-A^{NCP} and the CENP-HIKM/-LN complex. (B) Representative gel showing the result of the pull-down experiment. Bait was added as indicated above each lane. Prey was added as indicated below each lane. The gel was stained with CBB. (C) Graphical summary of the obtained results

MBP-CENP-C^{F} WT variant, the amount of bound CENP-A^{NCP} was considerably lower, indicating that CENP-HIKM/LN could only recruit one CENP-A^{NCP} to the MBP-CENP-C^{F} CENP-A binding mutant (Figure 3-15 C). Last, the MBP-CENP-C^{F} CENP-A/-HIKM/-LN binding mutant was unable to bind CENP-A^{NCP} nor CENP-HIKM/-LN. This experiment demonstrates, that CENP-HIKM and CENP-LN form a link between CENP-A and CENP-C even if there is no direct interaction between these two components. Furthermore, this result supports the previous localization experiment showing that CENP-C localizes at the centromere even when its nucleosome binding motifs have been mutated. The work *in vitro* strongly supports that the CENP-C^{F} CENP-A binding mutant is still able to interact with CENP-HIKM/-LN.

3.1.7 Dimerization of CENP-C is promoting centromere localization

Our localization studies demonstrate, that the centromere targeting of CENP-C depends on interactions with CENP-A and the CCAN members CENP-HIKM/-LN. Next, we aimed to investigate the contribution of the C-terminal Cupin dimerization domain to the centromere recruitment of CENP-C. In *S. cerevisiae* deletion of the Cupin domain results in temperature sensitive, slow growing strains (Cohen et al., 2008). In *X. laevis* a single point mutation within the Cupin domain reduces the signal of centromere-associated CENP-C by 40 % (Carroll et al., 2010). These findings demonstrate, that the Cupin domain might be important for the function of CENP-C. First, we checked if the purified C-terminal CENP-C construct MBP-CENP-C$^{721\text{-}943}$ dimerizes *in vitro*. Sedimentation velocity AUC analysis revealed, that this construct indeed forms a dimer (Figure 3-16 C).

Next, we tested the ability of mCherry-tagged C-terminal CENP-C constructs from human, *S. cerevisiae* and *D. melanogaster* to localize at centromeres in HeLa cells. A structural comparison of CENP-C Cupin domains revealed, that in organisms with regional centromeres the Cupin domains gained additional secondary structure elements which support dimerization (Chik et al., 2019). To test the ability of the mentioned Cupin domains to be recruited to the centromere, we co-transfected each of the three mCherry-Cupin constructs together with human GFP-CENP-C (Figure 3-16 A).

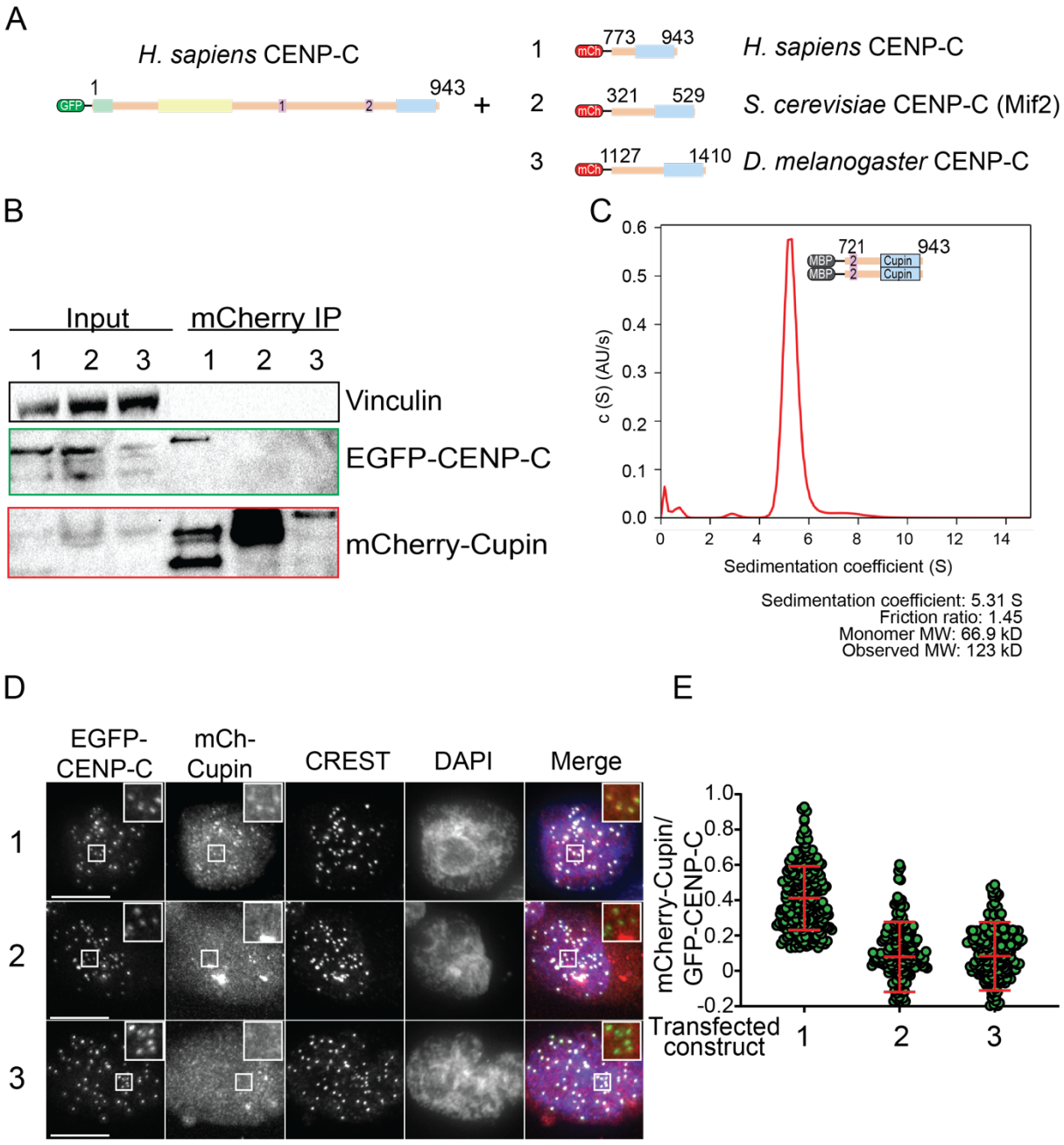

Figure 3-16 The Cupin domain of hs CENP-C localizes weakly at the centromere by dimerization with the full-length CENP-C protein

(A) Schematic showing the transiently transfected constructs for the experiments shown in B and D. Full-length GFP-tagged *hs* CENP-C was co-transfected with C-terminal CENP-C constructs containing the Cupin domains of either human, budding yeast or fly. (B) Immunoblot results of co-immunoprecipitation experiments from nuclear HeLa cell lysates. RFP-trap beads were used to immunoprecipitate the mCherry-tagged Cupin-domain constructs as indicated above each lane. Vinculin was detected as loading control of the input fractions. (C) Sedimentation velocity AUC results of MBP-CENP-C$^{721-943}$. The observed molecular weight of 123 kD indicates dimerization. (D) Representative IF images showing the fluorescence of EGFP-CENP-C and mCherry-Cupin constructs in fixed HeLa cells. The indicated co-transfected constructs are shown in A. Centromeres were visualized by CREST sera, DNA was stained with DAPI. Scale bars represent 10 µm. (E) Quantification of the results shown in D. Each point represents an individual centromere intensity. Red bars represent the mean values +/- standard deviation.

We found, that only the human mCherry-Cupin construct weakly co-localized with GFP-CENP-C, whereas the CENP-C Cupin domains from *D. melanogaster* and *S. cerevisiae* did not (Figure 3-16 D and E). To confirm this observation, we performed co-immunoprecipitation experiments with anti-mCherry nanobody coupled beads. The human mCherry-tagged Cupin construct, but not the ones from *D. melanogaster* and *S. cerevisiae*, interacted with GFP-CENP-C (Figure 3-16 B).Thus, our results indicate, that the Cupin domains from *D. melanogaster* and *S. cerevisiae* CENP-C cannot dimerize with the Cupin domain from human CENP-C. Furthermore, our results confirm a previous study reporting that the human Cupin domain weakly targets centromeres

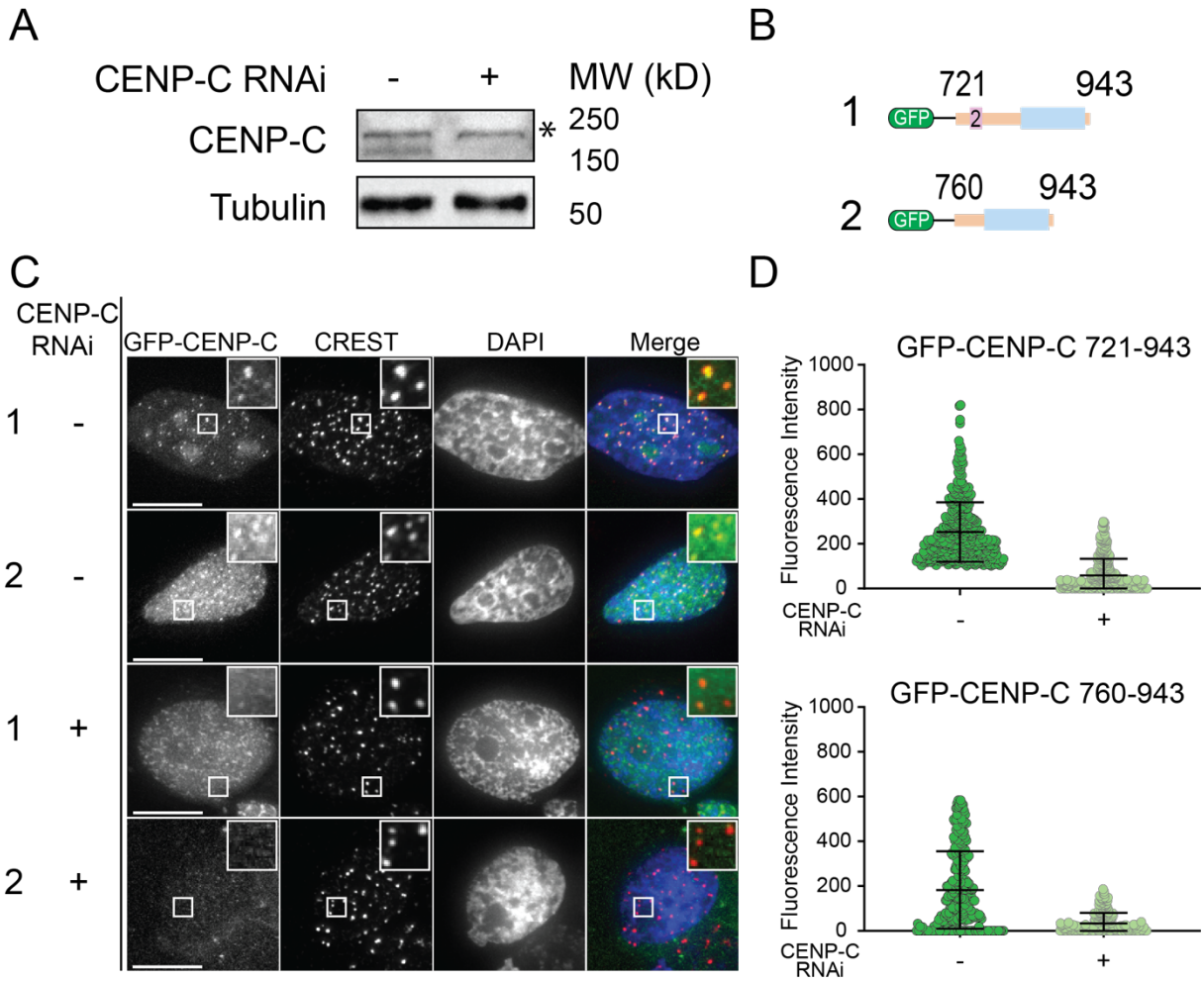

Figure 3-17 The CENP-C C-Terminus depends on endogenous CENP-C to localize at the centromere

(A) Immunoblot showing the RNAi depletion of CENP-C after 60 hours. The asterisk represents an unspecific band recognized by the CENP-C antibody. Tubulin was detected as loading control. (B) Schematic showing the expressed GFP-tagged CENP-C constructs of the experiment shown in C. (C) Representative IF images showing the fluorescence of the indicated expressed GFP-CENP-C constructs. Centromeres were visualized by CREST sera. Scale bars represent 10 µm. (D) Quantification of the results shown in C. Black bars represent the mean values +/- standard deviation.

(Trazzi et al., 2009). We hypothesized that the weak centromere targeting of the human Cupin domain construct depends on the presence of endogenous CENP-C. We therefore checked the centromere localization of two GFP-tagged C-terminal CENP-C constructs, CENP-C$^{721-943}$ and CENP-C$^{760-943}$ (Figure 3-17 B), in the presence and absence of endogenous CENP-C. While we induced the expression of the GFP-CENP-C constructs, we simultaneously treated cells with siRNA against CENP-C for 60 hours. We confirmed efficient depletion of CENP-C by Western Blot analysis (Figure 3-17 A). GFP-CENP-C$^{721-943}$, which harbours the conserved CENP-C motif and the Cupin domain, clearly localized at centromeres in the presence, but not in the absence, of endogenous CENP-C (Figure 3-17 C and D). Similarly, GFP-CENP-C$^{760-943}$, which lacks the conserved CENP-C motif, targeted centromeres in the presence of endogenous CENP-C, albeit much weaker than GFP-CENP-C$^{721-943}$. In CENP-C depleted cells, GFP-CENP-C$^{760-943}$ completely failed to localize like GFP-CENP-C$^{721-943}$. Thus, the Cupin domain itself does not promote centromere localization, but clearly depends on the presence of endogenous CENP-C to target the centromere.

Finally, we investigated the contribution of the Cupin domain to the centromere targeting in the context of full-length CENP-C. We created five GFP-CENP-C variants (Figure 3-18 A), namely WT GFP-CENP-C (1), GFP-CENP-C$^{1-772}$ (2) lacking the Cupin domain, GFP-CENP-C$^{1-772}$ fused to the Cupin domain of *S. cerevisiae* (3) or *D. melanogaster* (4) and CENP-C$^{1-772}$ fused to the LacI dimerization domain (5).

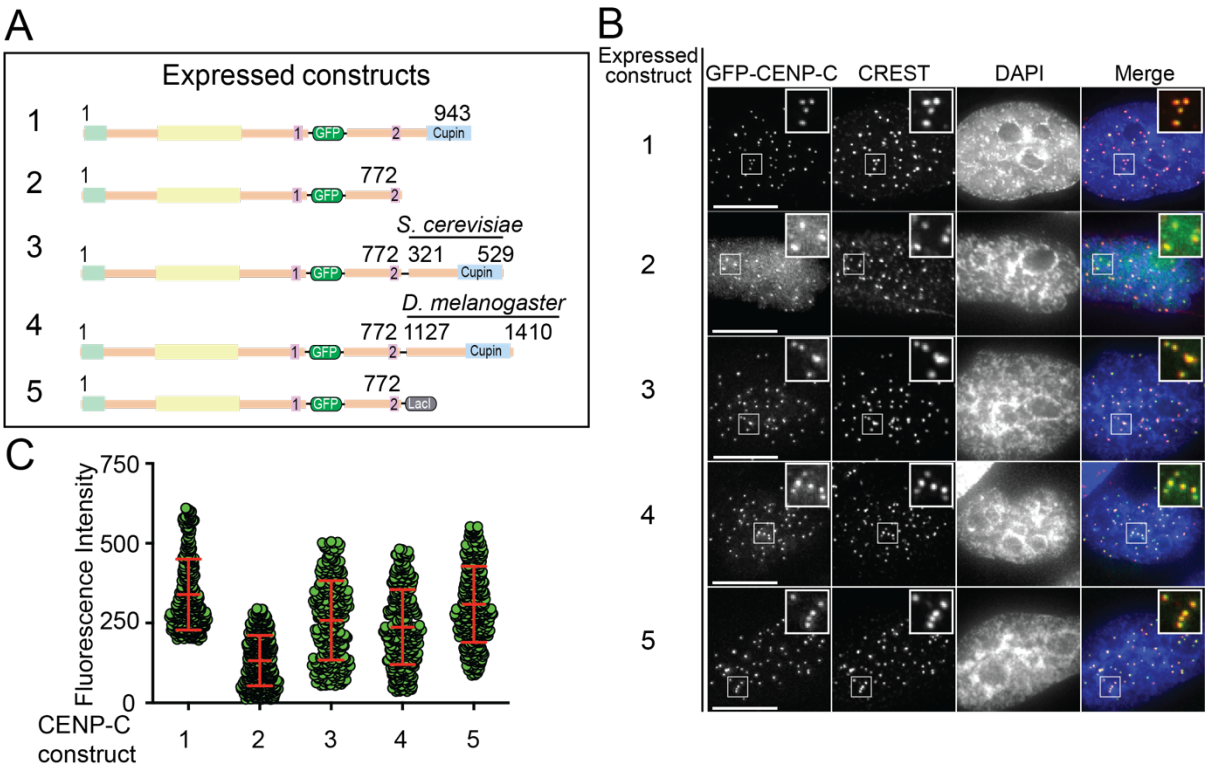

Figure 3-18 Dimerization of CENP-C facilitates centromere recruitment

(A) Schematic representation of the expressed GFP-CENP-C variants (B) Representative IF images of HeLa cells showing the centromere localization of the indicated GFP-CENP-C variants. CREST sera were used to visualize the centromere, and DNA was stained with DAPI. Scale bars represent 10 µm (C) Quantification of the results shown in B. Each individual point represents a centromere intensity. Red bars represent the mean value +/- standard deviation.

Remarkably, GFP-CENP-C$^{1\text{-}772}$ was recruited to the centromere much weaker than the other four expressed CENP-C variants (Figure 3-18 B and C). Furthermore, the two CENP-C chimeras and the LacI construct could localize at comparable, but slightly lower levels than WT GFP-CENP-C. These observations lead to the conclusion, that dimerization, no matter whether induced by the cognate human Cupin domain or by an orthologous Cupin domain, reinforces the affinity of CENP-C towards the centromere.

3.1.8 Reconstitution of defined recombinant kinetochore-dinucleosome particles

Having demonstrated that reconstituted CENP-C^{F} interacts with mono- and dinucleosomes as well as with the core CCAN members CENP-HIKM/-LN, we aimed to extend our biochemical reconstitution approach towards an as complete as possible recombinant kinetochore particle. We recently reconstituted a 26-subunit kinetochore particle, which contained nearly the entire CCAN and the KMN network (Pesenti et al.,

2018), but still lacked the CENP-TWSX complex and the full-length CENP-C protein. Besides CENP-C, that recruits the KMN network by its N-terminal MIS12 binding site, CENP-T forms a second axis providing connections towards the outer kinetochore in a CDK1 phosphorylation dependent manner (Gascoigne et al., 2011; Huis In 't Veld et al., 2016; Schleiffer et al., 2012; Screpanti et al., 2011). We therefore aimed to combine the CENP-C and CENP-T pathway on a dinucleosome structure to achieve the maximum recruitment of the outer kinetochore members by a completely reconstituted CCAN.

First, we reconstituted the CENP-C dependent pathway of MIS12/NDC80 complex recruitment. We immobilized either MBP-CENP-C^{F} WT or MBP-CENP-$C^{F\text{-}K10A/Y13A}$, a mutant unable to interact with the MIS12 complex (Screpanti et al., 2011), on amylose resin (Figure 3-19 A) and added the MIS12 and NDC80 complexes, either alone or in combination. The MIS12 complex used in this and all upcoming experiments contains a deletion mutant of DSN1, namely $DSN1^{\Delta 100\text{-}109}$, resulting in a ~90 fold tighter binding to CENP-C compared to the WT MIS12 complex due to the removal of an inhibitory fragment in DSN1 that binds to the CENP-C binding site in the Head1 region of the MIS12 complex (Petrovic et al., 2016). Neither CENP-C^{F} WT nor CENP-$C^{F\text{-}K10A/Y13A}$ were able to bind the NDC80 complex on its own (Figure 3-19 B).

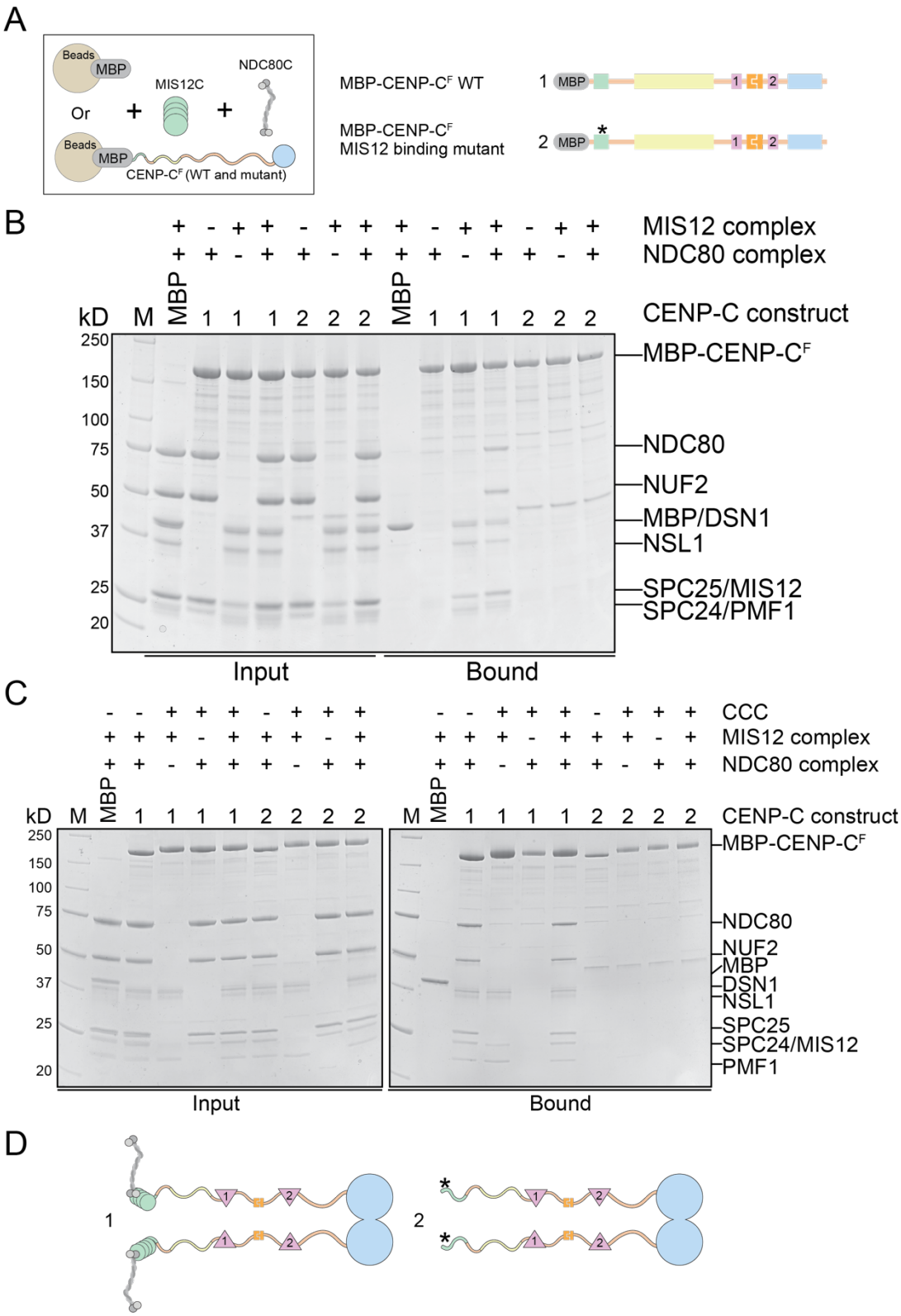

Figure 3-19 CENP-C recruits the NDC80 complex in a MIS12 complex dependent manner

(A) Schematic representation of the amylose-resin pull-down assay to determine the interaction between CENP-C^{WT}, CENP-C$^{K10A/Y13A}$, the MIS12 complex and the NDC80 complex. (B) Representative SDS-PAGE showing the result of the pull-down experiment. Bait was added as indicated above each lane. The gel was stained with CBB. (C) Representative SDS-PAGE of the pull-down experiment. In this experiment, CENP-C^{F} was additionally phosphorylated by CCC as indicated above each lane. (D) Graphical summary of the obtained results.

CENP-C^{F} WT interacted with the MIS12 complex and also with the NDC80 complex in a MIS12 complex dependent manner. In contrast, CENP-C$^{F\text{-}K10A/Y13A}$ was unable to bind the MIS12 complex and therefore could not interact with the NDC80 complex (Figure 3-19 B and D). We additionally checked, if phosphorylation of both CENP-C^{F} variants by CDK1-Cyclin B-CAK1 (CCC) would increase the amount of bound MIS12 or NDC80 complex. For this purpose, we phosphorylated CENP-C^{F} with CCC for 2 hours at 30 °C. Subsequently, we added the MIS12 and NDC80 complexes, either alone or in combination, and incubated the components for one further hour. After washing the beads, we could not see a difference of bound MIS12 and NDC80 complexes compared to unphosphorylated CENP-C^{F} in the SDS-PAGE. Thus, although both CENP-C^{F} variants were strongly phosphorylated by CCC, as can be seen in the SDS-PAGE (Figure 3-19 C), CCC phosphorylation did not alter the binding affinity between CENP-C and the MIS12 complex nor did it create additional binding sites.

Next, we aimed to reconstitute the CENP-T dependent pathway on solid phase. For this purpose, we co-purified Halo-tagged CENP-T together with MBP-tagged CENP-W. CENP-T can directly interact with two NDC80 complexes and can recruit one additional copy of NDC80 in a MIS12 complex dependent manner. All of these interactions depend on the CDK1 phosphorylation of three defined phosphorylation sites in CENP-T (Huis In 't Veld et al., 2016). In the pull-down experiment, we used two variants of CENP-TW, CENP-T^{WT}W and CENP-T$^{T11A/T85A}$W (Figure 3-20 A), which cannot bind the NDC80 complex (Huis In 't Veld et al., 2016). We incubated both CENP-TW variants either with an equimolar amount of MIS12 complex, a three-fold molar excess of NDC80 complex, or both. During the incubation, we added CCC to phosphorylate CENP-T. The efficient phosphorylation of CENP-T during the pull-down experiment was confirmed by SDS-PAGE (Figure 3-20 B), as we observed a shift of the CENP-T band in the bound fraction compared to the input fraction. As expected, CENP-T$^{T11A/T85A}$W did not bind the NDC80 complex in the absence of MIS12 complex, and the amount of recruited NDC80 complex was considered to be background binding. The addition of MIS12 complex enabled the recruitment of one NDC80 complex by CENP-T Ser201. In contrast, CENP-T^{WT}W interacted with the NDC80 complex in the absence of MIS12 complex. The amount of recruited NDC80 complex was visibly larger compared to the amount recruited by the NDC80 binding mutant in

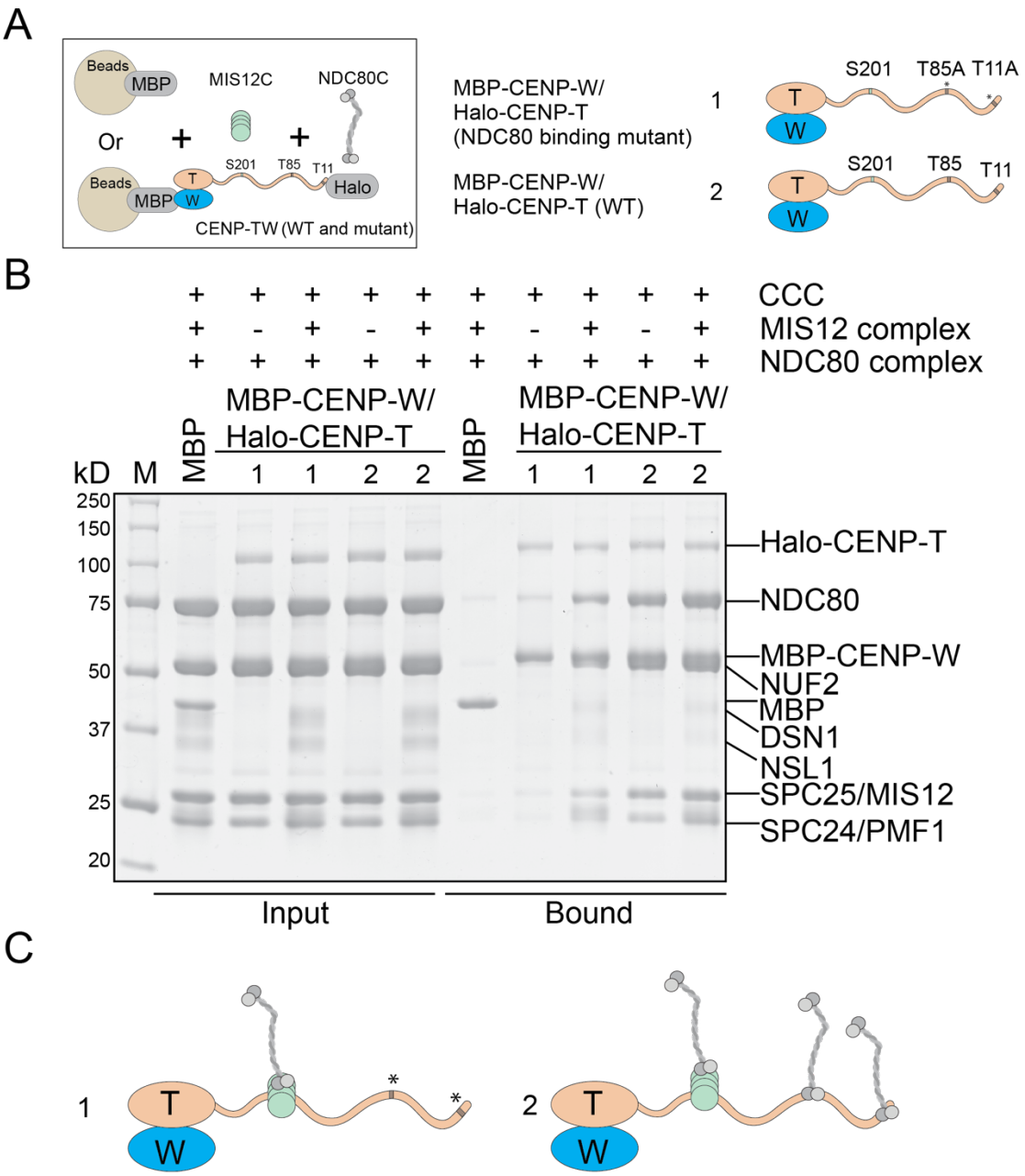

Figure 3-20 CENP-T recruits up to three NDC80 complexes

(A) Schematic representation of the amylose-resin pull-down experiment to determine the interaction between CENP-T^{WT}, CENP-T$^{T11A/T85A}$, the MIS12 complex and the NDC80 complex. (B) Representative gel showing the result of the pull-down experiment. Bait was added as indicated above each lane. Samples were phosphorylated by CCC as indicated above each lane. Gel was stained with CBB. (C) Graphical summary of the obtained results.

the presence of MIS12 complex, since CENP-T^{WT}W can directly bind two copies of NDC80 complex. Addition of MIS12 complex further enhanced the amount of recruited NDC80 complex. Quantification of the background subtracted NDC80 bands in the bound fractions of the four Halo-CENP-T/MBP-CENP-W pull-downs shown in Figure 3-20 B resulted in a ratio of 0:1:2.04:3.37 (from left to right). Thus, CENP-T needs to be phosphorylated by CDK1 at three phosphorylation sites for the maximum

recruitment of the NDC80 complex. Mutation of two CDK1 phosphorylation abolished the direct interaction between CENP-T$^{T11A/T85A}$W and two NDC80 complexes. The MIS12 complex, which binds to Ser201 of CENP-T, recruits one additional copy of NDC80 complex to CENP-T (Figure 3-20 C).

In the next experiment, we co-purified CENP-TW and CENP-XS, which form a stable, tetrameric complex (Nishino et al., 2012; Takeuchi et al., 2014). CENP-TWSX has been shown to interact weakly with the CENP-HIKM complex *in vitro* and to furthermore depend on CENP-HIKM for its centromere recruitment (Basilico et al., 2014). We hypothesized, that CENP-C^F bound to a CENP-A/H3 dinucleosome could provide a binding site for CENP-TWSX independently from CENP-HIKM. We furthermore tested the idea, that phosphorylation of CENP-C^F by CCC might enhance the binding of CENP-TWSX. We immobilized MBP-CENP-C^F bound to CENP-A/H3 dinucleosomes on amylose resin and added either CENP-TWSX alone, together with CENP-HIKM, together with CENP/-LN or together with CENP-HIKM/-LN (Figure 3-21 A). Furthermore, we tested all four conditions in the presence and absence of CCC phosphorylation. CENP-TWSX was already pre-phosphorylated by CCC during the purification. CENP-C was efficiently phosphorylated during the experiment as indicated by the shift of the CENP-C^F band in the bound fraction (Figure 3-21 B).

CENP-C^F bound to CENP-A/H3 dinucleosomes interacted with CENP-TWSX only weakly (Figure 3-21 B), and addition of CENP-LN did not enhance the binding. However, addition of CENP-HIKM, alone or in combination with CENP-LN, enhanced the binding of CENP-TWSX. Phosphorylation of CCC did not show any positive or negative effect, suggesting that CENP-C^F, although strongly phosphorylated by CCC, does not contain a CDK1 dependent binding site for CENP-TWSX. Thus, this experiment confirms that CENP-HIKM is the main interaction partner of CENP-TWSX. Despite previous reports of DNA binding by CENP-TW, the linker DNA of the dinucleosome did not strongly attract CENP-TWSX in the absence of CENP-HIKM.

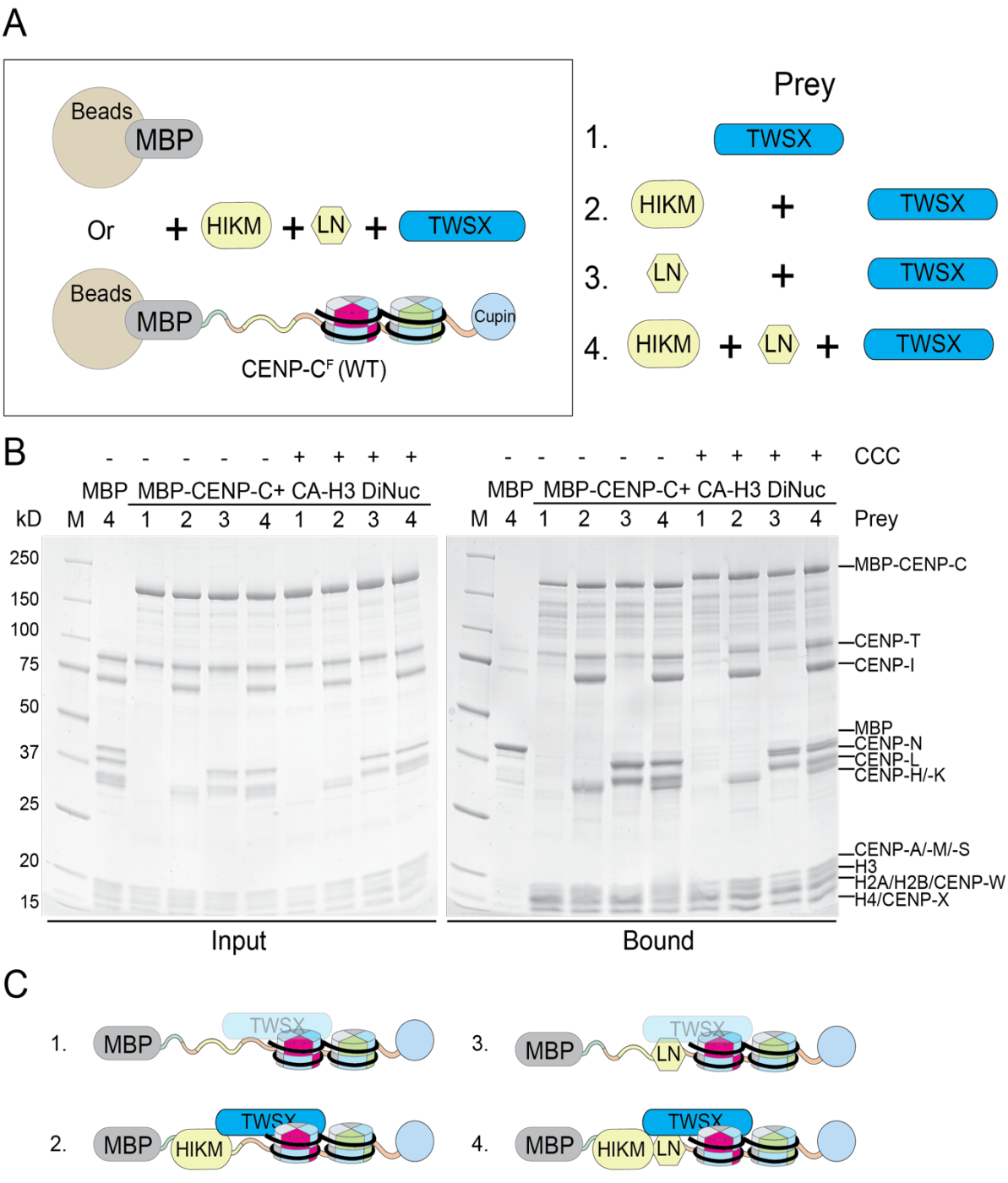

Figure 3-21 CENP-TWSX mainly interacts with the CENP-HIKM complex

(A) Schematic representation of the amylose-resin pull-down experiment to determine the binding partner of the CENP-TWSX complex (B) Representative gels showing the input fractions on the left side and the bound fractions on the right side. Prey was added as indicated by the numbers above each lane. Samples were unphosphorylated or phosphorylated by CCC as indicated. The gels were stained with CBB. (C) Graphical summary of the obtained results.

Finally, we reconstituted three kinetochore particles of different complexity immobilized on amylose resin (Figure 3-22 A). The minimal kinetochore particle contained MBP-CENP-C^{F} bound to CENP-A/H3 dinucleosomes, CENP-HIKM and CENP-LN. This kinetochore particle, due to the lack of CENP-T, can only interact with the outer kinetochore members through the CENP-C pathway. The second kinetochore particle additionally contained the CENP-OPQUR and CENP-TWSX complexes and therefore included the entire CCAN. The third particle we created was additionally phosphorylated by CCC to allow CENP-T to interact with the outer kinetochore members. We first reconstituted the CCAN particles as described. Subsequently, we added a sufficient amount of KMN (containing KNL1$^{2000-2316}$, MIS12 complex and NDC80 complex) to saturate the MIS12 binding sites of CENP-C^{F} and CENP-T (Figure 3-22 B). Last, after washing away the excess of unbound KMN, we additionally added amounts of NDC80 complex to CCAN complexes 2 and 3 sufficient to saturate the two NDC80 binding sites of CENP-T.

The CCAN particle 1 containing the core CCAN subunits recruited all the KMN network components through the N-terminal MIS12 binding site of CENP-C. In the bound fraction of CCAN particle 2 we could additionally identify all the proteins of the CENP-OPQUR and CENP-TWSX complexes. However, although we added twice the amount of KMN network to this sample and furthermore added an excess of NDC80 complex, we could, if at all, detect a very small increase of bound KMN components compared to particle 1 (Figure 3-22 C). This demonstrates, that CENP-T, if unphosphorylated, cannot interact with the outer kinetochore. The slight increase of the KMN band intensities compared to particle 1 could be explained by the micromolar concentrations we used in this experiment that would allow residual interactions between unphosphorylated CENP-T and the KMN network. Strikingly, the CCAN particle 3 phosphorylated by CCC recruited a significantly larger amount of the outer kinetochore proteins. However, the amount of incorporated CENP-TWSX in particle 2 and 3 appeared to be sub-stoichiometric compared to the rest of the CCAN. We therefore conclude, that we did not incorporate two copies of CENP-TWSX into the kinetochore particles, but most probably one. In case one phosphorylated CENP-TWSX complex

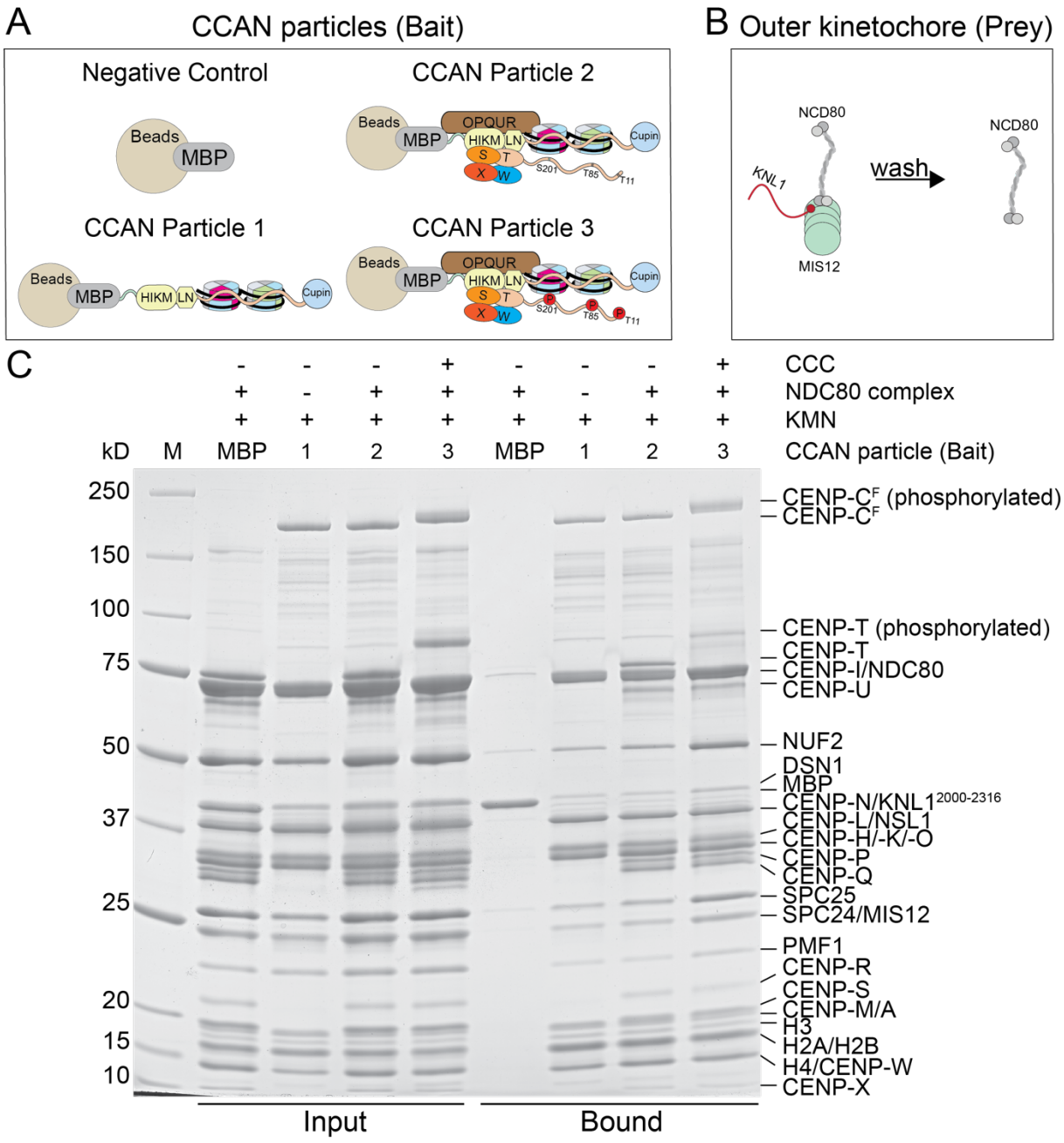

Figure 3-22 Reconstitution of a complete kinetochore particle

(A) Schematic representation of the different reconstituted CCAN particles immobilized on amylose-resin (B) Outer kinetochore members KMN and NDC80 complex were sequentially added as prey to the reconstituted particles shown in A. (C) Representative gel showing the result of the amylose pull-down experiment. Input fractions were loaded on the left side and the bound fractions on the right side of the gel. The reconstituted CCAN particle used as bait is indicated above each lane. The outer kinetochore members were added as indicated. Samples were unphosphorylated or phosphorylated by CCC as indicated. The gel was stained with CBB.

was present per CENP-C dimer in kinetochore particle 3, five NDC80 complexes should have been recruited, from which three are part of the KMN network and two are directly bound by CENP-T. Compared to particle 1, that does not contain CENP-TWSX and theoretically recruits two NDC80 complexes per CENP-C dimer, the band intensities of the NDC80 components would be increased by 150 %. Indeed, the band intensities of NDC80 and SPC25, which do not overlap with other protein bands in the SDS-PAGE, were increased by 245 % and 165 % in particle 3. Furthermore, the band intensities of the MIS12 complex members PMF1 and DSN1 were increased by 57 % and 34 % in particle 3 compared to particle 1. This strongly supports the assumption, that particle 3, in comparison with particle 1, contains one additional copy of the MIS12 complex which is recruited by CENP-T. Thus, we conclude, that particle 3 contains three MIS12 complexes and most likely five NDC80 complexes, whereas particle 1 contains two copies each of the MIS12 and the NDC80 complex.

However, to define the exact stoichiometry of the complex in a more quantitative manner, AUC experiments or quantitative mass spectrometry analyses will have to be performed. Nevertheless, we were able to reconstitute particles that contain the inner and outer kinetochore built on a full-length CENP-C protein bound to a CENP-A/H3 dinucleosome template. We furthermore demonstrated, that we need to incorporate both, CENP-C and CENP-T, to bind the maximum amount of outer kinetochore proteins. Furthermore, CENP-T had to be phosphorylated by CDK1 in order to recruit the KMN network.

3.2 Insights into the propagation of centromeric chromatin

In the second part of my PhD thesis, I will focus on the mechanism of CENP-A deposition, a crucial process that maintains the CENP-A levels at centromeres and occurs during early G1 phase. Although the CENP-A loading machinery, the Mis18 complex, has been identified and characterized in several recent studies, the mechanism of CENP-A replenishment remains poorly understood. The centromere receptor of the Mis18 complex has not been identified yet, but several studies proposed an interaction between CENP-C and M18BP1. To gain further insights into the complex CENP-A replenishment reaction, I first aimed to identify the interactome of the Mis18 complex by performing pull-down experiments from human cell lysates coupled with mass spectrometry analysis.

3.2.1 Identification of interaction partners of the CENP-A loading machinery

The Mis18 complex localizes at the centromere after mitotic exit in early G1 phase (Fujita et al., 2007). First, we wanted to confirm the G1 specific centromere localization of the Mis18 complex in HeLa cells. For that purpose, we generated a cell line, that stably co-expresses GFP-M18BP1 and mCherry-Mis18α. We treated the cells for 16 hours with 10 µM STLC to synchronize them in prometaphase (Figure 3-23 A). To achieve a homogenous cell population in a G1-like state, we did not wash out the STLC and let cells go through mitosis, but we treated the cells with a mixture of three mitotic kinase inhibitors to force cells out of mitosis rapidly. After having added 1 µM Reversine (MPS1 inhibitor), 9 µM RO3306, and 10 µM Roscovitine (CDK1 inhibitors), cells left mitosis within 20-30 minutes. We fixed cells 1 hour, 2 hours and 3 hours after mitotic release and checked the centromere localization of GFP-M18BP1 and mCherry-Mis18α. We detected both proteins at the centromere at all three time points. However, 1 hour after mitotic release nearly all centromeres were occupied by GFP-M18BP1 and mCherry-Mis18α, whereas after 2 and 3 hours many centromeres were already unoccupied. Furthermore, the mean signal intensities of the Mis18 complex proteins were strongly decreased after 3 hours (Figure 3-23 B and C). We subsequently performed pull-down experiments using RFP-trap and GFP-trap beads. We lysed cells 1 hour after mitotic release and purified the chromatin fraction by com-

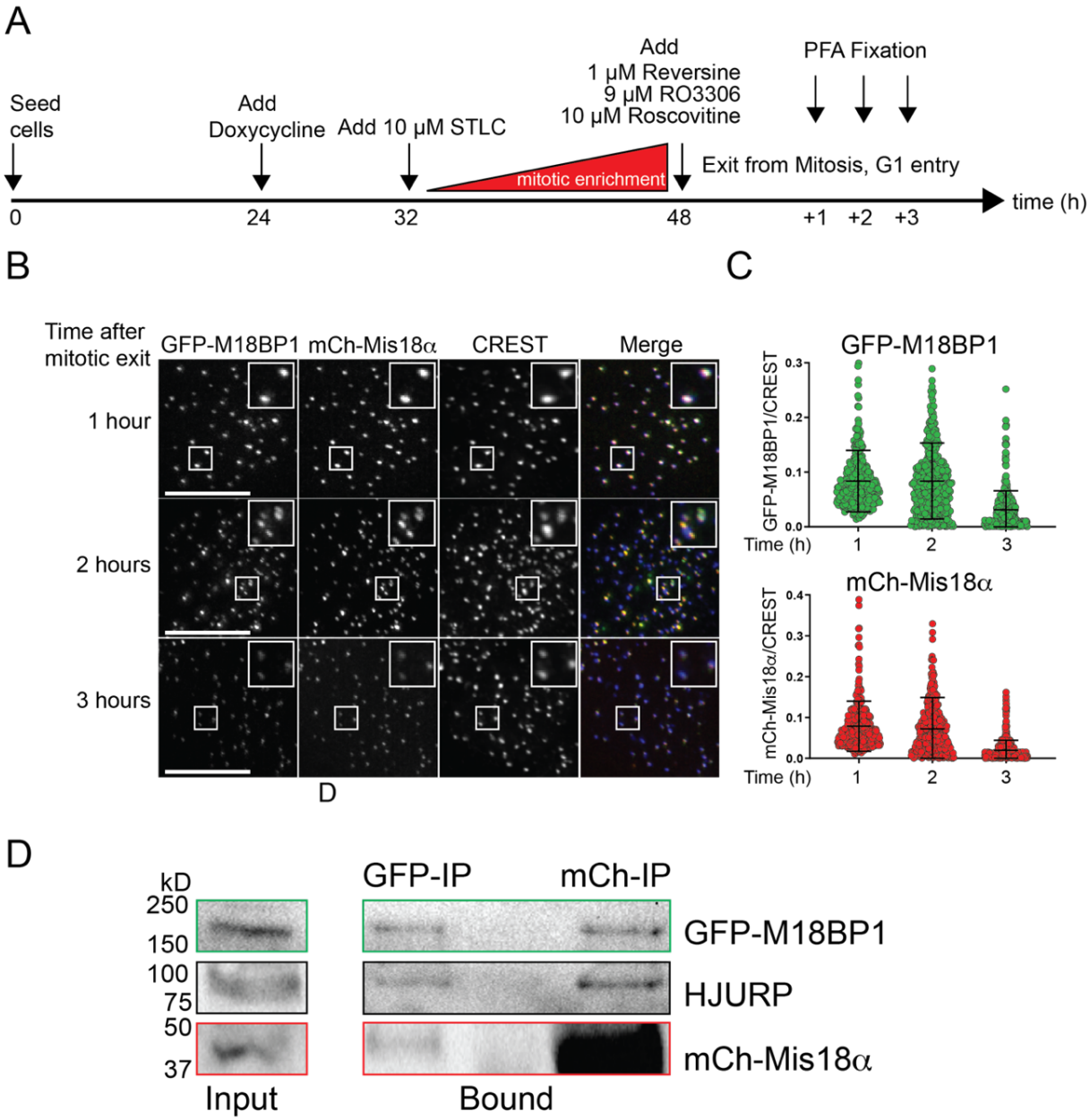

Figure 3-23 The Mis18 complex localizes at the centromere after mitotic exit

(A) Schematic showing the experimental procedure to investigate the time window of Mis18 complex centromere localization. Rapid mitotic exit was induced by addition of Reversine, RO3306 and Roscovitine to STLC arrested HeLa cells. Cells were fixed at the time points +1 h, +2 h and +3 h after mitotic exit. (B) Representative IF images showing fluorescence of GFP-M18BP1 and mCherry-Mis18α at the indicated time points. Centromeres were visualized by CREST sera. Scale bars represent 10 µm. (C) Quantification of the results shown in B. Each individual point represents a centromere intensity. Black bars represent the mean value +/- standard deviation. The fluorescent intensities of GFP-M18BP1 and mCherry-Mis18α were normalized to CREST. (D) Immunoblot results of co-immunoprecipitation experiments from nuclear HeLa cell lysates. GFP-Trap beads were used to immunoprecipitate GFP-M18BP1, RFP-Trap beads were used to immunoprecipitate mCherry-Mis18α from the same lysate. Cells were harvested and lysed one hour after mitotic exit.

bining sonication and benzonase treatments. mCherry-Mis18α was efficiently enriched on the RFP-trap beads, and furthermore we detected GFP-M18BP1 and HJURP, the CENP-A specific chaperone, by Western blotting (Figure 3-23 D). The co-immunoprecipitation of GFP-M18BP1 was less efficient, but HJURP and GFP-M18BP1 were detected at similar levels compared to the mCherry-Mis18α pull-down indicating that GFP-M18BP1 might be the limiting factor and mCherry-Mis18α was expressed at much higher levels.

Next, we analysed the IPs by mass spectrometry to identify proteins that specifically interact with the Mis18 complex in early G1 phase and that therefore could be potentially involved in the CENP-A replenishment reaction. We identified all core components of the CENP-A loading machinery in the mCherry-Mis18α and the GFP-M18BP1 IPs (Figure 3-24 A and B, highlighted in green). Strikingly, PLK1 was highly enriched in both IPs (highlighted in yellow), suggesting an important role of this particular kinase in the CENP-A loading reaction as it has been previously proposed (McKinley and Cheeseman, 2014). Furthermore, the pentameric Condensin II complex (highlighted in purple) was equally enriched in both IPs. Condensin II has been

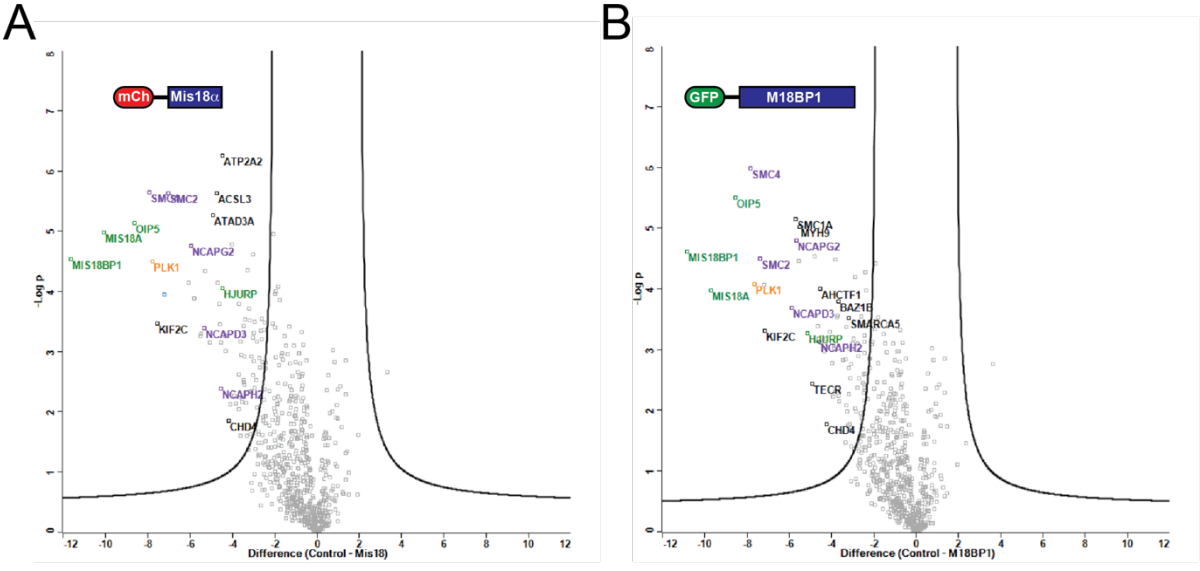

Figure 3-24 The Mis18 complex strongly interacts with PLK1 and the Condensin II complex

Volcano Blots showing the significant interaction partners of (A) mCherry-Mis18α and (B) GFP-M18BP1. The members of the Mis18 complex including HJURP are highlighted in green, PLK1 is highlighted in orange, the Condensin II complex is highlighted in purple. The y axis shows the negative logarithm of the p value, the x axis shows the binary logarithm of the fold change between the IP experiment and the control experiment. The black curves indicate a p-value of 0.05 with all the points left of the curve having a p-value <0.05. The samples were analysed as technical triplicates and potential candidates were omitted, if they were identified in less than two out of three measurements. The statistical analysis was performed with the software Perseus. OIP5 = Mis18β

proposed to be a crucial component for the CENP-A loading reaction (Barnhart-Dailey et al., 2017; Bernad et al., 2011). Although CENP-C was identified in the Mis18α and M18BP1 interactome, it was only enriched in one of three technical replicates and therefore not considered as a significant binding partner. Among the proteins, that were present in both IPs, we also identified CENP-V, components of the cohesin complex, the microtubule depolymerizer KIF2C and BAZ1B, which is part of the WICH chromatin remodeler complex. Due to its very high abundance in both IPs, we focused on PLK1 in our next experiments.

3.2.2 Investigating the interaction between PLK1 and the Mis18 complex

The PLK1 localization at the centromere has been shown to be dependent on M18BP1 (McKinley and Cheeseman, 2014). We confirmed a co-localization of M18BP1 and PLK1 in early G1 cells (Figure 3-25 A and B). PLK1 furthermore localized at the midbody since it is crucial for the initiation of cytokinesis (Petronczki et al., 2007). Strikingly, when we treated cells for 48 hours with M18BP1 siRNA, M18BP1 and PLK1 centromere localization was completely abolished. However, PLK1 still localized efficiently at the midbody. This observation implies that M18BP1 itself, or an Mis18 complex member, is the PLK1 receptor during early G1 phase enabling its centromere localization. Next, we wanted to investigate, whether the centromere localization of the Mis18 complex and PLK1 depends on the catalytic activity of PLK1 kinase. For that purpose, we treated cells co-expressing GFP-M18BP1 and mCherry-Mis18α with 10 µM BI2536, a specific small-molecule PLK1 inhibitor (Steegmaier et al., 2007), for 3 hours. Cells were additionally treated with siRNA against endogenous M18BP1.

We detected the Mis18 complex and PLK1 co-localizing at centromeres in early G1 cells, that were not treated with BI2536 (Figure 3-25 C and D). In cells treated with BI2536, GFP-M18BP1 and mCherry-Mis18α still localized at the centromere, but the signal intensities were reduced. Strikingly, the centromere localization of PLK1 was strongly impaired in most of the cells. Thus, the catalytic activity of PLK1 is indeed required for its efficient co-localization with the Mis18 complex at the centromere. Eight M18BP1 sites have been identified to be phosphorylated by PLK1 *in vitro* (McKinley and Cheeseman, 2014). Interestingly, an M18BP1 1-490 truncation mutant harbouring four of eight identified PLK1 phosphorylation sites localized at the centromere and

rescued CENP-A loading in the absence of endogenous M18BP1. Alanine substitutions of these four PLK1 sites abolished the ability of M18BP1 to localize at the centromere and load new CENP-A (McKinley and Cheeseman, 2014). From the four PLK1 sites, S93 is in close proximity to the binding sites of Mis18α and Mis18β, namely T40 and S110 (Pan et al., 2017). We decided to generate a stable cell line expressing the point mutant GFP-M18BP1^{S93A} and to check its ability to localize at the centromere in the presence and absence of endogenous M18BP1. Furthermore, we checked if M18BP1 is phosphorylated by PLK1 using a specific antibody against M18BP1 pT702 (McKinley and Cheeseman, 2014).

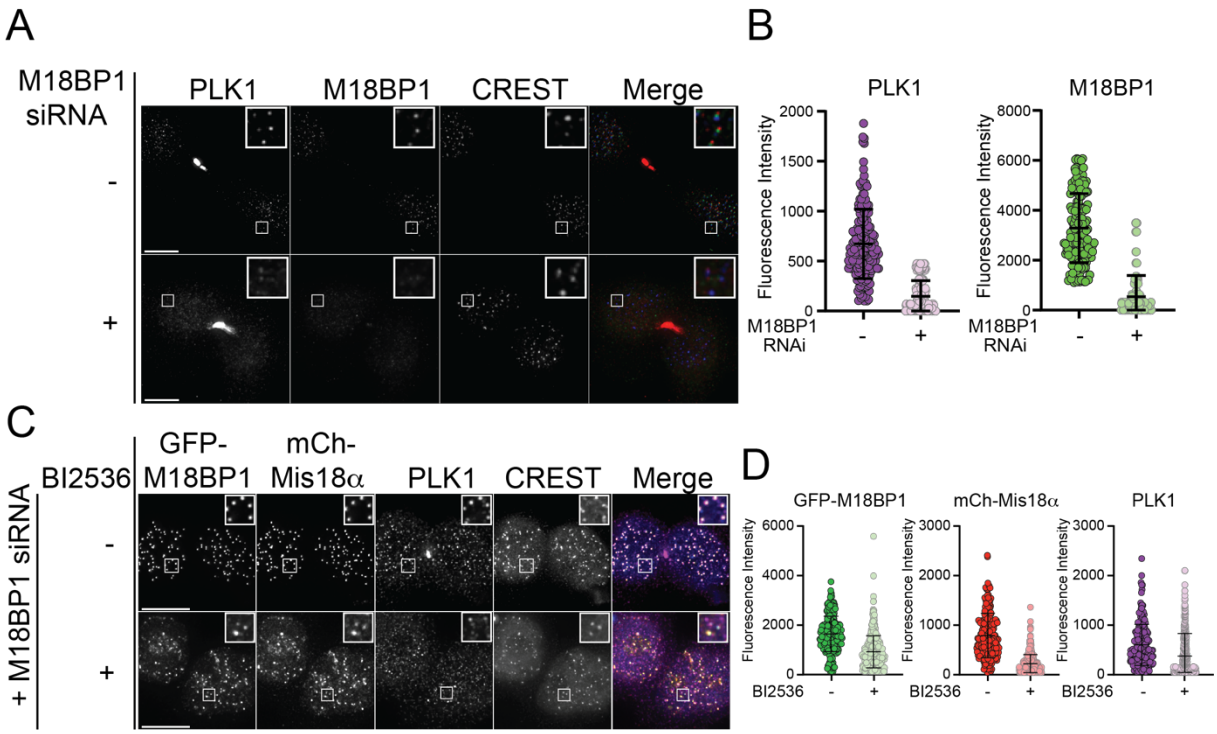

Figure 3-25 PLK1 and M18BP1 co-localize at the centromere in early G1 phase

(A) Representative IF images showing the fluorescence of PLK1 and M18BP1. Centromeres were visualized by CREST sera. Cells were treated with M18BP1 siRNA as indicated. Scale bars represent 10 µm. (B) Quantification of the results shown in A. Each point represents an individual centromere intensity. Black bars represent the mean value +/- standard deviation. (C) Representative IF images showing the fluorescence of GFP-M18BP1, mCherry-Mis18α and PLK1. Cells were treated with 10 µM PLK1 inhibitor BI2536 as indicated. Centromeres were visualized by CREST sera. Scale bars represent 10 µm. (D) Quantification of the results shown in C. The quantification was performed in the same way described in B.

GFP-M18BP1^{S93A} localized at the centromere in the presence of endogenous M18BP1 (Figure 3-26 A and B). We also detected a centromere signal of the M18BP1 pT702 antibody. In case we treated cells with 10 µM BI2536, both signals were severely reduced. In cells treated with M18BP1 siRNA, we did not detect a centromere signal of GFP-M18BP1^{S93A} and M18BP1 pT702, independently of BI2536 treatment. Thus, unlike WT GFP-M18BP1, the expressed GFP-M18BP1^{S93A} mutant depends on the presence of endogenous M18BP1 for its centromere localization, most likely mediated by oligomerization with the endogenous Mis18 complex proteins.

The M18BP1 pT702 antibody was unable to distinguish between endogenous and transgenic M18BP1 in IF. We therefore analysed the cell lysates of all four conditions by Western blotting (Figure 3-26 C and D). We detected two different species of M18BP1 using the pT702 antibody and an M18BP1 antibody, because the GFP-tagged transgene is 25 kD larger in size. We normalized all band intensities to the endogenous pT702 band of the untreated cells (first lane in Figure 3-26 C). In the untreated sample, the pT702 signal of endogenous M18BP1 was more than 10 times stronger compared to the expressed GFP-M18BP1^{S93A} mutant, although the transgene was present at higher levels than the endogenous protein. Treatment with BI2536 reduced the pT702 signal of endogenous M18BP1 by 80 %, while it abolished completely the signal of the transgene. When we treated cells with M18BP1 siRNA, we did not detect any endogenous signals of M18BP1 or M18BP1 pT702 indicating an efficient depletion.

Strikingly, the pT702 signal of the expressed point mutant was slightly increased in the absence of endogenous M18BP1. However, the normalized band intensity did not exceed 20 %. Thus, the alanine substitution of M18BP1 S93 caused a strong reduction of T702 PLK1 phosphorylation and a centromere localization defect in the absence of endogenous M18BP1. The S93 PLK1 phosphorylation site is therefore crucial for the phosphorylation of at least one further PLK1 site, T702. How the S93A substitution abrogates the phosphorylation of T702 and how PLK1 promotes the centromere localization of the Mis18 complex, remains to be investigated.

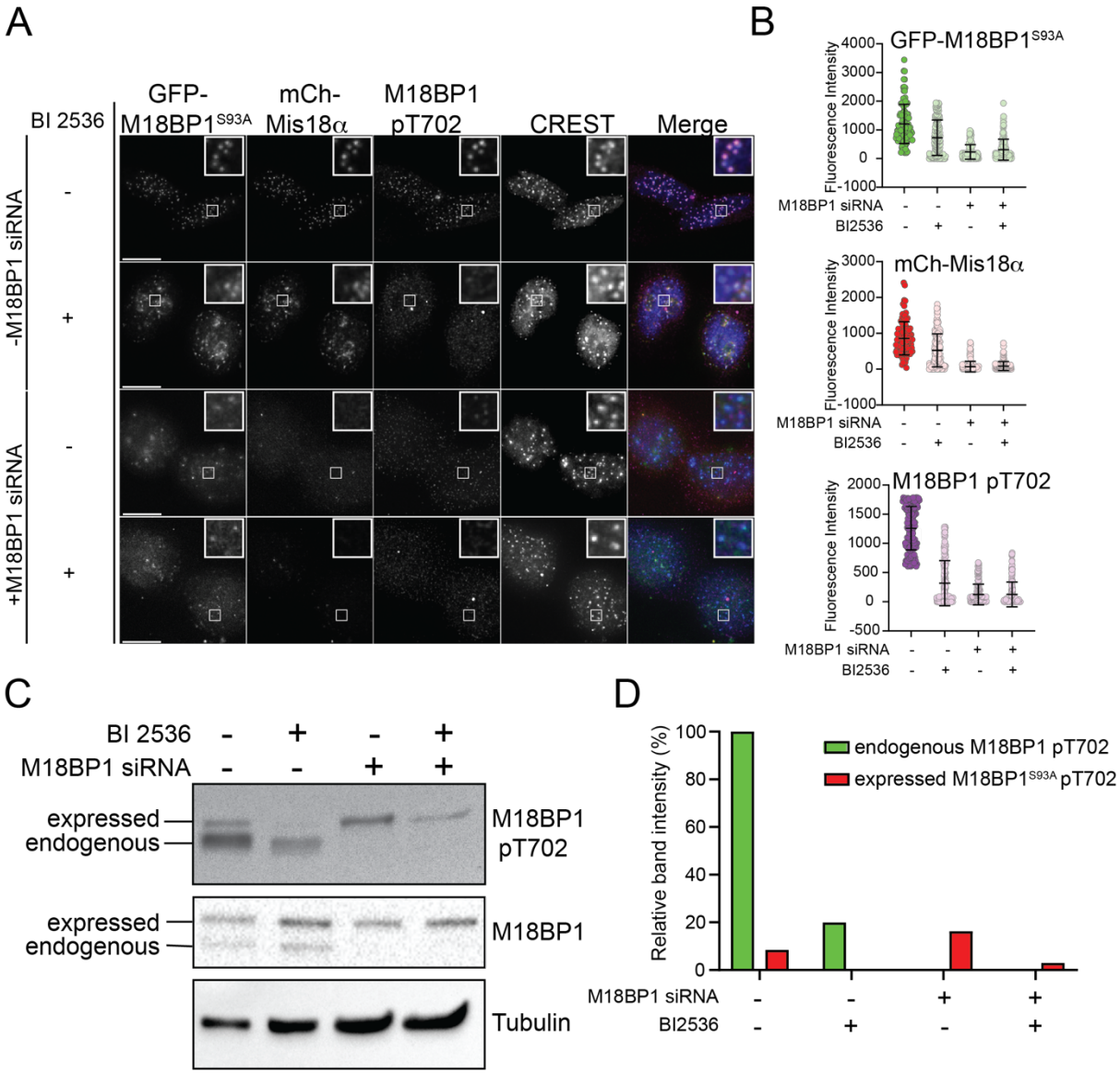

Figure 3-26 Ser93 of M18BP1 is a PLK1 phosphorylation site important for centromere localisation

(A) Representative IF images showing the fluorescence of GFP-M18BP1, mCherry-Mis18α and M18BP1pT702. Cells were treated with the PLK1 inhibitor BI2536 and M18BP1 siRNA as indicated. Centromeres were visualized by CREST sera. Scale bars represent 10 µm. (B) Quantification of results shown in A. Each point represents an individual centromere intensity. Black bars represent mean values +/- standard deviation. (C) Immunoblot showing the amount of phosphorylated T702 of M18BP1. Cells were treated as indicated above each lane. Tubulin is shown as a loading control. (D) Quantification of the pT702 Immunoblot shown in C. The measured intensities of phosphorylated T702 of endogenous and expressed M18BP1 were normalized to tubulin, which was used as an internal loading control. Subsequently, the intensities were normalized to the signal derived from the endogenous M18BP1 in lane 1.

3.2.3 The centromere localization of M18BP1 in early G1 phase requires CENP-C

Although the mass spectrometry analysis on the Mis18 complex IPs did not identify CENP-C as a prominent binding partner, we wanted to investigate whether the depletion of CENP-C using the AID system had a negative effect on the localization of M18BP1. We transiently transfected DLD1 CENP-C-AID cells with plasmids either co-expressing SNAP-M18BP1 and mCherry (1), SNAP-M18BP1 and WT mCherry-CENP-C (2) or SNAP-M18BP1 and mCherry-CENP-C lacking both nucleosome binding motifs (3) (Figure 3-27 B). Subsequently, we synchronized cells in G1 by a combined thymidine and STLC arrest. After washing out STLC, cells entered early G1 phase within 3 hours. We finally added a SNAP-SiR dye to the cells to ligate SNAP-M18BP1 with a fluorescent dye allowing its detection by fluorescence microscopy (Figure 3-27 A). We detected SNAP-M18BP1 localizing at centromeres in G1 cells, that were not treated with IAA and transfected with mCherry (Figure 3-27 C and D). However, IAA treatment severely reduced the ability of M18BP1 to localize at centromeres in cells transfected with mCherry. Expression of both mCherry-CENP-C variants rescued the centromere localization of M18BP1 to similar extents, although the CENP-C mutant localized much weakly than WT CENP-C. Thus, CENP-C, or a downstream CCAN component, is crucial for the recruitment of the Mis18 complex. However, the two nucleosome binding motifs of CENP-C do not seem to be necessary to recruit M18BP1. Thus, the exact binding site of the Mis18 complex still remains unclear and has to be defined in future cellular or *in vitro* experiments.

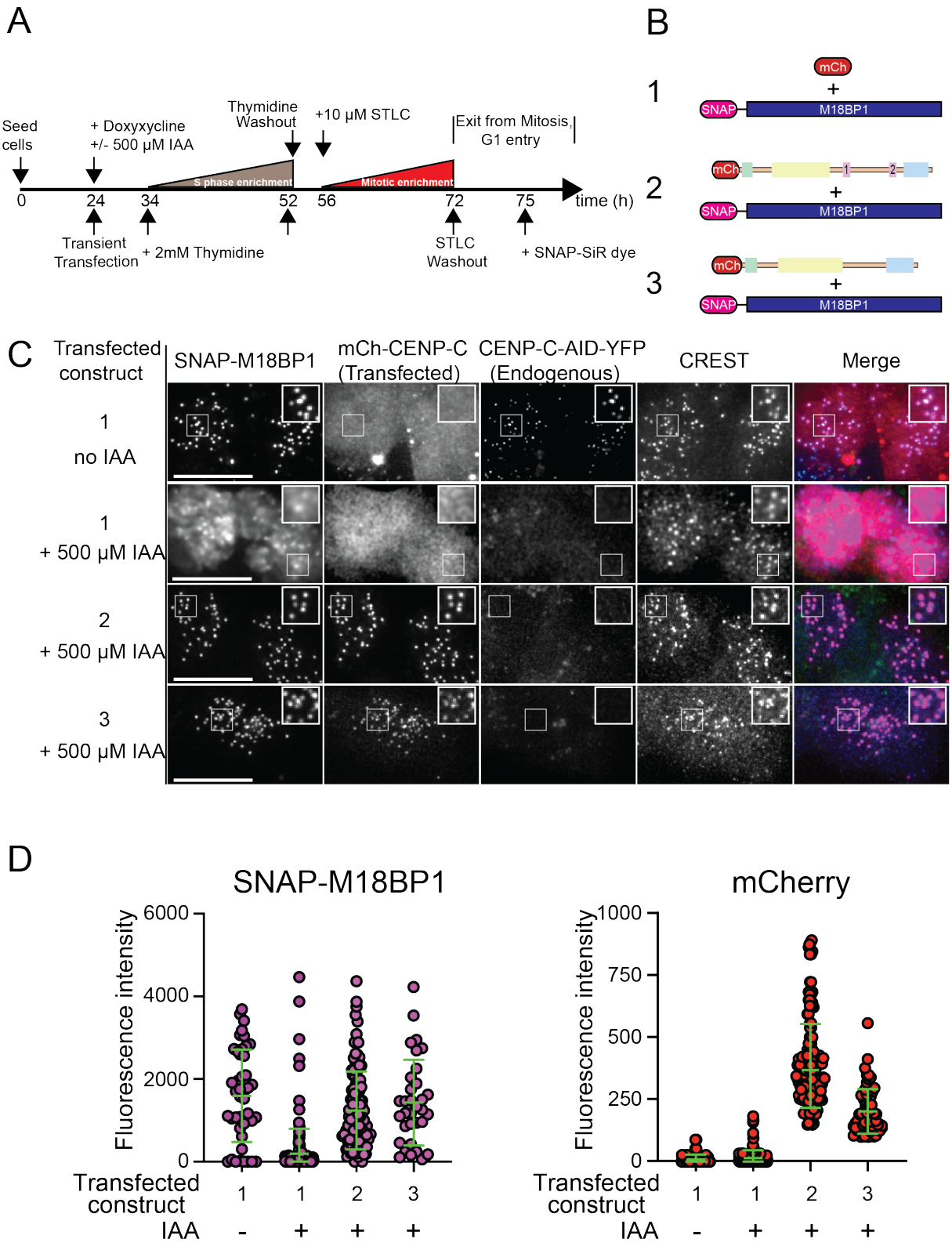

Figure 3-27 CENP-C is crucial for the centromere recruitment of M18BP1

(A) Schematic showing the experimental procedure to determine the interaction between CENP-C and M18BP1 in DLD-1 cells. To specifically label M18BP1, SNAP-SiR dye was added before the fixation of the cells. (B) Transfected constructs used in this experiment. (C) Representative IF images showing fluorescence of SNAP-M18BP1 after labelling with SNAP-SiR dye, mCherry-CENP-C and CENP-C-AID-YFP. Centromeres were visualized using CREST sera. Scale bars represent 10 µm. (D) Quantification of the results shown in C. Each individual point represents a centromere intensity. Green bars represent the mean value +/- standard deviation.

4 Discussion

On each human chromosome, the highly complex kinetochore provides a link between the centromeres and the spindle microtubules during mitosis, ensuring faithful chromosome segregation and genomic stability. Human regional centromeres are epigenetically defined by an enrichment of CENP-A nucleosomes which are embedded in megabase repeats of repetitive α-satellite DNA. In contrast to the point centromere of *S. cerevisiae*, that is defined by a single Cse4 nucleosome specifically recognized by Mif2, human CENP-C provides binding sites for two nucleosomes. The composition of the underlying dinucleosome structure might alternate during two key events in the cell cycle, which are linked to the CENP-A replenishment reaction in early G1 phase and the dilution of the CENP-A pool during DNA replication.

4.1 Biochemical and in-cell investigation of the human kinetochore architecture

This part of my PhD work focused on the biochemical reconstitution of full-length CENP-C, and the characterization of its interactions with centromeric nucleosomes as well as dinucleosomes of defined composition. Using reconstituted full-length CENP-C, I demonstrated that CENP-C binds two CENP-A mononucleosomes. Crosslinking experiments with CENP-A/H3 dinucleosomes revealed that the CENP-A portion preferentially binds to the central motif of CENP-C. By electroporating CENP-C into living human cells depleted of endogenous CENP-C, I confirmed the functionality of the recombinant protein during mitosis. Furthermore, I determined the crucial regions of CENP-C promoting its centromere recruitment. Last, I reconstituted extended kinetochore particles assembled on dinucleosome templates of different complexity. The amount of recruited outer kinetochore components could be controlled by the CDK1 phosphorylation status of CENP-T.

4.1.1 CENP-C interacts with two nucleosomes *in vitro*

We used two independent methods to demonstrate that reconstituted full-length CENP-C binds two CENP-A nucleosomes *in vitro*. First, we performed analytical SEC

experiments showing that one molar equivalent of CENP-C dimer binds two molar equivalents of CENP-A nucleosomes. When we inactivated one of two motifs, CENP-C only bound one molar equivalent of CENP-A. Using sedimentation velocity AUC, we furthermore deduced the stoichiometry of the CENP-C/nucleosome complexes from the obtained molecular weights. Again, we confirmed that if both CENP-C motifs are functional, one CENP-C dimer binds two CENP-A nucleosomes. Using amber codon suppression, we introduced the unnatural amino acid Bpa into close vicinity of both CENP-C motifs. UV light induced crosslinking revealed that the CENP-A portion of a CENP-A/H3 dinucleosome preferentially binds the central motif of CENP-C at saturating and sub-saturating concentrations.

The availability of a recombinant, well-behaved form of full-length CENP-C for our demanding *in vitro* experiments marks a critical achievement in the biochemical reconstitution of complex human kinetochore particles. Combining the results of the performed analytical SEC and AUC experiments, CENP-C unequivocally bridges two centromeric nucleosomes. Thus, our findings propose a dinucleosome structure to be the fundamental unit of the human centromere and confirm a previous ChIP study suggesting that CENP-C, CENP-B and CENP-T occupy a CENP-A dinucleosome over an alpha-satellite dimer (Thakur and Henikoff, 2016). CENP-C preferentially bound CENP-A over H3 mononucleosomes both in analytical SEC and in EMSA experiments. However, our competitive EMSA experiments revealed only modest selectivity of CENP-A over H3, as has been previously shown for the individual CENP-C motifs (Kato et al., 2013).

A fundamental, still unanswered question is, how the architecture of centromeric chromatin changes during the cell cycle in the context of CENP-A replenishment and CENP-A dilution. The currently accepted placeholder model predicts that each CENP-A nucleosome is distributed to one of the two arising sister chromatids during DNA replication, and that the resulting gap on the other sister chromatid is filled in by a histone H3.3 placeholder nucleosome (Dunleavy et al., 2011). The C-terminal CENP-C motif could be temporarily occupied by H3, since it has been shown to be less selective for CENP-A over H3 than the central motif (Kato et al., 2013). We reconstituted CENP-A/CENP-A and CENP-A/H3 dinucleosomes as well as CENP-C mutants in which we incorporated a photo-inducible crosslinking unnatural amino acid either C-terminal of the central or the C-terminal CENP-C motif. CENP-A

dinucleosomes crosslinked to both motifs at saturating and sub-saturating concentrations. However, at low dinucleosome concentrations, CENP-A/H3 dinucleosomes displayed a CENP-A band crosslinked to the central motif, but not to the conserved motif. Our crosslinking experiments were strongly limited by the fact that we could not detect crosslinked H3 in any of the samples. We speculate that H3 was either not bound tightly enough or could not be reached by the Bpa residue due to a binding mode that differs from CENP-A. However, our crosslinking experiments give a first hint that CENP-A preferentially binds to the central motif. Crosslinking mass spectrometry analyses have to be performed in the future to confirm this hypothesis.

If a CENP-A/CENP-A or CENP-A/H3 dinucleosome structure recapitulates the actual situation present *in vivo*, remains an outstanding question. Although the placeholder model postulated by Dunleavy et al. is generally accepted, there are other hypotheses for how CENP-A could be distributed and how the resulting centromere nucleosome structures could look like (Figure 4-1). Although the octameric structure of the CENP-A nucleosome has been determined in a crystal structure and has also been found to be the predominant form *in vivo*, tetrameric CENP-A hemisomes or tetrasomes have been postulated to be present in *D. melanogaster* as well as human interphase cells (Dalal et al., 2007; Dimitriadis et al., 2010; Furuyama et al., 2013; Furuyama and Henikoff, 2009; Hasson et al., 2013; Tachiwana et al., 2011). Furthermore, the composition of CENP-A nucleosomes has been claimed to cycle between octamers before DNA replication and tetramers after replication (Bui et al., 2012). Contrarily, in budding yeast one copy of Cse4 has been proposed to be present from telophase to G2 phase, whereas a second Cse4 molecule is incorporated during anaphase (Shivaraju et al., 2012). An intermediate model postulates that the parental CENP-A nucleosome would be split, and CENP-A would be mixed with H3 in the resulting nucleosome. These mixed CENP-A/H3 mononucleosomes have been identified in budding yeast and also in human, albeit at very low abundance (Foltz et al., 2006; Lochmann and Ivanov, 2012). Although the placeholder model with octameric CENP-A and H3.3 nucleosomes is currently the most accepted model in the field, the other models have not been disproved yet. All three models are compatible with a halving of the CENP-A pool during S-phase. In summary, CENP-C bridging two octameric nucleosomes, as demonstrated in this work, most likely represents a biologically

relevant structure, that serves as a template for the reconstitution of human kinetochore particles, as discussed in the later part of this work.

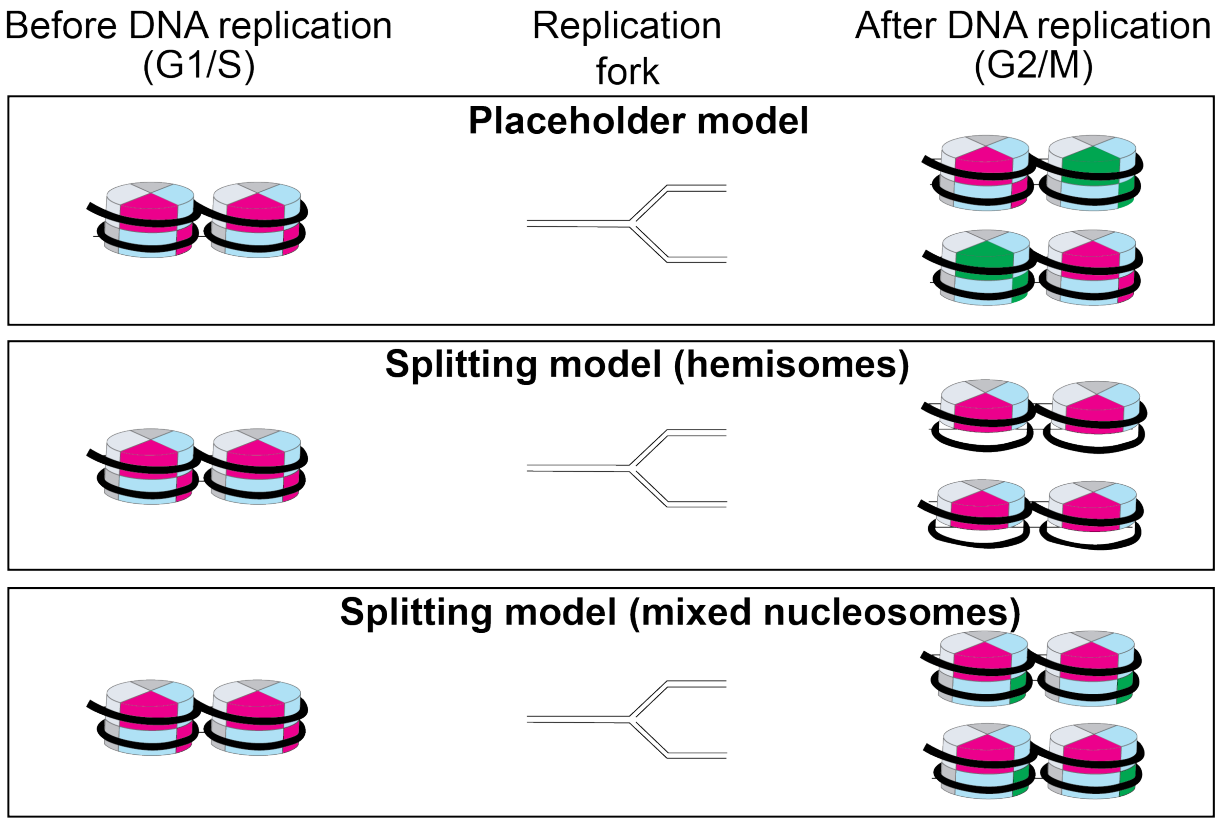

Figure 4-1 Models of centromeric nucleosome organization

According to the placeholder model, the complete CENP-A nucleosome (magenta) is distributed to one of the two arising sister chromatids during DNA replication. The resulting gaps are filled by a H3.3 placeholder nucleosome (green). This results in CENP-A/H3 or H3/CENP-A dinucleosomes. The H3.3 placeholder nucleosome is going to be evicted in early G1 phase and subsequently exchanged against a new CENP-A nucleosome. The splitting model predicts, that the CENP-A nucleosomes are split into hemisomes. Alternatively, H3.3 is incorporated into the CENP-A nucleosomes, resulting in mixed nucleosomes.

4.1.2 Electroporated recombinant CENP-C localizes at the centromere and allows cells to reach a state of chromosome congression

To test the functionality of reconstituted CENP-C in human cells, we used electroporation as a method for protein delivery. In previous studies, we successfully electroporated several subcomplexes of the inner and outer kinetochore like CENP-OPQUR, the NDC80 and MIS12 complexes as well as the corona proteins Spindly and CENP-E (Alex et al., 2019; Ciossani et al., 2018; Pesenti et al., 2018). As receptor cells, we used a human DLD-1 cell line with both alleles of CENP-C tagged with AID allowing for its rapid depletion within minutes (Hoffmann et al., 2016). Depletion of endogenous CENP-C in cells electroporated with mCherry resulted in a strong defective mitotic phenotype, since the majority of the cells were unable to align their chromosomes and to form a metaphase plate. This observation is in line with previous studies reporting mitotic arrest upon depletion of CENP-C (Fukagawa and Brown, 1997; Kwon et al., 2007; Orr and Sunkel, 2011; Shono et al., 2015). Electroporated mCherry-CENP-C localized at centromeres both in interphase and mitotic cells depleted of endogenous CENP-C. This result demonstrates once more, that electroporation is a suitable approach to introduce kinetochore proteins into human cells. Furthermore, it demonstrates that neither the N-terminal mCherry tag, nor the internal SpyCatcher-SpyTag sequence hinder CENP-C to efficiently target the centromere.

In the performed chromosome congression assay, electroporated mCherry-CENP-C enabled cells to align their chromosomes into a metaphase plate nearly at the same extent as observed in control cells that were not CENP-C depleted and electroporated with mCherry. This result provides further evidence for the functionality of reconstituted, electroporated CENP-C. Chromosome congression depends on CENP-OPQUR and on CENP-E, the localization of which depends on CENP-C (Bancroft et al., 2015; Liu et al., 2006; Pesenti et al., 2018). Although we did not check the localization of inner or outer kinetochore proteins in electroporated cells, the formation of metaphase plates indicates that electroporated CENP-C fulfils its role as the kinetochore "blueprint" (Klare et al., 2015). In future experiments, single cells could be followed by live microscopy to observe if also faithful chromosome segregation is promoted by recombinant CENP-C. Combining rapid AID induced degradation with

efficient protein delivery, these experiments provide the basis for the electroporation of larger kinetochore subcomplexes or even entire kinetochores in the future.

4.1.3 The centromere localization of CENP-C strongly depends on its homo-dimerization and interactions with the CCAN-members CENP-HIKM/-LN

We demonstrated that CENP-C, when electroporated into human cells, is able to functionally complement the loss of endogenous CENP-C. Using the same approach, we aimed to investigate, what are the determinants for the centromere recruitment of CENP-C. CENP-C serving as the scaffold of the kinetochore harbours binding sites for other kinetochore members as well as two nucleosome binding motifs. In our localization studies, we mutated the binding sites of CENP-HIKM/-LN and the nucleosome binding motifs, either alone or in combination. The localization of the CENP-A binding mutant was weaker compared to the WT protein; however, the centromere signals, despite being significantly lower, appeared sharp and perfectly co-localized with the centromere marker CREST. This result is in line with a recent study showing that interrupting the interaction between CENP-C and nucleosomes leads to a strong reduction of CENP-A after 24 hours (Guo et al., 2017). Thus, the fluorescent signal reduction we observed for the CENP-A binding mutant relative to the WT CENP-C protein was most likely a consequence of decreased CENP-A levels at the centromere and not of a weaker CENP-C localization per se.

The CENP-HIKM/-LN binding mutant showed a remarkably strong localization defect, that was much more pronounced compared to the CENP-A binding mutant. Furthermore, the signal was dispersed across the nucleus. This result might appear unexpected, since the nucleosome binding motifs of that mutant remained intact. However, CENP-C shows only a moderate, approximately 10-fold preference of CENP-A over H3 *in vitro* (Kato et al., 2013). In our competitive gel shift assays, in which we used a 1:1 ratio of CENP-A and H3 nucleosomes, CENP-C preferentially bound CENP-A, but started binding H3 when we added CENP-C in excess. A quantitative study revealed, that the genomic CENP-A:H3 ratio is about 1:1200, and therefore the preference of CENP-C towards CENP-A *in vitro* is not high enough to explain how CENP-C is selectively targeted to the centromere (Bodor et al., 2014). This is in clear contrast to the situation in *S. cerevisiae*, where Mif2 binds centromeric nucleosomes more than 1000-fold tighter than H3 nucleosomes due to a strong selectivity for both

Cse4 over H3 and centromeric over non-centromeric DNA (Xiao et al., 2017). Importantly, only 20 % of the total CENP-A pool has been found at the centromere in human RPE cells, whereas the rest is spread throughout the genome or is localized outside the nucleus (Bodor et al., 2014). We conclude, that CENP-C might be primarily attracted by the CCAN, which is concentrated at each centromere, for its recruitment and will subsequently bind CENP-A. We could support this idea in an *in vitro* pull-down experiment, where CENP-HIKM/-LN could mediate the interaction between CENP-A nucleosomes and a CENP-C mutant unable to bind CENP-A. Thus, although CENP-C has been shown to be upstream of CENP-HIKM, CENP-LN and CENP-T (Basilico et al., 2014; Klare et al., 2015; Pentakota et al., 2017; Tanaka et al., 2009), its own localization seems to be co-dependent on other CCAN members. A previous study in human DLD-1 cells proposed that specifically during interphase, but not in mitosis, CENP-C is reciprocally stabilized by CENP-HIKM/-LN (McKinley et al., 2015). The same cell cycle dependent relation has been reported in chicken (Kwon et al., 2007; Nagpal et al., 2015). The difference between interphase and mitosis could reflect different posttranslational modifications. One recent study claimed that CDK1 phosphorylation of a residue in close vicinity to the conserved CENP-C motif enhances the affinity to CENP-A (Watanabe et al., 2019). Since we did not synchronize the cells in our electroporation experiments, future studies are necessary to confirm a possible switch during the cell cycle.

In the second part of our localization studies, we focused on the C-terminal Cupin domain that promotes homo-dimerization of CENP-C in *S. cerevisiae*, *S. pombe* and *D. melanogaster* (Chik et al., 2019; Cohen et al., 2008; Medina-Pritchard et al., 2020; Xiao et al., 2017). We confirmed by AUC analysis that also the human Cupin domain dimerizes *in vitro*. Our co-localization studies of human CENP-C and the Cupin domains from human, *S. cerevisiae* and *D. melanogaster* revealed that only the human Cupin domain is able to interact with human CENP-C, which can be explained by striking amino acid variations between the Cupin domains of different organisms (Medina-Pritchard et al., 2020). The centromere localization of two human Cupin domain constructs, from which one additionally contained the conserved CENP-C motif, was dependent on endogenous CENP-C. This is in contrast to a recent study showing, that a C-terminal construct of CENP-C localizes at the centromere in mitosis (Watanabe et al., 2019). However, in the latter study endogenous CENP-C was rapidly

depleted using AID-tagged CENP-C, whereas we have used an RNAi based approach. Strikingly, a monomeric CENP-C truncation mutant lacking the Cupin domain localized weaker than WT CENP-C. Furthermore, CENP-C chimeras of human CENP-C$^{1-772}$ and the Cupin domains from *S. cerevisiae*, *D. melanogaster* or an artificial dimerization domain localized at the centromere nearly as well as WT CENP-C. Thus, homo-dimerization is an important mechanism promoting robust centromere recruitment of CENP-C as demonstrated previously in *X. laevis* (Carroll et al., 2010). Taken together with the previous results, the homo-dimerization of CENP-C and its interactions with other CCAN proteins provide additional selectivity that is necessary for its centromere targeting.

The Cupin domains of *S. pombe* and *D. melanogaster* have been shown to interact with Moa1 and CAL1, respectively (Chik et al., 2019; Medina-Pritchard et al., 2020). Importantly, CAL1, the CENP-A chaperone in *D. melanogaster*, can only interact with dimeric, but not with monomeric CENP-C in that organism (Roure et al., 2019). Thus, the Cupin domain carries a functional role besides dimerization. Furthermore, the C-terminal part of CENP-C has been proposed to interact with components of the Mis18 complex in mouse and frog (Dambacher et al., 2012; Moree et al., 2011). Therefore, also the Cupin domain of human CENP-C is likely to mediate interactions with other proteins, which has to be examined in the future.

4.1.4 Reconstitution of extended kinetochore particles on dinucleosome templates

Using MBP-tagged CENP-C^{F} as bait, we reconstituted the complete 16 subunit CCAN bound to CENP-A/H3 dinucleosomes. We further included all the outer kinetochore members except Zwint, resulting in recombinant kinetochore particles harbouring 25 kinetochore subunits and five additional histone proteins assembled in dinucleosome templates. For the first time, we have included CENP-TWSX into our reconstituted kinetochores which forms a stable tetrameric complex and, together with CENP-C, promotes the recruitment of the KMN network components (Gascoigne et al., 2011; Kim and Yu, 2015; Nishino et al., 2013; Nishino et al., 2012; Suzuki et al., 2015). Previous studies proposed, that the CENP-TWSX complex preferentially binds the linker DNA between two adjacent nucleosomes (Takeuchi et al., 2014; Thakur and Henikoff, 2016). Strikingly, *in vitro* CENP-TWSX complex binds equally well to a 100 bp linker DNA, regardless of whether the underlying dinucleosome contains H3 or

CENP-A (Takeuchi et al., 2014). Among the CCAN members, the CENP-HIKM complex has been shown to interact weakly with CENP-TWSX (Basilico et al., 2014). In our reconstitution, CENP-TWSX weakly interacted with CENP-C bound to CENP-A/H3 dinucleosomes. Importantly, phosphorylation of CENP-C by CDK1 did not increase the binding of CENP-TWSX, whereas addition of CENP-HIKM clearly enhanced the binding of CENP-TWSX. However, CENP-TWSX and also CENP-OPQUR appeared to be sub-stoichiometric in our kinetochore particles compared to CENP-C, CENP-HIKM and CENP-LN. This finding is surprising, because the pseudo-symmetry of the CENP-A nucleosome allows its binding to two CCAN modules (Weir et al., 2016). We conclude that only one copy of CENP-TWSX is present in the kinetochore particles, which might reflect the real stoichiometry or could be either caused by the absence of a critical posttranslational modification or reflect a missing binding partner. CENP-B, which binds to a defined 17 bp DNA sequence contained in the linker DNA of the dinucleosomes, would be one plausible candidate, since it has been found in the same complex bridging young alpha satellite dimers together with CENP-C and CENP-T (Thakur and Henikoff, 2016). Although no direct binding between CENP-B and CENP-T has been reported so far *in vitro*, an interaction between CENP-B and CENP-T has been proposed by *in vivo* FRET experiments (Hellwig et al., 2008).

In spite of the sub-stoichiometric incorporation of CENP-TWSX, we observed a strong increase of recruited KMN complex, particularly of the NDC80 complex members, upon phosphorylation of CENP-T by CDK1 kinase. This behaviour recapitulates the results from previous studies showing both *in vivo* and *in vitro* that CDK1 phosphorylation enables the binding of two NDC80 complexes and one additional KMN complex to CENP-T (Huis In 't Veld et al., 2016; Rago et al., 2015). As mentioned before, we assume that we have most likely one copy of CENP-TWSX incorporated in the kinetochore particles. In that case, the CDK1 phosphorylated kinetochore particle would contain two KMN complexes recruited by the CENP-C dimer, one KMN complex recruited by Ser201 of CENP-T and two additional NDC80 complexes recruited by Thr11 and Thr85 of CENP-T (Figure 4-2). As discussed above, we cannot exclude that we are still missing important components that will allow the incorporation of two CENP-TWSX complexes and will eventually lead to an even enhanced recruitment of the outer kinetochore complexes.

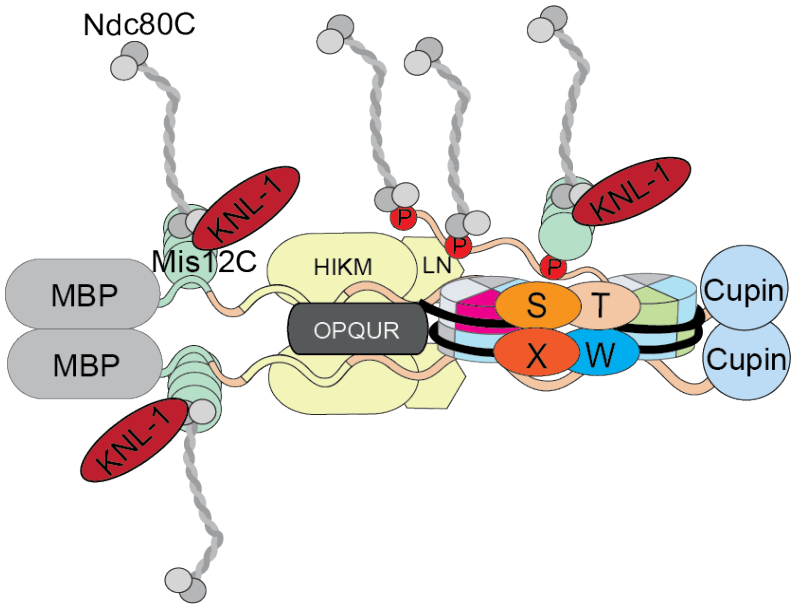

Figure 4-2 Proposed stoichiometry of the reconstituted kinetochore particle

The pseudo-symmetric CENP-A nucleosome binds one CENP-C dimer and two CENP-LN complexes. CENP-C recruits two HIKM complexes and at least one OPQUR and one CENP-TWSX complex. The N-Terminus of CENP-C recruits one KMN network per monomer. CENP-T recruits in a CDK1 phosphorylation dependent manner two NDC80 complexes and one additional KMN network.

4.2 Insights into the propagation of centromeric chromatin

In the second part of this work, I gained insights into the interactome of the Mis18 complex. Mass spectrometry analysis of M18BP1 and Mis18α IPs identified PLK1 as one of the most enriched interaction partners. I confirmed that PLK1 activity is necessary for the localization of the Mis18 complex at the centromere. Furthermore, I identified a crucial PLK1 phosphorylation site in M18BP1. Finally, I found that CENP-C depletion severely impairs the localization of M18BP1 in early G1 phase.

4.2.1 PLK1 activity is crucial for the centromere targeting of the Mis18 complex

We found PLK1 highly enriched in the M18BP1 and Mis18α IPs. The abundance of PLK1 in both IPs indicated, that PLK1 must be an important interacting protein, as has been reported in a previous study (McKinley and Cheeseman, 2014). We confirmed that depletion of M18BP1 prevents PLK1 from localizing at the centromere in early G1 phase. Using a PLK1 specific small molecule inhibitor (Steegmaier et al., 2007) we also demonstrated that the kinase activity of PLK1 promotes the G1 phase localization

of the Mis18 complex and PLK1 itself at the centromere. Inhibition of PLK1 catalytic activity has been previously shown to cause delocalization of PLK1 from centrosomes and kinetochores, suggesting a critical dependence of PLK1 localization on its own catalytical activity (Lenart et al., 2007). Mutation of a single PLK1 site in M18BP1, Ser93, into Ala had two consequences. First, the expressed M18BP1^{S93A} mutant was unable to localize at the centromere in the absence of endogenous M18BP1. Second, the phosphorylation of another PLK1 site, Thr702, was severely reduced. Thus, mutating only one of eight previously identified PLK1 phosphorylation sites in M18BP1 (McKinley and Cheeseman, 2014) was sufficient to significantly disrupt the interactions between both proteins. Interestingly, Ser93 is in close proximity to the binding region of Mis18α/Mis18β (Pan et al., 2017). Complex formation of M18BP1, Mis18α and Mis18β is inhibited by CDK1 activity, which is high during mitosis and is rapidly switched off at the metaphase to anaphase transition. How PLK1 phosphorylation of M18BP1 Ser93 permits the centromere localization of the Mis18 complex to the centromere, remains unclear. *In vitro*, PLK1 is not necessary for the interaction between M18BP1 and Mis18α/β (Pan et al., 2017).

The C-Terminus of PLK1 consists of two homologous Polo boxes forming the Polo box domain (PBD), which targets PLK1 to phosphoserine/threonine-containing motifs (Elia et al., 2003a; Elia et al., 2003b). CENP-U has been shown to be the mitotic receptor of PLK1 and the phosphorylation epitope necessary for the PBD binding was supposed to be created by PLK1 itself (Kang et al., 2011; Kang et al., 2006). Importantly, the PBD exhibits some specificity for Pro in the +1 position relative to the phosphorylation site, proposing an important role of Pro-directed kinases like CDK1 in priming the substrate for its interaction with PLK1 as proposed by several studies (Elia et al., 2003b; Golan et al., 2002; Soung et al., 2009; Zhang et al., 2009). To understand the interaction between M18BP1 and PLK1, it will be important to identify the binding site within M18BP1 that recruits PLK1 either in a CDK1 or PLK1 dependent manner. Although M18BP1 Ser93 has been shown to be phosphorylated by PLK1 *in vitro* (McKinley and Cheeseman, 2014), the surrounding sequence does not resemble the PBD binding motif (Elia et al., 2003a). Of note, M18BP1 Thr78 is another PLK1 consensus site (Santamaria et al., 2011) and could furthermore be a potential PBD docking site, although it has not been found to be phosphorylated by PLK1 and has not been mutated in the study by McKinley and Cheeseman. In future *in vitro*

experiments we will need to test which phosphorylation site in the N-Terminus of M18BP1 is responsible for the recruitment of PLK1 and if CDK1, PLK1, or even both kinases prime M18BP1 for the interaction with PLK1. Since the N-Terminus of M18BP1 is sufficient to load new CENP-A but still depends on PLK1 phosphorylation (McKinley and Cheeseman, 2014), we expect, that the site mediating the interaction with PLK1 must be included in the first 490 residues of M18BP1.

4.2.2 CENP-C is crucial for the centromere targeting of M18BP1

Using the DLD-1 CENP-C-AID-YFP cell line, we found that auxin induced depletion of CENP-C results in a strongly reduced centromere recruitment of M18BP1 in early G1 phase. Expression of WT CENP-C and a CENP-C mutant lacking the nucleosome binding motifs rescued M18BP1 localization. Thus, CENP-C is a critical component essential for the centromere recruitment of the Mis18 complex. Since CENP-C depletion leads to an overall destabilization of the CCAN, we cannot rule out that other CCAN members contribute to creating a binding site for M18BP1. At least one study proposed that also CENP-I, when tethered to ectopic alphoid LacO arrays, may directly interact with M18BP1 in the context of CENP-C RNAi (Shono et al., 2015). However, at endogenous centromeres CENP-HIKM directly depends on CENP-C for its localization (Klare et al., 2015). Thus, CENP-C might be the foundation of a composite binding site and further CCAN members could provide additional contact sites for the Mis18 complex.

The nucleosome binding motifs of CENP-C do not seem to be important for the recruitment of M18BP1 to the centromere. Contrarily, in *X. laevis*, the C-terminal CENP-C motif and the Cupin domain have been shown to be equally important for the interaction between *Xenopus* CENP-C and *Xenopus* M18BP1 *in vitro (Moree et al., 2011)*. Similarly, a C-terminal mouse CENP-C fragment, but not a fragment spanning the middle part or the N-Terminus, interacted with mouse M18BP1 (Dambacher et al., 2012). In future experiments, it will be important to investigate, which part of CENP-C provides the binding site for the Mis18 complex. The Cupin domain of CENP-C could be potentially involved in the recruitment, since in *D. melanogaster* it interacts with the CENP-A deposition factor CAL1 (Medina-Pritchard et al., 2020). Therefore, it will be crucial to test if substitution of the Cupin domain with an artificial dimerization domain shows a negative effect on M18BP1 recruitment.

5 Abstract

Kinetochores, large multi-protein assemblies on centromeric DNA, interact with spindle microtubules to mediate faithful chromosome segregation during mitosis. The inner part of the kinetochore, the 16-subunit constitutive centromere associated network (CCAN), flanks the centromere throughout the cell cycle and provides the structural foundation for the peripheral kinetochore subunits. Centromere protein (CENP)-C is a fundamental CCAN subunit that provides a foundation, either directly or indirectly, to all other kinetochore components onto the specialized centromeric chromatin. Recent biochemical reconstitution studies provided insights into the complex human kinetochore architecture but still lacked the full-length version of CENP-C. My PhD work aimed to characterize the interactions of recombinant full-length CENP-C with nucleosomes and the other kinetochore members *in vitro*. Furthermore, my work aimed to define the determinants for the centromere recruitment of CENP-C. Lastly, in my studies, I gained new insights into the propagation of centromeric chromatin.

Combining biochemical reconstitution and biophysical methods, I revealed that the full-length CENP-C protein binds two nucleosomes and that this interaction strictly depends on two conserved nucleosome binding motifs. Using dinucleosomes bound to full-length CENP-C as a template, a 30-subunit kinetochore particle was reconstituted containing all inner and outer kinetochore subcomplexes. Electroporation of CENP-C into living human cells showed that CENP-C depends on the interactions with nucleosomes and with the CCAN members CENP-HIKM/-LN for its proper recruitment to the centromere. Furthermore, homo-dimerization mediated by the Cupin-like domain was identified as a mechanism promoting affinity towards the centromere. Immunoprecipitation experiments from cell lysates combined with mass spectrometry analysis identified Polo-like kinase 1 (PLK1) as a crucial factor that promotes centromere propagation.

In conclusion, this work demonstrates that CENP-C can bridge two adjacent nucleosomes and suggests that the resulting dinucleosome structure might represent the fundamental unit of the human kinetochore. This structure furthermore provides the basis for the *in vitro* reconstitution of the entire inner and outer kinetochore by integrating the CENP-C and CENP-T dependent pathway.

6 Zusammenfassung

Kinetochore stellen Multi-Proteinkomplexe dar, die sich am Zentromer anlagern und während der Mitose die korrekte Aufteilung der Chromosomen bewerkstelligen, indem sie als Ankerpunkte für die Fasern des Spindelapparates dienen. Das innere Kinetochor, auch "Constitutive Centromere Associated Network" (CCAN) genannt, das aus 16 Untereinheiten besteht, flankiert das Zentromer während des gesamten Zellzyklus und bildet zudem die strukturelle Plattform für die äußeren Kinetochorproteine. Das "Centromere Protein (CENP)-C" stellt eine wichtige CCAN-Untereinheit dar und beinhaltet zwei benachbarte nukleosomenbindende Motive, darüber hinaus rekrutiert es entweder direkt oder indirekt alle weiteren Kinetochorproteine. Aktuelle biochemische Studien, die das Kinetochor *in vitro* nachbilden, liefern Einblicke in die komplexe Architektur des menschlichen Kinetochors, beinhalten aber nicht das vollständige CENP-C-Protein. Das Ziel meiner Doktorarbeit war, erstmals die Interaktion zwischen dem aufgereinigten, vollständigen CENP-C-Protein und Nukleosomen sowie den anderen Kinetochorproteinen *in vitro* zu charakterisieren. Außerdem sollte untersucht werden, wie genau CENP-C an das Zentromer rekrutiert wird. Darüber hinaus liefert meine Arbeit einen Einblick, wie das Zentromer-Chromatin in Zellen erhalten bleibt.

Durch biochemische Rekonstitution konnte ich unter Anwendung biophysikalischer Methoden zeigen, dass das vollständige CENP-C-Protein mit zwei Nukleosomen interagiert und dass diese Interaktion von der Intaktheit der beiden CENP-C-Motive abhängt. Ein Komplex aus CENP-C und Dinukleosomen diente des Weiteren als Grundlage für die Rekonstitution von Kinetochorpartikeln, die mit insgesamt 30 Untereinheiten sämtliche Teilkomplexe des inneren sowie äußeren Kinetochors enthalten. Die Elektroporation von CENP-C in lebende menschliche Zellen zeigte, dass CENP-C sowohl mit Nukleosomen als auch mit den CCAN-Untereinheiten CENP-HIKM/-LN interagieren muss, um zuverlässig an das Zentromer rekrutiert zu werden. Außerdem zeigte sich, dass die Homo-Dimerisierung der "Cupin"-Domäne die Affinität von CENP-C zum Zentromer erhöht. Zuletzt konnte die massenspektroskopische Analyse von Immunpräzipitationen aus Zelllysaten Polo-like Kinase 1 (PLK1) als bedeutenden Faktor identifizieren, der für die Konservierung des Zentromerchromatins benötigt wird.

Zusammenfassend zeigt diese Arbeit, dass zwei benachbarte Nukleosomen von CENP-C überbrückt werden und dass die resultierende Dinukleosomenstruktur die fundamentale Einheit des humanen Kinetochors repräsentieren könnte. Darüber hinaus dient diese Struktur als Grundgerüst für die *in vitro*-Rekonstitution des gesamten inneren und äußeren Kinetochors, was durch die Integration sowohl von CENP-C als auch von CENP-T ermöglicht wird.

7 Bibliography

Abraham, R.T. (2001). Cell cycle checkpoint signaling through the ATM and ATR kinases. Genes Dev *15*, 2177-2196.

Abrieu, A., Magnaghi-Jaulin, L., Kahana, J.A., Peter, M., Castro, A., Vigneron, S., Lorca, T., Cleveland, D.W., and Labbe, J.C. (2001). Mps1 is a kinetochore-associated kinase essential for the vertebrate mitotic checkpoint. Cell *106*, 83-93.

Alex, A., Piano, V., Polley, S., Stuiver, M., Voss, S., Ciossani, G., Overlack, K., Voss, B., Wohlgemuth, S., Petrovic, A.*, et al.* (2019). Electroporated recombinant proteins as tools for in vivo functional complementation, imaging and chemical biology. Elife *8*.

Ali-Ahmad, A., Bilokapic, S., Schafer, I.B., Halic, M., and Sekulic, N. (2019). CENP-C unwraps the human CENP-A nucleosome through the H2A C-terminal tail. EMBO Rep *20*, e48913.

Allu, P.K., Dawicki-McKenna, J.M., Van Eeuwen, T., Slavin, M., Braitbard, M., Xu, C., Kalisman, N., Murakami, K., and Black, B.E. (2019). Structure of the Human Core Centromeric Nucleosome Complex. Curr Biol *29*, 2625-2639 e2625.

Alushin, G.M., Musinipally, V., Matson, D., Tooley, J., Stukenberg, P.T., and Nogales, E. (2012). Multimodal microtubule binding by the Ndc80 kinetochore complex. Nat Struct Mol Biol *19*, 1161-1167.

Alushin, G.M., Ramey, V.H., Pasqualato, S., Ball, D.A., Grigorieff, N., Musacchio, A., and Nogales, E. (2010). The Ndc80 kinetochore complex forms oligomeric arrays along microtubules. Nature *467*, 805-810.

Amano, M., Suzuki, A., Hori, T., Backer, C., Okawa, K., Cheeseman, I.M., and Fukagawa, T. (2009). The CENP-S complex is essential for the stable assembly of outer kinetochore structure. J Cell Biol *186*, 173-182.

Amaro, A.C., Samora, C.P., Holtackers, R., Wang, E., Kingston, I.J., Alonso, M., Lampson, M., McAinsh, A.D., and Meraldi, P. (2010). Molecular control of kinetochore-microtubule dynamics and chromosome oscillations. Nat Cell Biol *12*, 319-329.

Amor, D.J., and Choo, K.H. (2002). Neocentromeres: role in human disease, evolution, and centromere study. Am J Hum Genet *71*, 695-714.

Andronov, L., Ouararhni, K., Stoll, I., Klaholz, B.P., and Hamiche, A. (2019). CENP-A nucleosome clusters form rosette-like structures around HJURP during G1. Nat Commun *10*, 4436.

Arellano, M., and Moreno, S. (1997). Regulation of CDK/cyclin complexes during the cell cycle. Int J Biochem Cell Biol *29*, 559-573.

Asbury, C.L. (2017). Anaphase A: Disassembling Microtubules Move Chromosomes toward Spindle Poles. Biology (Basel) *6*.

Bailey, A.O., Panchenko, T., Sathyan, K.M., Petkowski, J.J., Pai, P.J., Bai, D.L., Russell, D.H., Macara, I.G., Shabanowitz, J., Hunt, D.F.*, et al.* (2013). Posttranslational modification of CENP-A influences the conformation of centromeric chromatin. Proc Natl Acad Sci U S A *110*, 11827-11832.

Bancroft, J., Auckland, P., Samora, C.P., and McAinsh, A.D. (2015). Chromosome congression is promoted by CENP-Q- and CENP-E-dependent pathways. J Cell Sci *128*, 171-184.

Barnhart, M.C., Kuich, P.H., Stellfox, M.E., Ward, J.A., Bassett, E.A., Black, B.E., and Foltz, D.R. (2011). HJURP is a CENP-A chromatin assembly factor sufficient to form a functional de novo kinetochore. J Cell Biol *194*, 229-243.

Barnhart-Dailey, M.C., Trivedi, P., Stukenberg, P.T., and Foltz, D.R. (2017). HJURP interaction with the condensin II complex during G1 promotes CENP-A deposition. Mol Biol Cell *28*, 54-64.

Barra, V., Logsdon, G.A., Scelfo, A., Hoffmann, S., Herve, S., Aslanian, A., Nechemia-Arbely, Y., Cleveland, D.W., Black, B.E., and Fachinetti, D. (2019). Phosphorylation of CENP-A on serine 7 does not control centromere function. Nat Commun *10*, 175.

Basilico, F., Maffini, S., Weir, J.R., Prumbaum, D., Rojas, A.M., Zimniak, T., De Antoni, A., Jeganathan, S., Voss, B., van Gerwen, S.*, et al.* (2014). The pseudo GTPase CENP-M drives human kinetochore assembly. Elife *3*, e02978.

Bergmann, J.H., Rodriguez, M.G., Martins, N.M., Kimura, H., Kelly, D.A., Masumoto, H., Larionov, V., Jansen, L.E., and Earnshaw, W.C. (2011). Epigenetic engineering shows H3K4me2 is required for HJURP targeting and CENP-A assembly on a synthetic human kinetochore. EMBO J *30*, 328-340.

Bernad, R., Sanchez, P., Rivera, T., Rodriguez-Corsino, M., Boyarchuk, E., Vassias, I., Ray-Gallet, D., Arnaoutov, A., Dasso, M., Almouzni, G.*, et al.* (2011). Xenopus HJURP and condensin II are required for CENP-A assembly. J Cell Biol *192*, 569-582.

Black, B.E., Jansen, L.E., Maddox, P.S., Foltz, D.R., Desai, A.B., Shah, J.V., and Cleveland, D.W. (2007). Centromere identity maintained by nucleosomes assembled with histone H3 containing the CENP-A targeting domain. Mol Cell *25*, 309-322.

Blow, J.J., and Hodgson, B. (2002). Replication licensing--defining the proliferative state? Trends Cell Biol *12*, 72-78.

Bobkov, G.O.M., Gilbert, N., and Heun, P. (2018). Centromere transcription allows CENP-A to transit from chromatin association to stable incorporation. J Cell Biol *217*, 1957-1972.

Bobkov, G.O.M., Huang, A., van den Berg, S.J.W., Mitra, S., Anselm, E., Lazou, V., Schunter, S., Feederle, R., Imhof, A., Lusser, A.*, et al.* (2020). Spt6 is a maintenance factor for centromeric CENP-A. Nature Communications *11*.

Bodor, D.L., and Jansen, L.E. (2013). How two become one: HJURP dimerization drives CENP-A assembly. EMBO J *32*, 2090-2092.

Bodor, D.L., Mata, J.F., Sergeev, M., David, A.F., Salimian, K.J., Panchenko, T., Cleveland, D.W., Black, B.E., Shah, J.V., and Jansen, L.E. (2014). The quantitative architecture of centromeric chromatin. Elife *3*, e02137.

Bodor, D.L., Rodriguez, M.G., Moreno, N., and Jansen, L.E. (2012). Analysis of protein turnover by quantitative SNAP-based pulse-chase imaging. Curr Protoc Cell Biol *Chapter 8*, Unit8 8.

Boyer, L.A., Langer, M.R., Crowley, K.A., Tan, S., Denu, J.M., and Peterson, C.L. (2002). Essential role for the SANT domain in the functioning of multiple chromatin remodeling enzymes. Mol Cell *10*, 935-942.

Bui, M., Dimitriadis, E.K., Hoischen, C., An, E., Quenet, D., Giebe, S., Nita-Lazar, A., Diekmann, S., and Dalal, Y. (2012). Cell-cycle-dependent structural transitions in the human CENP-A nucleosome in vivo. Cell *150*, 317-326.

Camahort, R., Li, B., Florens, L., Swanson, S.K., Washburn, M.P., and Gerton, J.L. (2007). Scm3 is essential to recruit the histone h3 variant cse4 to centromeres and to maintain a functional kinetochore. Mol Cell *26*, 853-865.

Cao, S., Zhou, K., Zhang, Z., Luger, K., and Straight, A.F. (2018). Constitutive centromere-associated network contacts confer differential stability on CENP-A nucleosomes in vitro and in the cell. Mol Biol Cell *29*, 751-762.

Carmena, M., Wheelock, M., Funabiki, H., and Earnshaw, W.C. (2012). The chromosomal passenger complex (CPC): from easy rider to the godfather of mitosis. Nat Rev Mol Cell Biol *13*, 789-803.

Carroll, C.W., Milks, K.J., and Straight, A.F. (2010). Dual recognition of CENP-A nucleosomes is required for centromere assembly. J Cell Biol *189*, 1143-1155.

Carroll, C.W., Silva, M.C., Godek, K.M., Jansen, L.E., and Straight, A.F. (2009). Centromere assembly requires the direct recognition of CENP-A nucleosomes by CENP-N. Nat Cell Biol *11*, 896-902.

Cheeseman, I.M., Chappie, J.S., Wilson-Kubalek, E.M., and Desai, A. (2006). The conserved KMN network constitutes the core microtubule-binding site of the kinetochore. Cell *127*, 983-997.

Cheeseman, I.M., Hori, T., Fukagawa, T., and Desai, A. (2008). KNL1 and the CENP-H/I/K complex coordinately direct kinetochore assembly in vertebrates. Mol Biol Cell *19*, 587-594.

Chen, C.C., Bowers, S., Lipinszki, Z., Palladino, J., Trusiak, S., Bettini, E., Rosin, L., Przewloka, M.R., Glover, D.M., O'Neill, R.J.*, et al.* (2015). Establishment of Centromeric Chromatin by the CENP-A Assembly Factor CAL1 Requires FACT-Mediated Transcription. Dev Cell *34*, 73-84.

Chik, J.K., Moiseeva, V., Goel, P.K., Meinen, B.A., Koldewey, P., An, S., Mellone, B.G., Subramanian, L., and Cho, U.S. (2019). Structures of CENP-C cupin domains at regional centromeres reveal unique patterns of dimerization and recruitment functions for the inner pocket. J Biol Chem *294*, 14119-14134.

Chin, J.W., Martin, A.B., King, D.S., Wang, L., and Schultz, P.G. (2002). Addition of a photocrosslinking amino acid to the genetic code of Escherichiacoli. Proc Natl Acad Sci U S A *99*, 11020-11024.

Cho, U.S., and Harrison, S.C. (2011). Recognition of the centromere-specific histone Cse4 by the chaperone Scm3. Proc Natl Acad Sci U S A *108*, 9367-9371.

Ciferri, C., Pasqualato, S., Screpanti, E., Varetti, G., Santaguida, S., Dos Reis, G., Maiolica, A., Polka, J., De Luca, J.G., De Wulf, P.*, et al.* (2008). Implications for kinetochore-microtubule attachment from the structure of an engineered Ndc80 complex. Cell *133*, 427-439.

Cimini, D., and Degrassi, F. (2005). Aneuploidy: a matter of bad connections. Trends Cell Biol *15*, 442-451.

Ciossani, G., Overlack, K., Petrovic, A., Huis In 't Veld, P.J., Koerner, C., Wohlgemuth, S., Maffini, S., and Musacchio, A. (2018). The kinetochore proteins CENP-E and CENP-F directly and specifically interact with distinct BUB mitotic checkpoint Ser/Thr kinases. J Biol Chem *293*, 10084-10101.

Clarke, L., and Carbon, J. (1980). Isolation of a yeast centromere and construction of functional small circular chromosomes. Nature *287*, 504-509.

Cohen, R.L., Espelin, C.W., De Wulf, P., Sorger, P.K., Harrison, S.C., and Simons, K.T. (2008). Structural and functional dissection of Mif2p, a conserved DNA-binding kinetochore protein. Mol Biol Cell *19*, 4480-4491.

Cohen-Fix, O., Peters, J.M., Kirschner, M.W., and Koshland, D. (1996). Anaphase initiation in Saccharomyces cerevisiae is controlled by the APC-dependent degradation of the anaphase inhibitor Pds1p. Genes Dev *10*, 3081-3093.

Conde e Silva, N., Black, B.E., Sivolob, A., Filipski, J., Cleveland, D.W., and Prunell, A. (2007). CENP-A-containing nucleosomes: easier disassembly versus exclusive centromeric localization. J Mol Biol *370*, 555-573.

Dalal, Y., Wang, H., Lindsay, S., and Henikoff, S. (2007). Tetrameric structure of centromeric nucleosomes in interphase Drosophila cells. PLoS Biol *5*, e218.

Dambacher, S., Deng, W., Hahn, M., Sadic, D., Frohlich, J., Nuber, A., Hoischen, C., Diekmann, S., Leonhardt, H., and Schotta, G. (2012). CENP-C facilitates the recruitment of M18BP1 to centromeric chromatin. Nucleus *3*, 101-110.

Dechassa, M.L., Wyns, K., Li, M., Hall, M.A., Wang, M.D., and Luger, K. (2011). Structure and Scm3-mediated assembly of budding yeast centromeric nucleosomes. Nat Commun *2*, 313.

DeLuca, K.F., Lens, S.M., and DeLuca, J.G. (2011). Temporal changes in Hec1 phosphorylation control kinetochore-microtubule attachment stability during mitosis. J Cell Sci *124*, 622-634.

Dimitriadis, E.K., Weber, C., Gill, R.K., Diekmann, S., and Dalal, Y. (2010). Tetrameric organization of vertebrate centromeric nucleosomes. Proc Natl Acad Sci U S A *107*, 20317-20322.

Dunleavy, E.M., Almouzni, G., and Karpen, G.H. (2011). H3.3 is deposited at centromeres in S phase as a placeholder for newly assembled CENP-A in G(1) phase. Nucleus *2*, 146-157.

Dunleavy, E.M., Roche, D., Tagami, H., Lacoste, N., Ray-Gallet, D., Nakamura, Y., Daigo, Y., Nakatani, Y., and Almouzni-Pettinotti, G. (2009). HJURP is a cell-cycle-dependent maintenance and deposition factor of CENP-A at centromeres. Cell *137*, 485-497.

Earnshaw, W.C., and Cooke, C.A. (1991). Analysis of the distribution of the INCENPs throughout mitosis reveals the existence of a pathway of structural changes in the chromosomes during metaphase and early events in cleavage furrow formation. J Cell Sci *98 (Pt 4)*, 443-461.

Earnshaw, W.C., and Migeon, B.R. (1985). Three related centromere proteins are absent from the inactive centromere of a stable isodicentric chromosome. Chromosoma *92*, 290-296.

Earnshaw, W.C., and Rothfield, N. (1985). Identification of a family of human centromere proteins using autoimmune sera from patients with scleroderma. Chromosoma *91*, 313-321.

Elia, A.E., Cantley, L.C., and Yaffe, M.B. (2003a). Proteomic screen finds pSer/pThr-binding domain localizing Plk1 to mitotic substrates. Science *299*, 1228-1231.

Elia, A.E., Rellos, P., Haire, L.F., Chao, J.W., Ivins, F.J., Hoepker, K., Mohammad, D., Cantley, L.C., Smerdon, S.J., and Yaffe, M.B. (2003b). The molecular basis for phosphodependent substrate targeting and regulation of Plks by the Polo-box domain. Cell *115*, 83-95.

Eot-Houllier, G., Magnaghi-Jaulin, L., Fulcrand, G., Moyroud, F.X., Monier, S., and Jaulin, C. (2018). Aurora A-dependent CENP-A phosphorylation at inner centromeres protects bioriented chromosomes against cohesion fatigue. Nat Commun *9*, 1888.

Falk, S.J., Guo, L.Y., Sekulic, N., Smoak, E.M., Mani, T., Logsdon, G.A., Gupta, K., Jansen, L.E., Van Duyne, G.D., Vinogradov, S.A.*, et al.* (2015). Chromosomes. CENP-C reshapes and stabilizes CENP-A nucleosomes at the centromere. Science *348*, 699-703.

Fang, J., Liu, Y., Wei, Y., Deng, W., Yu, Z., Huang, L., Teng, Y., Yao, T., You, Q., Ruan, H.*, et al.* (2015). Structural transitions of centromeric chromatin regulate the cell cycle-dependent recruitment of CENP-N. Genes Dev *29*, 1058-1073.

Fisher, R.P., and Morgan, D.O. (1994). A novel cyclin associates with MO15/CDK7 to form the CDK-activating kinase. Cell *78*, 713-724.

Foltz, D.R., Jansen, L.E., Bailey, A.O., Yates, J.R., 3rd, Bassett, E.A., Wood, S., Black, B.E., and Cleveland, D.W. (2009). Centromere-specific assembly of CENP-a nucleosomes is mediated by HJURP. Cell *137*, 472-484.

Foltz, D.R., Jansen, L.E., Black, B.E., Bailey, A.O., Yates, J.R., 3rd, and Cleveland, D.W. (2006). The human CENP-A centromeric nucleosome-associated complex. Nat Cell Biol *8*, 458-469.

French, B.T., and Straight, A.F. (2019). CDK phosphorylation of Xenopus laevis M18BP1 promotes its metaphase centromere localization. EMBO J *38*.

French, B.T., Westhorpe, F.G., Limouse, C., and Straight, A.F. (2017). Xenopus laevis M18BP1 Directly Binds Existing CENP-A Nucleosomes to Promote Centromeric Chromatin Assembly. Dev Cell *42*, 190-199 e110.

Fujita, Y., Hayashi, T., Kiyomitsu, T., Toyoda, Y., Kokubu, A., Obuse, C., and Yanagida, M. (2007). Priming of centromere for CENP-A recruitment by human hMis18alpha, hMis18beta, and M18BP1. Dev Cell *12*, 17-30.

Fukagawa, T., and Brown, W.R. (1997). Efficient conditional mutation of the vertebrate CENP-C gene. Hum Mol Genet *6*, 2301-2308.

Fukagawa, T., and Earnshaw, W.C. (2014). The centromere: chromatin foundation for the kinetochore machinery. Dev Cell *30*, 496-508.

Furuyama, S., and Biggins, S. (2007). Centromere identity is specified by a single centromeric nucleosome in budding yeast. Proc Natl Acad Sci U S A *104*, 14706-14711.

Furuyama, T., Codomo, C.A., and Henikoff, S. (2013). Reconstitution of hemisomes on budding yeast centromeric DNA. Nucleic Acids Res *41*, 5769-5783.

Furuyama, T., and Henikoff, S. (2009). Centromeric nucleosomes induce positive DNA supercoils. Cell *138*, 104-113.

Gascoigne, K.E., Takeuchi, K., Suzuki, A., Hori, T., Fukagawa, T., and Cheeseman, I.M. (2011). Induced ectopic kinetochore assembly bypasses the requirement for CENP-A nucleosomes. Cell *145*, 410-422.

Gibson, D.G., Young, L., Chuang, R.Y., Venter, J.C., Hutchison, C.A., 3rd, and Smith, H.O. (2009). Enzymatic assembly of DNA molecules up to several hundred kilobases. Nat Methods *6*, 343-345.

Golan, A., Yudkovsky, Y., and Hershko, A. (2002). The cyclin-ubiquitin ligase activity of cyclosome/APC is jointly activated by protein kinases Cdk1-cyclin B and Plk. J Biol Chem *277*, 15552-15557.

Goutte-Gattat, D., Shuaib, M., Ouararhni, K., Gautier, T., Skoufias, D.A., Hamiche, A., and Dimitrov, S. (2013). Phosphorylation of the CENP-A amino-terminus in mitotic centromeric chromatin is required for kinetochore function. Proc Natl Acad Sci U S A *110*, 8579-8584.

Gunbin, K.V., Suslov, V.V., Turnaev, II, Afonnikov, D.A., and Kolchanov, N.A. (2011). Molecular evolution of cyclin proteins in animals and fungi. BMC Evol Biol *11*, 224.

Guo, L.Y., Allu, P.K., Zandarashvili, L., McKinley, K.L., Sekulic, N., Dawicki-McKenna, J.M., Fachinetti, D., Logsdon, G.A., Jamiolkowski, R.M., Cleveland, D.W.*, et al.* (2017). Centromeres are maintained by fastening CENP-A to DNA and directing an arginine anchor-dependent nucleosome transition. Nat Commun *8*, 15775.

Guse, A., Carroll, C.W., Moree, B., Fuller, C.J., and Straight, A.F. (2011). In vitro centromere and kinetochore assembly on defined chromatin templates. Nature *477*, 354-358.

Hara, M., Ariyoshi, M., Okumura, E.I., Hori, T., and Fukagawa, T. (2018). Multiple phosphorylations control recruitment of the KMN network onto kinetochores. Nat Cell Biol *20*, 1378-1388.

Hartwell, L.H., and Weinert, T.A. (1989). Checkpoints: controls that ensure the order of cell cycle events. Science *246*, 629-634.

Hasson, D., Panchenko, T., Salimian, K.J., Salman, M.U., Sekulic, N., Alonso, A., Warburton, P.E., and Black, B.E. (2013). The octamer is the major form of CENP-A nucleosomes at human centromeres. Nat Struct Mol Biol *20*, 687-695.

Hayashi, T., Fujita, Y., Iwasaki, O., Adachi, Y., Takahashi, K., and Yanagida, M. (2004). Mis16 and Mis18 are required for CENP-A loading and histone deacetylation at centromeres. Cell *118*, 715-729.

Hayden, J.H., Bowser, S.S., and Rieder, C.L. (1990). Kinetochores capture astral microtubules during chromosome attachment to the mitotic spindle: direct visualization in live newt lung cells. J Cell Biol *111*, 1039-1045.

Hellwig, D., Munch, S., Orthaus, S., Hoischen, C., Hemmerich, P., and Diekmann, S. (2008). Live-cell imaging reveals sustained centromere binding of CENP-T via CENP-A and CENP-B. J Biophotonics *1*, 245-254.

Hinshaw, S.M., and Harrison, S.C. (2013). An Iml3-Chl4 heterodimer links the core centromere to factors required for accurate chromosome segregation. Cell Rep *5*, 29-36.

Hinshaw, S.M., and Harrison, S.C. (2019). The structure of the Ctf19c/CCAN from budding yeast. Elife *8*.

Hoffmann, S., Dumont, M., Barra, V., Ly, P., Nechemia-Arbely, Y., McMahon, M.A., Herve, S., Cleveland, D.W., and Fachinetti, D. (2016). CENP-A Is Dispensable for Mitotic Centromere Function after Initial Centromere/Kinetochore Assembly. Cell Rep *17*, 2394-2404.

Hori, T., Amano, M., Suzuki, A., Backer, C.B., Welburn, J.P., Dong, Y., McEwen, B.F., Shang, W.H., Suzuki, E., Okawa, K.*, et al.* (2008a). CCAN makes multiple contacts with centromeric DNA to provide distinct pathways to the outer kinetochore. Cell *135*, 1039-1052.

Hori, T., Okada, M., Maenaka, K., and Fukagawa, T. (2008b). CENP-O class proteins form a stable complex and are required for proper kinetochore function. Mol Biol Cell *19*, 843-854.

Hori, T., Shang, W.H., Hara, M., Ariyoshi, M., Arimura, Y., Fujita, R., Kurumizaka, H., and Fukagawa, T. (2017). Association of M18BP1/KNL2 with CENP-A Nucleosome Is Essential for Centromere Formation in Non-mammalian Vertebrates. Dev Cell *42*, 181-189 e183.

Hornung, P., Troc, P., Malvezzi, F., Maier, M., Demianova, Z., Zimniak, T., Litos, G., Lampert, F., Schleiffer, A., Brunner, M.*, et al.* (2014). A cooperative mechanism drives budding yeast kinetochore assembly downstream of CENP-A. J Cell Biol *206*, 509-524.

Howard, A., and Pelc, S.R. (1953). Synthesis of Desoxyribonucleic Acid in Normal and Irradiated Cells and Its Relation to Chromosome Breakage. International Journal of Radiation Biology and Related Studies in Physics, Chemistry and Medicine *49*, 207-218.

Hoyt, M.A., Totis, L., and Roberts, B.T. (1991). S. cerevisiae genes required for cell cycle arrest in response to loss of microtubule function. Cell *66*, 507-517.

Hu, H., Liu, Y., Wang, M., Fang, J., Huang, H., Yang, N., Li, Y., Wang, J., Yao, X., Shi, Y.*, et al.* (2011). Structure of a CENP-A-histone H4 heterodimer in complex with chaperone HJURP. Genes Dev *25*, 901-906.

Huis In 't Veld, P.J., Jeganathan, S., Petrovic, A., Singh, P., John, J., Krenn, V., Weissmann, F., Bange, T., and Musacchio, A. (2016). Molecular basis of outer kinetochore assembly on CENP-T. Elife *5*.

Hwang, L.H., Lau, L.F., Smith, D.L., Mistrot, C.A., Hardwick, K.G., Hwang, E.S., Amon, A., and Murray, A.W. (1998). Budding yeast Cdc20: a target of the spindle checkpoint. Science *279*, 1041-1044.

Jansen, L.E., Black, B.E., Foltz, D.R., and Cleveland, D.W. (2007). Propagation of centromeric chromatin requires exit from mitosis. J Cell Biol *176*, 795-805.

Jeronimo, C., Poitras, C., and Robert, F. (2019). Histone Recycling by FACT and Spt6 during Transcription Prevents the Scrambling of Histone Modifications. Cell Rep *28*, 1206-1218 e1208.

Kang, Y.H., Park, C.H., Kim, T.S., Soung, N.K., Bang, J.K., Kim, B.Y., Park, J.E., and Lee, K.S. (2011). Mammalian polo-like kinase 1-dependent regulation of the PBIP1-CENP-Q complex at kinetochores. J Biol Chem *286*, 19744-19757.

Kang, Y.H., Park, J.E., Yu, L.R., Soung, N.K., Yun, S.M., Bang, J.K., Seong, Y.S., Yu, H., Garfield, S., Veenstra, T.D.*, et al.* (2006). Self-regulated Plk1 recruitment to kinetochores by the Plk1-PBIP1 interaction is critical for proper chromosome segregation. Mol Cell *24*, 409-422.

Kapoor, T.M., Lampson, M.A., Hergert, P., Cameron, L., Cimini, D., Salmon, E.D., McEwen, B.F., and Khodjakov, A. (2006). Chromosomes can congress to the metaphase plate before biorientation. Science *311*, 388-391.

Kato, H., Jiang, J., Zhou, B.R., Rozendaal, M., Feng, H., Ghirlando, R., Xiao, T.S., Straight, A.F., and Bai, Y. (2013). A conserved mechanism for centromeric nucleosome recognition by centromere protein CENP-C. Science *340*, 1110-1113.

Khodjakov, A., Copenagle, L., Gordon, M.B., Compton, D.A., and Kapoor, T.M. (2003). Minus-end capture of preformed kinetochore fibers contributes to spindle morphogenesis. J Cell Biol *160*, 671-683.

Kim, I.S., Lee, M., Park, K.C., Jeon, Y., Park, J.H., Hwang, E.J., Jeon, T.I., Ko, S., Lee, H., Baek, S.H.*, et al.* (2012). Roles of Mis18alpha in epigenetic regulation of centromeric chromatin and CENP-A loading. Mol Cell *46*, 260-273.

Kim, S., and Yu, H. (2015). Multiple assembly mechanisms anchor the KMN spindle checkpoint platform at human mitotic kinetochores. J Cell Biol *208*, 181-196.

Kiyomitsu, T., Murakami, H., and Yanagida, M. (2011). Protein interaction domain mapping of human kinetochore protein Blinkin reveals a consensus motif for binding of spindle assembly checkpoint proteins Bub1 and BubR1. Mol Cell Biol *31*, 998-1011.

Klare, K., Weir, J.R., Basilico, F., Zimniak, T., Massimiliano, L., Ludwigs, N., Herzog, F., and Musacchio, A. (2015). CENP-C is a blueprint for constitutive centromere-associated network assembly within human kinetochores. J Cell Biol *210*, 11-22.

Knoepfler, P.S., and Eisenman, R.N. (1999). Sin meets NuRD and other tails of repression. Cell *99*, 447-450.

Kral, L. (2015). Possible identification of CENP-C in fish and the presence of the CENP-C motif in M18BP1 of vertebrates. F1000Res *4*, 474.

Krassovsky, K., Henikoff, J.G., and Henikoff, S. (2012). Tripartite organization of centromeric chromatin in budding yeast. Proc Natl Acad Sci U S A *109*, 243-248.

Kulaeva, O.I., Hsieh, F.K., Chang, H.W., Luse, D.S., and Studitsky, V.M. (2013). Mechanism of transcription through a nucleosome by RNA polymerase II. Biochim Biophys Acta *1829*, 76-83.

Kunitoku, N., Sasayama, T., Marumoto, T., Zhang, D., Honda, S., Kobayashi, O., Hatakeyama, K., Ushio, Y., Saya, H., and Hirota, T. (2003). CENP-A phosphorylation by Aurora-A in prophase is required for enrichment of Aurora-B at inner centromeres and for kinetochore function. Dev Cell *5*, 853-864.

Kwon, M.S., Hori, T., Okada, M., and Fukagawa, T. (2007). CENP-C is involved in chromosome segregation, mitotic checkpoint function, and kinetochore assembly. Mol Biol Cell *18*, 2155-2168.

Lagana, A., Dorn, J.F., De Rop, V., Ladouceur, A.M., Maddox, A.S., and Maddox, P.S. (2010). A small GTPase molecular switch regulates epigenetic centromere maintenance by stabilizing newly incorporated CENP-A. Nat Cell Biol *12*, 1186-1193.

Lang, J., Barber, A., and Biggins, S. (2018). An assay for de novo kinetochore assembly reveals a key role for the CENP-T pathway in budding yeast. Elife *7*.

Lechner, J., and Carbon, J. (1991). A 240 kd multisubunit protein complex, CBF3, is a major component of the budding yeast centromere. Cell *64*, 717-725.

Lenart, P., Petronczki, M., Steegmaier, M., Di Fiore, B., Lipp, J.J., Hoffmann, M., Rettig, W.J., Kraut, N., and Peters, J.M. (2007). The small-molecule inhibitor BI 2536 reveals novel insights into mitotic roles of polo-like kinase 1. Curr Biol *17*, 304-315.

Li, R., and Murray, A.W. (1991). Feedback control of mitosis in budding yeast. Cell *66*, 519-531.

Liu, C., and Mao, Y. (2016). Diaphanous formin mDia2 regulates CENP-A levels at centromeres. J Cell Biol *213*, 415-424.

Liu, S.T., Rattner, J.B., Jablonski, S.A., and Yen, T.J. (2006). Mapping the assembly pathways that specify formation of the trilaminar kinetochore plates in human cells. J Cell Biol *175*, 41-53.

Lochmann, B., and Ivanov, D. (2012). Histone H3 localizes to the centromeric DNA in budding yeast. PLoS Genet *8*, e1002739.

Locke, D.P., Hillier, L.W., Warren, W.C., Worley, K.C., Nazareth, L.V., Muzny, D.M., Yang, S.P., Wang, Z., Chinwalla, A.T., Minx, P.*, et al.* (2011). Comparative and demographic analysis of orang-utan genomes. Nature *469*, 529-533.

Logsdon, G.A., Barrey, E.J., Bassett, E.A., DeNizio, J.E., Guo, L.Y., Panchenko, T., Dawicki-McKenna, J.M., Heun, P., and Black, B.E. (2015). Both tails and the centromere targeting domain of CENP-A are required for centromere establishment. J Cell Biol *208*, 521-531.

Logsdon, G.A., Gambogi, C.W., Liskovykh, M.A., Barrey, E.J., Larionov, V., Miga, K.H., Heun, P., and Black, B.E. (2019). Human Artificial Chromosomes that Bypass Centromeric DNA. Cell *178*, 624-639 e619.

Luger, K., Mader, A.W., Richmond, R.K., Sargent, D.F., and Richmond, T.J. (1997). Crystal structure of the nucleosome core particle at 2.8 A resolution. Nature *389*, 251-260.

Maddox, P.S., Hyndman, F., Monen, J., Oegema, K., and Desai, A. (2007). Functional genomics identifies a Myb domain-containing protein family required for assembly of CENP-A chromatin. J Cell Biol *176*, 757-763.

Magidson, V., O'Connell, C.B., Loncarek, J., Paul, R., Mogilner, A., and Khodjakov, A. (2011). The spatial arrangement of chromosomes during prometaphase facilitates spindle assembly. Cell *146*, 555-567.

Maiato, H., Rieder, C.L., and Khodjakov, A. (2004). Kinetochore-driven formation of kinetochore fibers contributes to spindle assembly during animal mitosis. J Cell Biol *167*, 831-840.

Malvezzi, F., Litos, G., Schleiffer, A., Heuck, A., Mechtler, K., Clausen, T., and Westermann, S. (2013). A structural basis for kinetochore recruitment of the Ndc80 complex via two distinct centromere receptors. EMBO J *32*, 409-423.

Manuelidis, L. (1978). Chromosomal localization of complex and simple repeated human DNAs. Chromosoma *66*, 23-32.

Marques, A., and Pedrosa-Harand, A. (2016). Holocentromere identity: from the typical mitotic linear structure to the great plasticity of meiotic holocentromeres. Chromosoma *125*, 669-681.

Marshall, O.J., Marshall, A.T., and Choo, K.H. (2008). Three-dimensional localization of CENP-A suggests a complex higher order structure of centromeric chromatin. J Cell Biol *183*, 1193-1202.

McDonald, S.M., Close, D., Xin, H., Formosa, T., and Hill, C.P. (2010). Structure and biological importance of the Spn1-Spt6 interaction, and its regulatory role in nucleosome binding. Mol Cell *40*, 725-735.

McIntosh, J.R. (2016). Mitosis. Cold Spring Harb Perspect Biol *8*.

McKinley, K.L., and Cheeseman, I.M. (2014). Polo-like kinase 1 licenses CENP-A deposition at centromeres. Cell *158*, 397-411.

McKinley, K.L., Sekulic, N., Guo, L.Y., Tsinman, T., Black, B.E., and Cheeseman, I.M. (2015). The CENP-L-N Complex Forms a Critical Node in an Integrated Meshwork of Interactions at the Centromere-Kinetochore Interface. Mol Cell *60*, 886-898.

Medina-Pritchard, B., Lazou, V., Zou, J., Byron, O., Abad, M.A., Rappsilber, J., Heun, P., and Jeyaprakash, A.A. (2020). Structural basis for centromere maintenance by Drosophila CENP-A chaperone CAL1. EMBO J *39*, e103234.

Melters, D.P., Pitman, M., Rakshit, T., Dimitriadis, E.K., Bui, M., Papoian, G.A., and Dalal, Y. (2019). Intrinsic elasticity of nucleosomes is encoded by histone variants and calibrated by their binding partners. Proc Natl Acad Sci U S A *116*, 24066-24074.

Mendenhall, M.D., and Hodge, A.E. (1998). Regulation of Cdc28 cyclin-dependent protein kinase activity during the cell cycle of the yeast Saccharomyces cerevisiae. Microbiol Mol Biol Rev *62*, 1191-1243.

Mitra, S., Bodor, D.L., David, A.F., Abdul-Zani, I., Mata, J.F., Neumann, B., Reither, S., Tischer, C., and Jansen, L.E.T. (2020). Genetic screening identifies a SUMO protease dynamically maintaining centromeric chromatin. Nat Commun *11*, 501.

Mizuguchi, G., Xiao, H., Wisniewski, J., Smith, M.M., and Wu, C. (2007). Nonhistone Scm3 and histones CenH3-H4 assemble the core of centromere-specific nucleosomes. Cell *129*, 1153-1164.

Moree, B., Meyer, C.B., Fuller, C.J., and Straight, A.F. (2011). CENP-C recruits M18BP1 to centromeres to promote CENP-A chromatin assembly. J Cell Biol *194*, 855-871.

Morgan, D.O. (1995). Principles of CDK regulation. Nature *374*, 131-134.

Moroi, Y., Peebles, C., Fritzler, M.J., Steigerwald, J., and Tan, E.M. (1980). Autoantibody to centromere (kinetochore) in scleroderma sera. Proc Natl Acad Sci U S A *77*, 1627-1631.

Muller, S., Montes de Oca, R., Lacoste, N., Dingli, F., Loew, D., and Almouzni, G. (2014). Phosphorylation and DNA binding of HJURP determine its centromeric recruitment and function in CenH3(CENP-A) loading. Cell Rep *8*, 190-203.

Mullis, K., Faloona, F., Scharf, S., Saiki, R., Horn, G., and Erlich, H. (1986). Specific enzymatic amplification of DNA in vitro: the polymerase chain reaction. Cold Spring Harb Symp Quant Biol *51 Pt 1*, 263-273.

Murray, A.W., Solomon, M.J., and Kirschner, M.W. (1989). The role of cyclin synthesis and degradation in the control of maturation promoting factor activity. Nature *339*, 280-286.

Musacchio, A. (2015). The Molecular Biology of Spindle Assembly Checkpoint Signaling Dynamics. Curr Biol *25*, R1002-1018.

Nagpal, H., Hori, T., Furukawa, A., Sugase, K., Osakabe, A., Kurumizaka, H., and Fukagawa, T. (2015). Dynamic changes in CCAN organization through CENP-C during cell-cycle progression. Mol Biol Cell *26*, 3768-3776.

Nardi, I.K., Zasadzinska, E., Stellfox, M.E., Knippler, C.M., and Foltz, D.R. (2016). Licensing of Centromeric Chromatin Assembly through the Mis18alpha-Mis18beta Heterotetramer. Mol Cell *61*, 774-787.

Niikura, Y., Kitagawa, R., Ogi, H., Abdulle, R., Pagala, V., and Kitagawa, K. (2015). CENP-A K124 Ubiquitylation Is Required for CENP-A Deposition at the Centromere. Dev Cell *32*, 589-603.

Nilsson, J., Yekezare, M., Minshull, J., and Pines, J. (2008). The APC/C maintains the spindle assembly checkpoint by targeting Cdc20 for destruction. Nat Cell Biol *10*, 1411-1420.

Nishimura, K., Fukagawa, T., Takisawa, H., Kakimoto, T., and Kanemaki, M. (2009). An auxin-based degron system for the rapid depletion of proteins in nonplant cells. Nature Methods *6*, 917-922.

Nishino, T., Rago, F., Hori, T., Tomii, K., Cheeseman, I.M., and Fukagawa, T. (2013). CENP-T provides a structural platform for outer kinetochore assembly. EMBO J *32*, 424-436.

Nishino, T., Takeuchi, K., Gascoigne, K.E., Suzuki, A., Hori, T., Oyama, T., Morikawa, K., Cheeseman, I.M., and Fukagawa, T. (2012). CENP-T-W-S-X forms a unique centromeric chromatin structure with a histone-like fold. Cell *148*, 487-501.

Ohtsubo, M., Theodoras, A.M., Schumacher, J., Roberts, J.M., and Pagano, M. (1995). Human cyclin E, a nuclear protein essential for the G1-to-S phase transition. Mol Cell Biol *15*, 2612-2624.

Ohzeki, J., Bergmann, J.H., Kouprina, N., Noskov, V.N., Nakano, M., Kimura, H., Earnshaw, W.C., Larionov, V., and Masumoto, H. (2012). Breaking the HAC Barrier: histone H3K9 acetyl/methyl balance regulates CENP-A assembly. EMBO J *31*, 2391-2402.

Ohzeki, J., Shono, N., Otake, K., Martins, N.M., Kugou, K., Kimura, H., Nagase, T., Larionov, V., Earnshaw, W.C., and Masumoto, H. (2016). KAT7/HBO1/MYST2 Regulates CENP-A Chromatin Assembly by Antagonizing Suv39h1-Mediated Centromere Inactivation. Dev Cell *37*, 413-427.

Ohzeki, J.i. (2002). CENP-B box is required for de novo centromere chromatin assembly on human alphoid DNA. The Journal of Cell Biology *159*, 765-775.

Okada, M., Cheeseman, I.M., Hori, T., Okawa, K., McLeod, I.X., Yates, J.R., 3rd, Desai, A., and Fukagawa, T. (2006). The CENP-H-I complex is required for the efficient incorporation of newly synthesized CENP-A into centromeres. Nat Cell Biol *8*, 446-457.

Okada, M., Okawa, K., Isobe, T., and Fukagawa, T. (2009). CENP-H-containing complex facilitates centromere deposition of CENP-A in cooperation with FACT and CHD1. Mol Biol Cell *20*, 3986-3995.

Okada, T., Ohzeki, J., Nakano, M., Yoda, K., Brinkley, W.R., Larionov, V., and Masumoto, H. (2007). CENP-B controls centromere formation depending on the chromatin context. Cell *131*, 1287-1300.

Orr, B., and Sunkel, C.E. (2011). Drosophila CENP-C is essential for centromere identity. Chromosoma *120*, 83-96.

Palmer, D.K., O'Day, K., Wener, M.H., Andrews, B.S., and Margolis, R.L. (1987). A 17-kD centromere protein (CENP-A) copurifies with nucleosome core particles and with histones. J Cell Biol *104*, 805-815.

Pan, D., Klare, K., Petrovic, A., Take, A., Walstein, K., Singh, P., Rondelet, A., Bird, A.W., and Musacchio, A. (2017). CDK-regulated dimerization of M18BP1 on a Mis18 hexamer is necessary for CENP-A loading. Elife *6*.

Pan, D., Walstein, K., Take, A., Bier, D., Kaiser, N., and Musacchio, A. (2019). Mechanism of centromere recruitment of the CENP-A chaperone HJURP and its implications for centromere licensing. Nat Commun *10*, 4046.

Panchenko, T., Sorensen, T.C., Woodcock, C.L., Kan, Z.Y., Wood, S., Resch, M.G., Luger, K., Englander, S.W., Hansen, J.C., and Black, B.E. (2011). Replacement of histone H3 with CENP-A directs global nucleosome array condensation and loosening of nucleosome superhelical termini. Proc Natl Acad Sci U S A *108*, 16588-16593.

Pardee, A.B. (1974). A restriction point for control of normal animal cell proliferation. Proc Natl Acad Sci U S A *71*, 1286-1290.

Paweletz, N. (2001). Walther Flemming: Pioneer of mitosis research. Nature reviews Molecular cell biology *2*, 72-75.

Pekgoz Altunkaya, G., Malvezzi, F., Demianova, Z., Zimniak, T., Litos, G., Weissmann, F., Mechtler, K., Herzog, F., and Westermann, S. (2016). CCAN Assembly Configures Composite Binding Interfaces to Promote Cross-Linking of Ndc80 Complexes at the Kinetochore. Curr Biol *26*, 2370-2378.

Pentakota, S., Zhou, K., Smith, C., Maffini, S., Petrovic, A., Morgan, G.P., Weir, J.R., Vetter, I.R., Musacchio, A., and Luger, K. (2017). Decoding the centromeric nucleosome through CENP-N. Elife *6*.

Perpelescu, M., Nozaki, N., Obuse, C., Yang, H., and Yoda, K. (2009). Active establishment of centromeric CENP-A chromatin by RSF complex. J Cell Biol *185*, 397-407.

Pesenti, M.E., Prumbaum, D., Auckland, P., Smith, C.M., Faesen, A.C., Petrovic, A., Erent, M., Maffini, S., Pentakota, S., Weir, J.R.*, et al.* (2018). Reconstitution of a 26-Subunit Human Kinetochore Reveals Cooperative Microtubule Binding by CENP-OPQUR and NDC80. Mol Cell *71*, 923-939 e910.

Pesenti, M.E., Weir, J.R., and Musacchio, A. (2016). Progress in the structural and functional characterization of kinetochores. Curr Opin Struct Biol *37*, 152-163.

Petronczki, M., Glotzer, M., Kraut, N., and Peters, J.M. (2007). Polo-like kinase 1 triggers the initiation of cytokinesis in human cells by promoting recruitment of the RhoGEF Ect2 to the central spindle. Dev Cell *12*, 713-725.

Petrovic, A., Keller, J., Liu, Y., Overlack, K., John, J., Dimitrova, Y.N., Jenni, S., van Gerwen, S., Stege, P., Wohlgemuth, S.*, et al.* (2016). Structure of the MIS12 Complex

and Molecular Basis of Its Interaction with CENP-C at Human Kinetochores. Cell *167*, 1028-1040 e1015.

Petrovic, A., Mosalaganti, S., Keller, J., Mattiuzzo, M., Overlack, K., Krenn, V., De Antoni, A., Wohlgemuth, S., Cecatiello, V., Pasqualato, S.*, et al.* (2014). Modular assembly of RWD domains on the Mis12 complex underlies outer kinetochore organization. Mol Cell *53*, 591-605.

Petrovic, A., Pasqualato, S., Dube, P., Krenn, V., Santaguida, S., Cittaro, D., Monzani, S., Massimiliano, L., Keller, J., Tarricone, A.*, et al.* (2010). The MIS12 complex is a protein interaction hub for outer kinetochore assembly. J Cell Biol *190*, 835-852.

Przewloka, M.R., Venkei, Z., Bolanos-Garcia, V.M., Debski, J., Dadlez, M., and Glover, D.M. (2011). CENP-C is a structural platform for kinetochore assembly. Curr Biol *21*, 399-405.

Rago, F., Gascoigne, K.E., and Cheeseman, I.M. (2015). Distinct organization and regulation of the outer kinetochore KMN network downstream of CENP-C and CENP-T. Curr Biol *25*, 671-677.

Richter, M.M., Poznanski, J., Zdziarska, A., Czarnocki-Cieciura, M., Lipinszki, Z., Dadlez, M., Glover, D.M., and Przewloka, M.R. (2016). Network of protein interactions within the Drosophila inner kinetochore. Open Biol *6*, 150238.

Rieder, C.L. (1982). The formation, structure, and composition of the mammalian kinetochore and kinetochore fiber. Int Rev Cytol *79*, 1-58.

Rieder, C.L., Cole, R.W., Khodjakov, A., and Sluder, G. (1995). The checkpoint delaying anaphase in response to chromosome monoorientation is mediated by an inhibitory signal produced by unattached kinetochores. J Cell Biol *130*, 941-948.

Rogers, S., Wells, R., and Rechsteiner, M. (1986). Amino acid sequences common to rapidly degraded proteins: the PEST hypothesis. Science *234*, 364-368.

Roulland, Y., Ouararhni, K., Naidenov, M., Ramos, L., Shuaib, M., Syed, S.H., Lone, I.N., Boopathi, R., Fontaine, E., Papai, G.*, et al.* (2016). The Flexible Ends of CENP-A Nucleosome Are Required for Mitotic Fidelity. Mol Cell *63*, 674-685.

Roure, V., Medina-Pritchard, B., Lazou, V., Rago, L., Anselm, E., Venegas, D., Jeyaprakash, A.A., and Heun, P. (2019). Reconstituting Drosophila Centromere Identity in Human Cells. Cell Rep *29*, 464-479 e465.

Salmon, E.D., Cimini, D., Cameron, L.A., and DeLuca, J.G. (2005). Merotelic kinetochores in mammalian tissue cells. Philos Trans R Soc Lond B Biol Sci *360*, 553-568.

Sanchez-Pulido, L., Pidoux, A.L., Ponting, C.P., and Allshire, R.C. (2009). Common ancestry of the CENP-A chaperones Scm3 and HJURP. Cell *137*, 1173-1174.

Sandmann, M., Talbert, P., Demidov, D., Kuhlmann, M., Rutten, T., Conrad, U., and Lermontova, I. (2017). Targeting of Arabidopsis KNL2 to Centromeres Depends on the Conserved CENPC-k Motif in Its C Terminus. Plant Cell *29*, 144-155.

Santamaria, A., Wang, B., Elowe, S., Malik, R., Zhang, F., Bauer, M., Schmidt, A., Silljé, H.H.W., Körner, R., and Nigg, E.A. (2011). The Plk1-dependent Phosphoproteome of the Early Mitotic Spindle. Molecular & Cellular Proteomics *10*.

Sathyan, K.M., Fachinetti, D., and Foltz, D.R. (2017). alpha-amino trimethylation of CENP-A by NRMT is required for full recruitment of the centromere. Nat Commun *8*, 14678.

Schagger, H., and von Jagow, G. (1987). Tricine-sodium dodecyl sulfate-polyacrylamide gel electrophoresis for the separation of proteins in the range from 1 to 100 kDa. Anal Biochem *166*, 368-379.

Schleiffer, A., Maier, M., Litos, G., Lampert, F., Hornung, P., Mechtler, K., and Westermann, S. (2012). CENP-T proteins are conserved centromere receptors of the Ndc80 complex. Nat Cell Biol *14*, 604-613.

Schuh, M., Lehner, C.F., and Heidmann, S. (2007). Incorporation of Drosophila CID/CENP-A and CENP-C into centromeres during early embryonic anaphase. Curr Biol *17*, 237-243.

Screpanti, E., De Antoni, A., Alushin, G.M., Petrovic, A., Melis, T., Nogales, E., and Musacchio, A. (2011). Direct binding of Cenp-C to the Mis12 complex joins the inner and outer kinetochore. Curr Biol *21*, 391-398.

Shang, W.H., Hori, T., Toyoda, A., Kato, J., Popendorf, K., Sakakibara, Y., Fujiyama, A., and Fukagawa, T. (2010). Chickens possess centromeres with both extended tandem repeats and short non-tandem-repetitive sequences. Genome Res *20*, 1219-1228.

Shang, W.H., Hori, T., Westhorpe, F.G., Godek, K.M., Toyoda, A., Misu, S., Monma, N., Ikeo, K., Carroll, C.W., Takami, Y.*, et al.* (2016). Acetylation of histone H4 lysine 5 and 12 is required for CENP-A deposition into centromeres. Nat Commun *7*, 13465.

Sharma, A.B., Dimitrov, S., Hamiche, A., and Van Dyck, E. (2019). Centromeric and ectopic assembly of CENP-A chromatin in health and cancer: old marks and new tracks. Nucleic Acids Res *47*, 1051-1069.

Shelby, R.D., Monier, K., and Sullivan, K.F. (2000). Chromatin assembly at kinetochores is uncoupled from DNA replication. J Cell Biol *151*, 1113-1118.

Sherr, C.J. (1994). G1 phase progression: cycling on cue. Cell *79*, 551-555.

Shivaraju, M., Unruh, J.R., Slaughter, B.D., Mattingly, M., Berman, J., and Gerton, J.L. (2012). Cell-cycle-coupled structural oscillation of centromeric nucleosomes in yeast. Cell *150*, 304-316.

Shono, N., Ohzeki, J., Otake, K., Martins, N.M., Nagase, T., Kimura, H., Larionov, V., Earnshaw, W.C., and Masumoto, H. (2015). CENP-C and CENP-I are key connecting factors for kinetochore and CENP-A assembly. J Cell Sci *128*, 4572-4587.

Shrestha, R.L., Conti, D., Tamura, N., Braun, D., Ramalingam, R.A., Cieslinski, K., Ries, J., and Draviam, V.M. (2017). Aurora-B kinase pathway controls the lateral to end-on conversion of kinetochore-microtubule attachments in human cells. Nat Commun *8*, 150.

Shuaib, M., Ouararhni, K., Dimitrov, S., and Hamiche, A. (2010). HJURP binds CENP-A via a highly conserved N-terminal domain and mediates its deposition at centromeres. Proc Natl Acad Sci U S A *107*, 1349-1354.

Silva, M.C., Bodor, D.L., Stellfox, M.E., Martins, N.M., Hochegger, H., Foltz, D.R., and Jansen, L.E. (2012). Cdk activity couples epigenetic centromere inheritance to cell cycle progression. Dev Cell *22*, 52-63.

Song, K., Gronemeyer, B., Lu, W., Eugster, E., and Tomkiel, J.E. (2002). Mutational analysis of the central centromere targeting domain of human centromere protein C, (CENP-C). Exp Cell Res *275*, 81-91.

Soung, N.K., Park, J.E., Yu, L.R., Lee, K.H., Lee, J.M., Bang, J.K., Veenstra, T.D., Rhee, K., and Lee, K.S. (2009). Plk1-dependent and -independent roles of an ODF2 splice variant, hCenexin1, at the centrosome of somatic cells. Dev Cell *16*, 539-550.

Spiller, F., Medina-Pritchard, B., Abad, M.A., Wear, M.A., Molina, O., Earnshaw, W.C., and Jeyaprakash, A.A. (2017). Molecular basis for Cdk1-regulated timing of Mis18 complex assembly and CENP-A deposition. EMBO Rep *18*, 894-905.

Stankovic, A., Guo, L.Y., Mata, J.F., Bodor, D.L., Cao, X.J., Bailey, A.O., Shabanowitz, J., Hunt, D.F., Garcia, B.A., Black, B.E*., et al.* (2017). A Dual Inhibitory Mechanism Sufficient to Maintain Cell-Cycle-Restricted CENP-A Assembly. Mol Cell *65*, 231-246.

Steegmaier, M., Hoffmann, M., Baum, A., Lenart, P., Petronczki, M., Krssak, M., Gurtler, U., Garin-Chesa, P., Lieb, S., Quant, J*., et al.* (2007). BI 2536, a potent and selective inhibitor of polo-like kinase 1, inhibits tumor growth in vivo. Curr Biol *17*, 316-322.

Stellfox, M.E., Bailey, A.O., and Foltz, D.R. (2013). Putting CENP-A in its place. Cell Mol Life Sci *70*, 387-406.

Stellfox, M.E., Nardi, I.K., Knippler, C.M., and Foltz, D.R. (2016). Differential Binding Partners of the Mis18alpha/beta YIPPEE Domains Regulate Mis18 Complex Recruitment to Centromeres. Cell Rep *15*, 2127-2135.

Subramanian, L., Medina-Pritchard, B., Barton, R., Spiller, F., Kulasegaran-Shylini, R., Radaviciute, G., Allshire, R.C., and Arockia Jeyaprakash, A. (2016). Centromere localization and function of Mis18 requires Yippee-like domain-mediated oligomerization. EMBO Rep *17*, 496-507.

Sudakin, V., Chan, G.K., and Yen, T.J. (2001). Checkpoint inhibition of the APC/C in HeLa cells is mediated by a complex of BUBR1, BUB3, CDC20, and MAD2. J Cell Biol *154*, 925-936.

Sudakin, V., Ganoth, D., Dahan, A., Heller, H., Hershko, J., Luca, F.C., Ruderman, J.V., and Hershko, A. (1995). The cyclosome, a large complex containing cyclin-selective ubiquitin ligase activity, targets cyclins for destruction at the end of mitosis. Mol Biol Cell *6*, 185-197.

Suzuki, A., Badger, B.L., and Salmon, E.D. (2015). A quantitative description of Ndc80 complex linkage to human kinetochores. Nat Commun *6*, 8161.

Suzuki, N., Nakano, M., Nozaki, N., Egashira, S.-i., Okazaki, T., and Masumoto, H. (2004). CENP-B Interacts with CENP-C Domains Containing Mif2 Regions Responsible for Centromere Localization. Journal of Biological Chemistry *279*, 5934-5946.

Tachiwana, H., Kagawa, W., Shiga, T., Osakabe, A., Miya, Y., Saito, K., Hayashi-Takanaka, Y., Oda, T., Sato, M., Park, S.Y.*, et al.* (2011). Crystal structure of the human centromeric nucleosome containing CENP-A. Nature *476*, 232-235.

Takeuchi, K., Nishino, T., Mayanagi, K., Horikoshi, N., Osakabe, A., Tachiwana, H., Hori, T., Kurumizaka, H., and Fukagawa, T. (2014). The centromeric nucleosome-like CENP-T-W-S-X complex induces positive supercoils into DNA. Nucleic Acids Res *42*, 1644-1655.

Tanaka, K., Chang, H.L., Kagami, A., and Watanabe, Y. (2009). CENP-C functions as a scaffold for effectors with essential kinetochore functions in mitosis and meiosis. Dev Cell *17*, 334-343.

Tanaka, T.U. (2010). Kinetochore-microtubule interactions: steps towards bi-orientation. EMBO J *29*, 4070-4082.

Thakur, J., and Henikoff, S. (2016). CENPT bridges adjacent CENPA nucleosomes on young human alpha-satellite dimers. Genome Res *26*, 1178-1187.

Tian, T., Li, X., Liu, Y., Wang, C., Liu, X., Bi, G., Zhang, X., Yao, X., Zhou, Z.H., and Zang, J. (2018). Molecular basis for CENP-N recognition of CENP-A nucleosome on the human kinetochore. Cell Res *28*, 374-378.

Tien, J.F., Umbreit, N.T., Gestaut, D.R., Franck, A.D., Cooper, J., Wordeman, L., Gonen, T., Asbury, C.L., and Davis, T.N. (2010). Cooperation of the Dam1 and Ndc80 kinetochore complexes enhances microtubule coupling and is regulated by aurora B. J Cell Biol *189*, 713-723.

Toth, A., Ciosk, R., Uhlmann, F., Galova, M., Schleiffer, A., and Nasmyth, K. (1999). Yeast cohesin complex requires a conserved protein, Eco1p(Ctf7), to establish cohesion between sister chromatids during DNA replication. Genes Dev *13*, 320-333.

Trazzi, S., Bernardoni, R., Diolaiti, D., Politi, V., Earnshaw, W.C., Perini, G., and Della Valle, G. (2002). In vivo functional dissection of human inner kinetochore protein CENP-C. J Struct Biol *140*, 39-48.

Trazzi, S., Perini, G., Bernardoni, R., Zoli, M., Reese, J.C., Musacchio, A., and Della Valle, G. (2009). The C-terminal domain of CENP-C displays multiple and critical functions for mammalian centromere formation. PLoS One *4*, e5832.

Uhlmann, F., Bouchoux, C., and Lopez-Aviles, S. (2011). A quantitative model for cyclin-dependent kinase control of the cell cycle: revisited. Philos Trans R Soc Lond B Biol Sci *366*, 3572-3583.

Uhlmann, F., Lottspeich, F., and Nasmyth, K. (1999). Sister-chromatid separation at anaphase onset is promoted by cleavage of the cohesin subunit Scc1. Nature *400*, 37-42.

Vermeulen, K., Van Bockstaele, D.R., and Berneman, Z.N. (2003). The cell cycle: a review of regulation, deregulation and therapeutic targets in cancer. Cell Prolif *36*, 131-149.

Voullaire, L.E., Slater, H.R., Petrovic, V., and Choo, K.H. (1993). A functional marker centromere with no detectable alpha-satellite, satellite III, or CENP-B protein: activation of a latent centromere? Am J Hum Genet *52*, 1153-1163.

Wang, H., Hu, X., Ding, X., Dou, Z., Yang, Z., Shaw, A.W., Teng, M., Cleveland, D.W., Goldberg, M.L., Niu, L.*, et al.* (2004). Human Zwint-1 specifies localization of Zeste White 10 to kinetochores and is essential for mitotic checkpoint signaling. J Biol Chem *279*, 54590-54598.

Watanabe, R., Hara, M., Okumura, E.I., Herve, S., Fachinetti, D., Ariyoshi, M., and Fukagawa, T. (2019). CDK1-mediated CENP-C phosphorylation modulates CENP-A binding and mitotic kinetochore localization. J Cell Biol *218*, 4042-4062.

Wei, R.R., Schnell, J.R., Larsen, N.A., Sorger, P.K., Chou, J.J., and Harrison, S.C. (2006). Structure of a central component of the yeast kinetochore: the Spc24p/Spc25p globular domain. Structure *14*, 1003-1009.

Wei, R.R., Sorger, P.K., and Harrison, S.C. (2005). Molecular organization of the Ndc80 complex, an essential kinetochore component. Proc Natl Acad Sci U S A *102*, 5363-5367.

Weir, J.R., Faesen, A.C., Klare, K., Petrovic, A., Basilico, F., Fischbock, J., Pentakota, S., Keller, J., Pesenti, M.E., Pan, D.*, et al.* (2016). Insights from biochemical reconstitution into the architecture of human kinetochores. Nature *537*, 249-253.

Westhorpe, F.G., Fuller, C.J., and Straight, A.F. (2015). A cell-free CENP-A assembly system defines the chromatin requirements for centromere maintenance. J Cell Biol *209*, 789-801.

Xiao, H., Wang, F., Wisniewski, J., Shaytan, A.K., Ghirlando, R., FitzGerald, P.C., Huang, Y., Wei, D., Li, S., Landsman, D.*, et al.* (2017). Molecular basis of CENP-C association with the CENP-A nucleosome at yeast centromeres. Genes & Development *31*, 1958-1972.

Yamagishi, Y., Yang, C.H., Tanno, Y., and Watanabe, Y. (2012). MPS1/Mph1 phosphorylates the kinetochore protein KNL1/Spc7 to recruit SAC components. Nat Cell Biol *14*, 746-752.

Yan, K., Yang, J., Zhang, Z., McLaughlin, S.H., Chang, L., Fasci, D., Ehrenhofer-Murray, A.E., Heck, A.J.R., and Barford, D. (2019). Structure of the inner kinetochore CCAN complex assembled onto a centromeric nucleosome. Nature *574*, 278-282.

Yu, Z., Zhou, X., Wang, W., Deng, W., Fang, J., Hu, H., Wang, Z., Li, S., Cui, L., Shen, J.*, et al.* (2015). Dynamic phosphorylation of CENP-A at Ser68 orchestrates its cell-cycle-dependent deposition at centromeres. Dev Cell *32*, 68-81.

Zakeri, B., Fierer, J.O., Celik, E., Chittock, E.C., Schwarz-Linek, U., Moy, V.T., and Howarth, M. (2012). Peptide tag forming a rapid covalent bond to a protein, through engineering a bacterial adhesin. Proc Natl Acad Sci U S A *109*, E690-697.

Zasadzinska, E., Barnhart-Dailey, M.C., Kuich, P.H., and Foltz, D.R. (2013). Dimerization of the CENP-A assembly factor HJURP is required for centromeric nucleosome deposition. EMBO J *32*, 2113-2124.

Zasadzinska, E., Huang, J., Bailey, A.O., Guo, L.Y., Lee, N.S., Srivastava, S., Wong, K.A., French, B.T., Black, B.E., and Foltz, D.R. (2018). Inheritance of CENP-A Nucleosomes during DNA Replication Requires HJURP. Dev Cell *47*, 348-362 e347.

Zeitlin, S.G., Shelby, R.D., and Sullivan, K.F. (2001). CENP-A is phosphorylated by Aurora B kinase and plays an unexpected role in completion of cytokinesis. J Cell Biol *155*, 1147-1157.

Zhang, D., Martyniuk, C.J., and Trudeau, V.L. (2006). SANTA domain: a novel conserved protein module in Eukaryota with potential involvement in chromatin regulation. Bioinformatics *22*, 2459-2462.

Zhang, X., Chen, Q., Feng, J., Hou, J., Yang, F., Liu, J., Jiang, Q., and Zhang, C. (2009). Sequential phosphorylation of Nedd1 by Cdk1 and Plk1 is required for targeting of the gammaTuRC to the centrosome. J Cell Sci *122*, 2240-2251.

Acknowledgements

First, I would like to thank Prof. Dr. Andrea Musacchio for giving me the opportunity to work in his lab, for scientific discussions and for continuously supporting me during the past years. I would also like to thank Prof. Dr. Stefan Westermann for being the second supervisor of my PhD thesis.

My sincere thanks go to my TAC members Dr. Heinz Neumann and Dr. Peter Bieling for their valuable suggestions.

I would like to give special thanks to Dr. Dongqing Pan for his invaluable scientific advice, his mentoring and his reliable support in the lab.

Furthermore, I want to thank Doro Vogt, Annika Take, Lisa Schulze and Dr. Duccio Conti for creating a nice working atmosphere and for making the daily work in the lab more joyful.

I would like to thank Dr. Tanja Bange and Franziska Müller for the processing and analysis of my mass spectrometry samples. Furthermore, I thank Dr. Stefano Maffini for his support at the microscope.

I would like to express my gratitude to many people in the lab for their support and helpful discussions: Dr. Arsen Petrovic, Dr. Giuseppe Ciossani, Dr. Valentina Piano, Dr. Marion Pesenti, Dr. Soumitra Polley, Dr. Pim Huis in ’t Veld, Dr. Nico Schmidt, Dr. Hefei Wang and Dr. Kathrin Ostholt.

I want to specially thank Antje Peukert for her very kind support in all non-scientific matters as well as Dr. Lucia Sironi and Christa Hornemann from the IMPRS for the organization of many helpful workshops and events.

I would also like to thank the Collaborative Research Center 1093 and especially Dr. Lydia Didt for offering and organizing an excellent scientific training program.

Last, I want to thank my family for the strong support during the past years.

Curriculum Vitae

Der Lebenslauf ist in der Online-Version aus Gründen des Datenschutzes nicht enthalten.

Affidavit

Erklärung:

Hiermit erkläre ich, gem. § 7 Abs. (2) e) + g) der Promotionsordnung der Fakultät für Biologie zur Erlangung des Dr. rer. nat., dass ich keine anderen Promotionen bzw. Promotionsversuche in der Vergangenheit durchgeführt habe und dass diese Arbeit von keiner anderen Fakultät/Fachbereich abgelehnt worden ist.

Dortmund, 29.09.2020 K. Walstein

Kai Walstein

Erklärung:

Hiermit erkläre ich, gem. § 7 Abs. (2) d) + f) der Promotionsordnung der Fakultät für Biologie zur Erlangung des Dr. rer. nat., dass ich die vorliegende Dissertation selbständig verfasst und mich keiner anderen als der angegebenen Hilfsmittel bedient, bei der Abfassung der Dissertation nur die angegeben Hilfsmittel benutzt und alle wörtlich oder inhaltlich übernommenen Stellen als solche gekennzeichnet habe.

Dortmund, 29.09.2020 K. Walstein

Kai Walstein

29.09.2020

Erklärung:

Hiermit erkläre ich, gem. § 6 Abs. (2) g) der Promotionsordnung der Fakultät für Biologie zur Erlangung der Dr. rer. nat., dass ich das Arbeitsgebiet, dem das Thema „Reconstitution and Characterization of Kinetochore Units Assembled on Centromeric Nucleosome Templates“ zuzuordnen ist, in Forschung und Lehre vertrete und den Antrag von Herrn Kai Walstein befürworte und die Betreuung auch im Falle eines Weggangs, wenn nicht wichtige Gründe dem entgegenstehen, weiterführen werde.

Mit freundlichen Grüßen

Andrea Musacchio